

Project	Advies Schadebeoordeling IMG WP2.4 Modelberekeningen schade in gebouwen ten gevolge van diepe bodemdaling
Report number	
Internal Reference	
Date	September 8, 2023
Version	2
Status	Cover Letter

Cover Letter

Before you lies a document containing additional appendixes to the original report titled "Computational modelling checks of masonry building damage due to deep subsidence" [1], issued in February of 2021.

In November of 2022, a review of the report was published by an independent, peer review committee [3]. To adequately address the commentary provided by this review, we deem necessary to provide additional background to the observations and conclusions discussed in the text of the original study. These four additional appendixes expand thus on the study and further support its main findings.

The observations from the peer review that are addressed by the appendixes can be summarised by the following two points:

- Insufficient underpinning of the worst case scenarios explored and suggestions on worse situations to contemplate: stiffer masonry, more vulnerable foundations, and no connections to transversal walls;
- No quantification of the probability of damage.

In the original report, the modelling checks concluded that damage due to deep subsidence was not a reasonable expectation given the low soil strain and curvatures. The peer review challenged this conclusion and asked for a quantitative probability of damage. To address the first bullet point, appendixes H and I were conceived, while appendix G was drafted tackle the second point and illustrate the location of the worst-cases along the probability spectrum; however, it couldn't quantify precise probabilities. In discussion with TNO and IMG, it was clear that further quantification would be helpful and so appendix J was added with an estimation of the probabilities; see Figure J.0 below. Its results have served to emphasize the message of the original report: that deep subsidence, in a direct sense, is unlikely to lead to visible damage in masonry buildings.

In addition to the appendixes, point-by-point replies, including comments not addressed by this new text, have been gathered in two tables: (A) about the commentary regarding observations using InSAR; and (B), with the individual comments about the aforementioned modelling study. These tables are also attached.

Accompanying the appendixes attached, a formal response letter to the peer review, based on the results herein and accompanying study by TNO [2], gathers the final conclusions of this study.

The Authors,
Delft, 8 of September of 2023

[1] Rots, J.G., Korswagen, P.A., Longo, M. (2021). Computational modelling checks of masonry building damage due to deep subsidence. Including appendixes A-F. Delft University of Technology. Report number 01, Version 05, February 18, 2021.

[2] M. Pluymaekers (2023). Memo: Additional analysis subsidence evaluation Norg. TNO AGE 23-10.024, August 2023

[3] Peer Review: Direct and indirect cause of building damages related to deep subsidence and heave due to gas extraction in Groningen and gas extraction and storage in Norg (2022). Movares. 2 November 2022. D79-CWS-HS-RAP-22007458

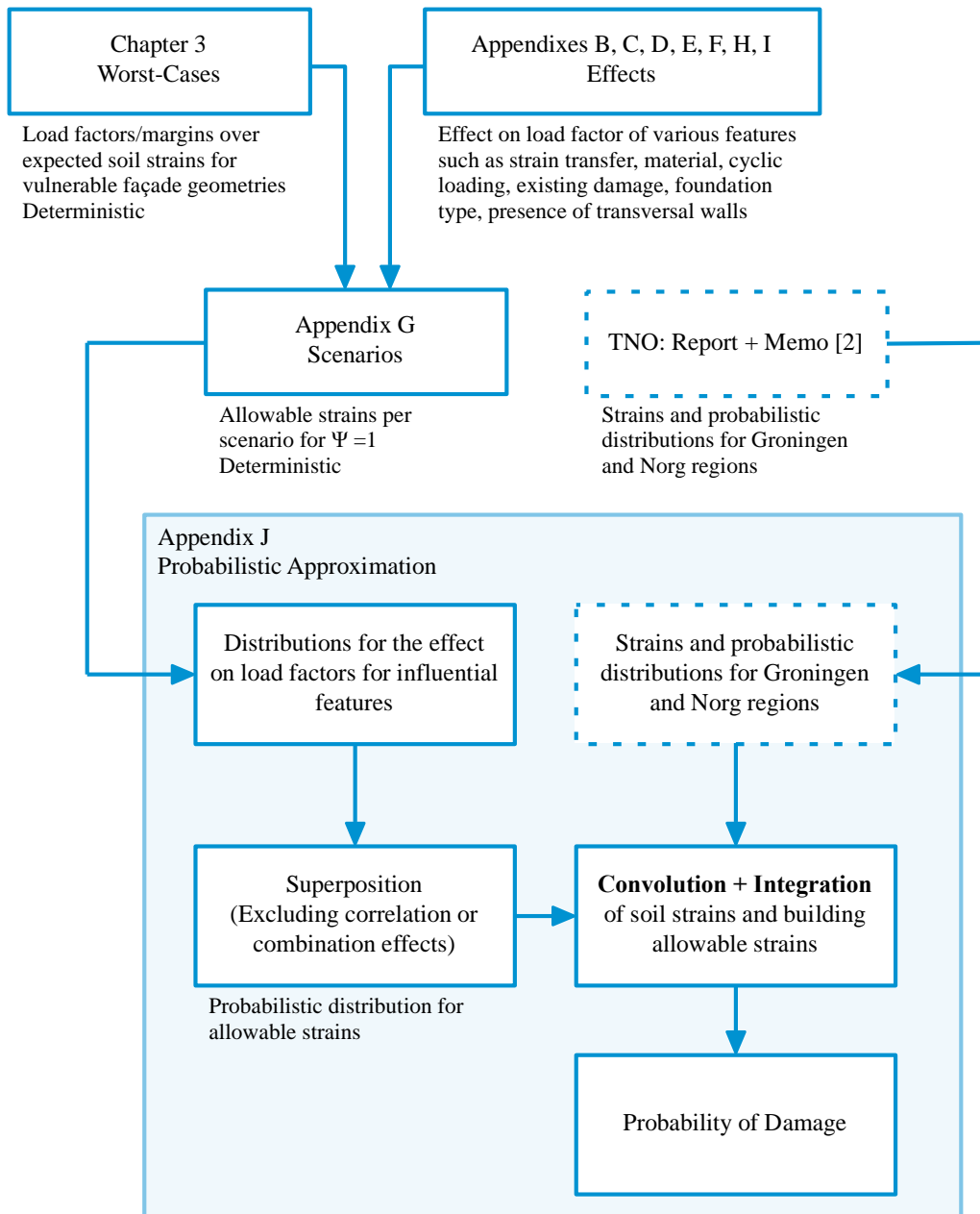


Figure J.0. Flowchart illustrating the composition of the study reaching a quantification of the probability of damage in Appendix J.

Project	Advies Schadebeoordeling IMG WP 2.4 Modelberekeningen schade in gebouwen ten gevolge van diepe bodemdaling
Report number	01
Internal Reference	
Date	8 September 2023
Version	06
Status	Final

Appendixes G, H, I and J to

COMPUTATIONAL MODELLING CHECKS OF MASONRY BUILDING DAMAGE DUE TO DEEP SUBSIDENCE

Work-Package 2.4

Client: IMG

Authors Paul Korswagen
 P.A.KorswagenEguren@tudelft.nl
 Michele Longo
 M.Longo@tudelft.nl
 Jan Rots
 J.G.Rots@tudelft.nl

Address Delft University of Technology
 Faculty of Civil Engineering and Geosciences
 Stevinweg 1, 2628 CN, Delft

 <p> Faculty of Civil Engineering and Geosciences Stevinweg 1 2628 CN Delft PO 5048 2600 GA Delft www.citg.tudelft.nl </p>		Appendixes to Report	
		Title: Appendixes G, H, I and J: Computational modelling checks of masonry building damage due to deep subsidence	
		Author(s): Paul A. Korswagen E. Michele Longo Jan G. Rots	
		Date: September 8, 2023	
Client(s): IMG		Version: 06	Status: Final
Project number:	Project name: Advies Schadebeoordeling IMG WP 2.4 Modelberekeningen schade in gebouwen ten gevolge van diepe bodemdaling		File reference:
Cite as: Korswagen P.A., Longo M., Rots J.G. (2023). Appendixes G, H, I and J: Computational modelling checks of masonry building damage due to deep subsidence. Delft University of Technology. Report number 01, Version 06, September 8, 2023.			

Copyright statement

All rights reserved. No part of this publication may be reproduced, stored in a retrieval system of any nature, or transmitted, in any form or by any means, electronic, mechanical, photocopying, recording or otherwise, without the prior written permission of TU Delft.

Liability statement

TU Delft and those who have contributed to this publication did exercise the greatest care in putting together this publication. However, the possibility should not be excluded that it contains errors and imperfections. Any use of this publication and data from it is entirely on the own responsibility of the user. For everybody who has contributed to this publication, TU Delft disclaims any liability for damage that could result from the use of this publication and data from it, unless the damage results from malice or gross negligence on the part of TU Delft and/or those who have contributed to this publication.

Table of Contents

<u>TABLE OF CONTENTS</u>	3
<u>APPENDIX H: EXPLORATIONS OF HORIZONTAL STRAIN TRANSFER WITH COUPLED SOIL-STRUCTURE MODELS</u>	5
H.1 INTRODUCTION	5
H.2 LITERATURE STUDY	5
H.3 METHOD	6
H.4 RESULTS	7
H.5 DISCUSSION	8
H.6 CONCLUSIONS	9
H.7 REFERENCES	9
<u>APPENDIX I: VULNERABLE FEATURES - ADDITIONAL MODELLING CHECK OF STIFF MASONRY, THIN FOUNDATIONS, AND NO TRANSVERSAL WALLS</u>	10
I.1 INTRODUCTION	10
I.2 METHOD	10
I.3 RESULTS	11
I.4 CONCLUSIONS	12
<u>APPENDIX G: QUALITATIVE PROBABILISTIC DESCRIPTION OF WORST-CASE SCENARIOS</u>	13
G.1 INTRODUCTION	13
G.2 METHOD	14
G.2.1. SUMMARY OF DUTCH BUILDINGS.....	14
G.2.2. SCENARIOS.....	16
G.2.3 STRAINS AND CURVATURES DUE TO DEEP SUBSIDENCE.....	21
G.3 RESULTS	22
G.4 CONCLUSIONS	26
G.5 REFERENCES	27
<u>APPENDIX J: CONVOLUTION FOR THE PROBABILITY OF BUILDING DAMAGE DUE TO HORIZONTAL SOIL STRAINS FOR BUILDINGS OF SCENARIO E</u>	28
J.1. INTRODUCTION.....	28
J.2. DISTRIBUTIONS FOR BUILDING VULNERABILITY	29
J.2.1. MATERIAL STRENGTH.....	29
J.2.2. FOUNDATION SIZE	29
J.2.3. GEOMETRY	30
J.2.4. PRE-DAMAGE	31
J.2.5. CYCLIC EFFECTS	31
J.2.6. STRAIN TRANSFER	31
J.2.7. RESULTS: SUPERPOSITION FOR A DISTRIBUTION OF ALLOWABLE STRAIN	32
J.3 CONVOLUTION OF FIELD STRAINS AND BUILDING VULNERABILITY.....	33
J.3.1. OVERVIEW OF HORIZONTAL FIELD STRAINS.....	33
J.3.2. CONVOLUTION WITH BUILDING FRAGILITY	37
J.3.3. INTERSECTION WITH BAG BUILDING DATABASE	40

J.4 DISCUSSION	43
J.5 CONCLUSIONS	44
J.6 REFERENCES	46

Appendix H: Explorations of horizontal strain transfer with coupled soil-structure models

H.1 Introduction

In most of the models of this study, the conservative approach has been taken and soil deformations have been directly applied at the base of foundations, forcing buildings to deform. In reality, the presence of the stiffer building also affects the deformations that appear on the soil; see Figure H.1 and Figure G.5. This means that the soil-structure problem is a coupled one: complex and with a large variability. This appendix conducts a preliminary study of what is agreed upon in literature, both numerical and experimental state-of-the-art. Moreover, it presents the results of an exploratory modelling campaign to determine what transfer ratios of strain to the structures are reasonable for the situation of Dutch soil and buildings. This is performed in the context of large horizontal strains and limited curvatures corresponding to the combination typical of deep subsidence phenomena.

H.2 Literature Study

Potts and Addenbrooke [1] determined that the amount of deformation transferred to a structure depends on the relative stiffness between the structure and the underlying soil. Their publication is cited in most studies treating the matter and their conclusions are widely agreed upon and expanded on. They also concluded that the shape of the greenfield subsidence due to tunnelling would be affected by the presence of a structure. Incidentally, they also determined thresholds for damage of buildings: at a horizontal strain of 800 $\mu\text{m}/\text{m}$ cracks of up to 1 mm may appear. In combination with a deflection ratio of 0.5‰, the permissible horizontal strain reduces to 500 $\mu\text{m}/\text{m}$. For tunnelling-induced subsidence, the curvatures of the soil are much more important.

Al Heib et al. [2] conducted physical models on scaled specimen of 3D buildings to observe the transfer of soil strain to a structure. The models consisted of a foundation, represented by a polycarbonate base filled with small bags of lead powder (load) upon which a superstructure made from sugar or wooden blocks is placed, and which rests on a container with sand. A comparison is made against a flexible ‘foundation’ of silicon. The sand is deformed by means of a hydraulic jack. An initial test without the building also compares the greenfield situation. From their results, it can be observed that the ground horizontal displacement when the structure is present is 10% smaller than the greenfield displacement. Similarly, the stiff polycarbonate foundation shows only 15% of the greenfield displacement, while the flexible silicone foundation shows 31% of the horizontal displacements. They conclude: “The physical model simulated also a masonry structure. It appears to be a very useful tool for studying the soil-interaction phenomena. A stiff structure behaves like a cantilever beam and ground displacements transferred to the structure are smaller than for a flexible structure.”

In a similar study, Caudron et al. [3] used scaled physical models to reproduce tunnelling or underground cavity collapses and assess the behaviour of a moment-frame and masonry structure on an instrumented footing foundation. They investigated the effect of the building position along the subsidence trough. The structure at the edges of the subsidence, where the horizontal strain is tensile, displayed only 8% of the greenfield horizontal strain, while the building in the centre of the trough, subjected to compressive horizontal strains, acquired 9% of the strain.

Further, Dalgic et al. [4] also conducted physical tests but on a larger scale and on 2D façades. Here, a foundation beam is deformed underneath the scaled façade. While soil-structure interaction is thus not included, the angular distortion that appears on the structures is related to damage, and damage patterns can be used to calibrate numerical models. These are similar to the patterns presented in this study.

Liu and Xu [5] investigated the effects of surface horizontal strains on soil-building interactions from a theoretical perspective at the local scale. They explored the effect of several parameters, among which the friction between soil and foundation. They concluded that a larger friction angle will also

lead to more damage in the building; however, they contemplated large values of horizontal strain of at least 1000 $\mu\text{m/m}$. Nonetheless, they also observed that a longer foundation will lead to higher building stresses when subjected to horizontal soil strain. Similarly, the presence of transverse walls will also increase the transfer of strain. Yet, much of the transfer is due to the contact pressure at the sides of the foundations and can only occur with compressive horizontal strains.

Ritter et al. [6] conducted centrifuge models, where the self-weight of scale models can be magnified to match the effect of gravity on the real-scale situation. Ritter et al. [7] also discusses the soil-structure interaction from experiments where the situation of greenfield and building presence are compared. Here, the strains in the soil block are measured during the centrifuge tests mimicking tunnelling excavations. The tests reveal how the presence of a building severely reduces the strains that appear in the soil. For the longest, flexible buildings, they observed transfers of horizontal strain of up to 40% of the greenfield situation.

Finally, Ren et al. [8] conducted early computational explorations on how to predict subsidence and horizontal displacements and determine the area of influence based on the size and shape of a mining intrusion. Their computations were also compared against field measurements. Their results indicate an order of magnitude for the horizontal strains to expect. In most cases, the strains are higher than those investigated herein.

Additional studies by Giardina et al. [9] or Mair et al. [10] have also been consulted; these study the effects of tunnelling on buildings. The first concludes that modelling strategies must consider a no-tension interface between building and soil, while the latter emphasizes the importance of employing earth pressure balance shields and compensation grouting to prevent surface subsidence that affects buildings.

H.3 Method

A plane stress shallow-soil model is used to explore the influence of the surrounding soil on the transfer of strains to a building positioned atop the first soil layer; see Figure H.1. Five different horizontal strains can be distinguished: first, on the model without the building, the horizontal strain throughout the top soil layer would be fairly constant and is denoted ϵ_{GF} , the greenfield strain. This is the strain usually determined with geomechanical models and other calculation methods. The presence of a relatively stiff building, however, affects the local strain distribution. In an identical model, the strain at the base of the variable soil layer might differ slightly; this is identified as the applied horizontal strain, ϵ_A . Underneath the stiff foundation, the strain is identified as ϵ_F and, if the soil and building are fully connected, will be identical to the strain measured at the foundation, ϵ_M . In some models, the non-linear behaviour of the soil-foundation interface is explored and ϵ_F and ϵ_M will differ. Finally, for completeness, the strain at the top of the building is also registered, ϵ_T .

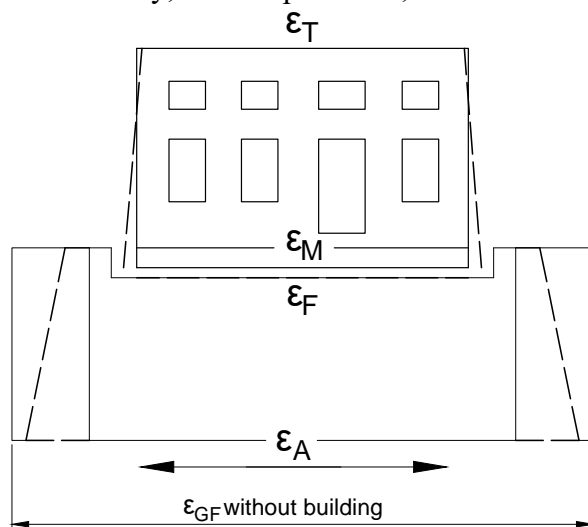


Figure H.1. Scheme of horizontal strains ϵ at various locations close to the structure.

In this preliminary computational study, for compatibility with the soil model, the building is replaced by a block of 5x4 m, with a thickness of 0.21 m. The top soil layer is modelled 2 m deep and 11 m long; see Figure H.2. The building is linear-elastic with a Young's Modulus of 5 GPa; this means that if the soil has a Young's Modulus of 400 MPa, the building would be 2.6 times stiffer than the soil.

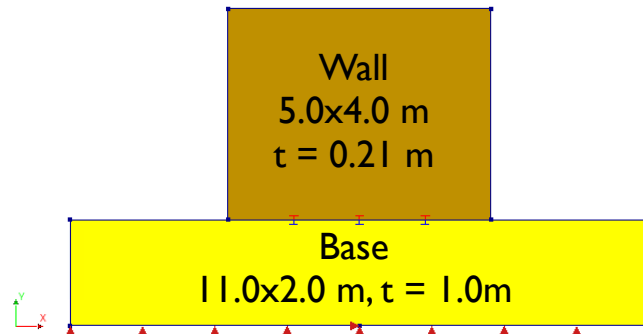


Figure H.2. Scheme of a building on top of a soil layer.

The horizontal strain is prescribed to the soil block. This recreates the effect of enforcing a displacement on both lateral edges of the soil block such that a uniform strain appears, as is the case of the greenfield scenario. In the case with the building, the strain distribution is not uniform and varies around the foundation of the building.

Six model variations are contemplated as the result of 2 parameters: the stiffness of the soil block and the type of interface between the soil and building. For the latter, a slipping and non-slipping interface are compared, while for the soil, a stiff sand, a flexible peat, and an unrealistic steel-like soil, are explored. The slipping interface considers Coulomb friction without cohesion; the friction coefficient is consistent with the type of soil.

H.4 Results

The results of the six models in terms of horizontal strain at various points in the model are summarised in Table H.1. A large value of strain was applied; however, for the linear-elastic model, the actual value is irrelevant. For the models with a slip soil-foundation interface, the large strain is representative of the large values required for slip to occur. Conversely, the models without slip are characteristic of the behaviour when horizontal strain values are small.

For these models, the softest soil (clay) deforms because of the structure and thus the presence of the structure can be inferred at the depth of 2 metres. The most restrictive structure, without slip, leads to the largest effect on the soil. However, the strain measured at the structure itself is in the order of 6%. When the soil is relatively stiff, such as a densely-packed sand, the transfer is about 35% but, if slip is possible, then only about 7% is again transferred. If the soil is infinitely stiff (or the structure is very flexible) however, then most of the strain is transferred. Nonetheless, if slip can occur, then the foundation is likely to slip in such a way that only a tiny amount of strain is transferred (about 1%). It follows that in situations where the soil is even softer, such as peat or organic soil, the transfer will be reduced; for this reason, very soft soils have not been included in this preliminary model and relatively high E moduli have been employed for the other soil types.

Table H.1. Results of the exploratory coupled soil-structure models.
Nominal applied strain: 10^{-2} or 1 cm/m or 10^4 000 $\mu\text{m/m}$ (100%).

Soil	Young's Modulus MPa	ϵ_{GF} Nominal horizontal strain applied (tension)	Interface Type	ϵ_s Depth: 2 m	ϵ_r Right underneath foundation	ϵ_m Measured at Foundation
Soft	45	100	Non-slip	72.26	6.7	
			Slip	88.10	17.32	6.09
Stiff	395		Non-slip	86.29	35.2	
			Slip	105.98	95.81	5.51
Infinitely stiff	200000		Non-slip	99.95	99.5	
			Slip	99.99	100.04	1.19

As an example, Figure H.3 shows the case of the soft soil with a non-slipping interface. One can observe that underneath the structure, the strain in the soil is reduced. At the centre, this effect is greatest. Moreover, the restraint provided by the structure atop causes bending in the soil block which explains the results higher than the applied strain in table H.1. At a larger depth, this effect diminishes so that at the edges of the soil block, the horizontal strain is constant.

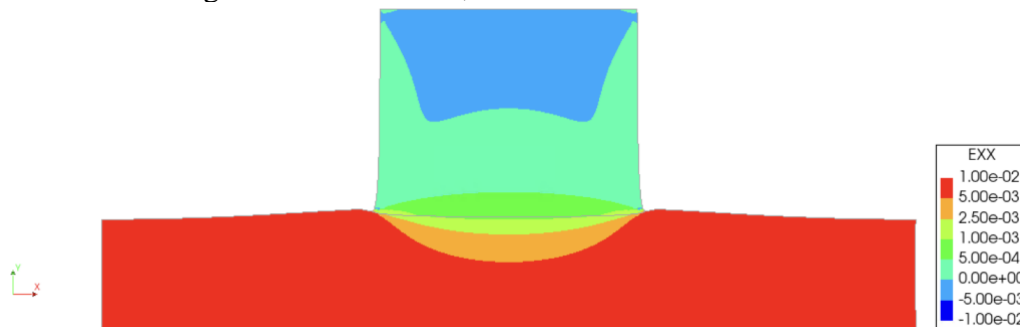


Figure H.3. Structure with non-slip interface on soft soil.

H.5 Discussion

The coupled model serves to investigate not only the effect of the soil deformation on the building, but also the effect of the building on the soil. It is clear that a structure, in most cases much stiffer than the upper layers of the soil, will provide a constraint and limit the deformation in the soil and thus the deformations to which the building itself is subjected to. Consequently, any effect that reduces the stiffness of the structure, or increases the stiffness of the soil, will lead to higher horizontal strains in the structure; it is expected that the same trend will occur for curvatures, but this has not been explored in this appendix. It follows, that longer buildings (with a large L/H ratio) will be more flexible from the perspective of the soil. Similarly, buildings with many openings, or structures with existing cracks, will present a more flexible constraint and experience higher strains. Moreover, the behaviour of soil is non-linear; at larger strains, most soils become more flexible. Ultimately, it is important to characterise the stiffness ratio between the soil and the building, then, regardless of the characteristics of the building (with openings or as a solid wall depicted in this section), the transfer of strains can be quantified for any given ratio; see [7].

These effects have not been looked into in this explorative appendix so they cannot be quantified; they remain as limitations of the employed approach.

H.6 Conclusions

This exploratory coupled model, where a constant strain is applied to a soil block, reproduces the observations from literature: the building affects the strain distribution in the soil depending on their stiffness relationship. A stiff building on a flexible soil will reduce the strains in the soil close to the building. Consequently, only a small amount of the horizontal strains expected in the greenfield situation will be measurable on a structure. This is particularly the case for larger values of strain, where (partial) slip between soil and foundation could be expected. On a stiff soil, like densely packed sand, a masonry façade is shown to display about 35% of the horizontal strain; this is also found in literature for both numerical simulations and scaled experimental tests.

While additional situations may be explored, such as the case of flexible or pre-damaged buildings, non-linear soil behaviour, or combinations with soil curvatures in addition to horizontal strain, these models show that a transfer of 50% will be a very conservative assumption for the case of most Dutch buildings with shallow foundations. This is valid for effects of deep subsidence where small horizontal strains, in the order of 10 to 30 $\mu\text{m}/\text{m}$, are dominant in respect to negligible curvatures, in the order of 100 nrad/m . The situation for larger strains or in combination with larger curvatures, has not been explored herein.

H.7 References

1. Potts and Addenbrooke (1997)
D.M. Potts DM, T.I Addenbrooke (1997). A structure's influence on tunnelling-induced ground movements. *Proceedings of the Institution of Civil Engineers-Geotechnical Engineering*. 1997;125:109-25.
2. Al Heib et al. (2013)
M. Al Heib, H.L. Nghiem, Fabrice, Emeriault (2013). Understanding Sinkhole Consequences on Masonry Structures Using Large Small-Scale Physical Modeling. *International Conference on Case Histories in Geotechnical Engineering*, 12
3. Caudron et al. (2008)
M. Caudron, M. Al Heib, F. Emeriault (2008). Collapses of underground cavities and soil-structure interactions - influences of the position of the structure relative to the cavity. *International Association for Computer Methods and Advances in Geomechanics (IACMAG)*.
4. Dalgic et al. (2023)
K.D. Dalgic, B. Gulen, Y. Liu, S. Acikgoz, H. Burd, M. Marasli, A. Ilki (2023). Masonry buildings subjected to settlements: Half-scale testing, detailed measurements, and insights into behaviour. *Engineering Structures* 278 (2023) 115233. doi.org/10.1016/j.engstruct.2022.115233
5. Liu & Xu (2022)
X. Liu, L. Xu (2022). Soil-Building Interaction under Surface Horizontal Strain Induced by Underground Mining. *Advances in Civil Engineering Volume 2022, Article ID 2425936*. doi.org/10.1155/2022/2425936
6. Ritter et al. (2020)
S. Ritter, G. Giardina, A. Franza, M.J. DeJong (2020). Building Deformation Caused by Tunneling: Centrifuge Modeling. *Journal of Geotechnical and Geoenvironmental Engineering*. 10.1061/%28ASCE%29GT.1943-5606.0002223
7. Ritter et al. (2017)
S. Ritter, G. Giardina, M. J. DeJong and R. J. Mair (2017). Influence of building characteristics on tunnelling-induced ground movements. *Géotechnique* 67, No. 10, 926–937 doi.org/10.1680/jgeot.SIP17.P.138
8. Giardina et al. (2015)
Giardina, G., DeJong, M. J. & Mair, R. J. (2015). Interaction between surface structures and tunnelling in sand: centrifuge and computational modelling. *Tunn. Undergr. Space Technol.* 50, 465–478, doi.org/10.1016/j.tust.2015.07.016.
9. Ren et al. (1987)
G. Ren, D.J. Reddish, B.N. Whittaker (1987). Mining Subsidence and Displacement Prediction Using Influence Function Methods. *Mining Science and Technology*, 5 (1987) 89-104. doi
10. Mair and Taylor (1997)
Mair, R. J. & Taylor, R. N. (1997). Theme lecture: bored tunneling in the urban environment. In *Proceedings of the 14th international conference on soil mechanics and foundation engineering, Hamburg, 6–12 September 1997*, pp. 2353–2385. Rotterdam, the Netherlands: Balkema.

Appendix I: Vulnerable features - additional modelling check of stiff masonry, thin foundations, and no transversal walls

I.1 Introduction

In section 3 of the main text, the model set with the basic features is explored. The basic set includes three façade geometries, a masonry foundation, standard NPR 9998 material, and the maximum soil strains are fully transferred to the foundation (100%). In appendixes B to F, varying features are further explored, such as the effect of cyclic loading or existing damage in the masonry buildings; see also appendix G for an overview of the scenarios. In this appendix, the effects of other potentially-vulnerable features is investigated. Three features, and their combination, are included: a reduced foundation, no connection to transversal walls, and a very stiff masonry.

I.2 Method

The basic model cases treated in Chapter 3 include:

- Quadratic plane stress elements meshed at 200 mm with the non-linear Engineering Masonry Model; see material properties in Appendix A.
- A foundation with identical elements as the façades, only varying in thickness.
- A connection with transversal walls consisting of vertical, elastic, linear beam elements with a Young's modulus of 1/3 of the wall material and a section equal to one thickness.
- Gravity load and overburden depending on the façade geometry and configuration.
- Direct, 100% transfer or application of the soil deformation (horizontal strain and curvature) at the base of the foundation.
- This deformation is applied over 20 steps using a Quasi-Newton secant, increment-iterative method satisfying all displacement, force, and energy norms with a tolerance of 1%, 1%, and 0.01% respectively.
- Second order effects are also considered using the Total Lagrange geometrical non-linearity.

For additional details, the reader is referred to Chapter 3 and its corresponding appendixes.

These models of the three façades (A, B, and C) are modified herein to consider:

- No connection to transversal walls. The main set of models includes beam elements on each side to mimic the contribution of the walls transversal to the façades. These beam elements are only a few bricks thick and were introduced following studies that determined that including the transversal walls led to more accurate model results. For these models, the connection to transversal walls is fully removed.
- Stiff masonry. For the standard models, values suggested by the Dutch guideline, NPR 9998, are used to characterise the masonry material. In appendix D, additional scenarios with reduced strength are investigated. For the new models, a stiffer masonry is considered since it might be more vulnerable to applied soil deformations (when applied directly at 100%). The strength is kept at standard values but the Young's moduli are enlarged by a factor of 2. From 5 GPa and 2.5 GPa for vertical and horizontal Young's moduli, the values are set to 10 GPa and 5 GPa, respectively.
- A thinner foundation. The masonry foundation of 60 x 60 cm is made less stiff by reducing its width to 40 cm. As in the standard case, the unreinforced masonry foundation is assigned the same material properties as the rest of the façade, which also makes it more vulnerable.
- Finally, a model set displaying all three aforementioned features is also studied.

I.3 Results

In Table I.1. the results are shown in terms of the amplification factor required to reach visible damage measured by a Ψ value of 1. This means that soil strains are magnified until damage becomes visible. On the first row, the table also shows which amplification factors were needed for the main model set. As expected, the vulnerable features lead to a reduction of the factor for virtually all cases. In the case of sagging settlement shapes however, the disconnection from transversal walls can be beneficial as illustrated by façades B and C. The thinner foundation results in little reduction. In contrast, the much stiffer façades see magnification factors reduced by almost 40%. When all three features are combined in a single model, the effects do not add up linearly, but result instead in a slight additional reduction over the worst case. The lowest amplification factor reaches a value of 2.3 for the hogging case of façade A. Hogging occurs at two locations: for heave at the centre of the gas field in Norg when the gas reservoir is fully pumped up, and for subsidence, when the gas field is empty at the perimeter of the subsidence trough. Heave is associated with the largest soil strains at the centre including hogging curvatures and dominant horizontal strains in tension. The magnification factor refers to this situation, as the second case at the perimeter of the trough displays much lower strains. Façade A, shown in Figure I.1, is a long façade, thus more susceptible to soil deformations, with small windows where cracks are localised, especially due to the very stiff masonry assumed.

Table I.1. Results of the four model sets investigated. Load amplification factors to reach Psi=1.

Variation	Façade A		Façade B		Façade C	
	Sagging	Hogging	Sagging	Hogging	Sagging	Hogging
Original (Chapter 3)	10.85	5.50	6.90	6.00	12.50	7.00
Effect: No transversal walls	10.40	3.00	7.20	4.20	13.00	5.00
Effect: Double E masonry	7.30	3.50	4.70	3.80	8.80	4.40
Effect: Reduced foundation thickness t	10.70	5.30	6.70	6.00	12.10	6.90
A model with all three effects combined	6.70	2.30	5.00	3.10	8.60	3.70

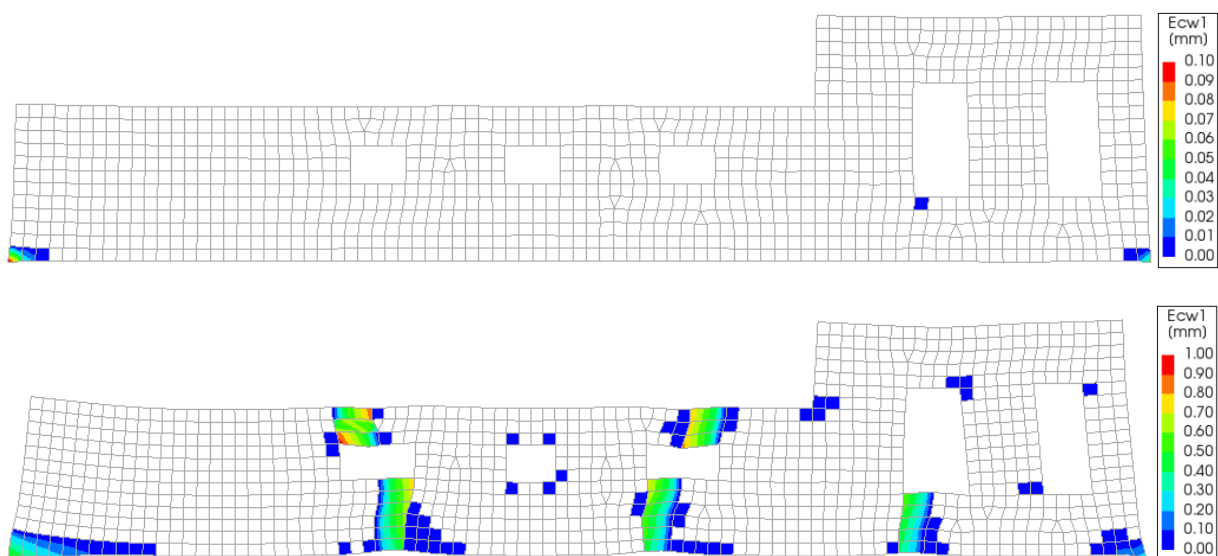


Figure I.1. Illustration of visible crack damage from the FEM model for the case of hogging of façade A for Psi=1 (top, load factor of 2.3, worst situation of Table I.1) and Psi=2.5 (bottom, load factor of 6.0) for the combination of all three vulnerable features.

An important case is highlighted in Figure I.1; it also depicts the case of wider cracks that go through the unreinforced foundation for the situation of $\Psi=2.5$. The exaggerated deformed shape makes the applied horizontal strains visible. As an important note, the removal of the transversal walls leads to delamination cracks at the corners of the façade, (one of the reasons why including them results in more accurate models); these delamination cracks are read as damage but in reality, they would likely not be visible. This means that the values output by these models are conservative in the sense that they overestimate damage. Moreover, the figure also depicts the situation for $\Psi=2.5$ associated to cracks of up to 1 mm in width. These cracks are more visible and correspond to a less strict threshold for light damage. More importantly, the load factor required to cause this damage is significantly higher (about 2.5 times larger) than the just-visible cracks of $\Psi=1$. While the case of $\Psi=2.5$ is not included in Table I.1 and is not the focus of this appendix, it is presented to emphasize the strictness of the $\Psi=1.0$ criterion.

Finally, in these models, a 100% transfer of horizontal strains is applied. The transversal walls, representing additional embedment, would increase the strain transfer if the 100% was not enforced. Hence, comparing models with and without transversal walls, when strain transfer is determined from a coupled soil model (Appendix H) or from a soil-structure interface, would likely show that the cases with transversal walls become more damaged; the damage picture is also more realistic.

I.4 Conclusions

This appendix summarises the brief study into the effect of three vulnerable features, namely: the disconnection of façades from transversal walls which may provide some beneficial constraint, the reduction of width of unreinforced masonry foundations to account for extremely flexible foundations, and the doubling of masonry stiffness to observe the cases of façades sensitive to soil deformations. The results from the FEM models show that indeed, all three effects, independently and in combination, lead to increased vulnerability; however, a margin remains, meaning that soil deformations, fully applied to the base of the models (100% transfer) need to be amplified to reach visible damage ($\Psi=1.0$). In comparison to the original models, a reduction of the amplification factor by 40% to 60% is observed. These effects are further employed in Appendix G, Table G.1.

Appendix G: Qualitative probabilistic description of worst-case scenarios

G.1 Introduction

In this report, the method of worst-case scenarios has been employed. This approach is valid when the full extent of the variability of a hazard, or more importantly, the variability of the response, cannot be comprehensively characterised. Indeed, in the case of building damage due to deep subsidence, three aspects need to be fully characterised for the probability of damage to be accurately calculated:

- The behaviour of the ground surface in response to deep subsidence due to gas storage and extraction,
- The damage initiation and propagation in buildings in response to soil deformations,
- The interaction between the behaviour of a building and the deformations of the soil.

Furthermore, the variability of these three aspects needs also to be understood. So, building typologies, configurations, materials and conditions, together with soil properties, stratigraphy, water tables and local phenomena, all must be thoroughly discerned. In the efforts to evaluate the safety of Dutch buildings in regard to earthquake vibrations, information about the types of buildings present is reasonably extensive. Also, soil properties, within a micro-zonation area, are well defined. Nonetheless, the structural typologies defined to assess the response of buildings against dynamic soil movements and dynamic lateral loads do not necessarily correspond to typologies that categorise the response of buildings when subjected to static settlement-type soil deformations. For example, whether low buildings are founded on shallow or deep foundations is not relevant when assessing their seismic vulnerability, but this would be extremely important when evaluating their response towards ground deformations. Similarly, the composition of the soil has been established for its effect on dynamic amplification, and sometimes also risk of compaction, but how the different types of soil interact with a building when deformations originate from the deep soil, has not been determined. Moreover, soil-structure effects such as the transfer of horizontal displacements between the lower soil layers and the foundations of buildings have not been extensively studied, especially for small deformations potentially linked with light damage. Consequently, in the state of the art to evaluate building response towards soil deformations, knowledge is still missing both for buildings in general and for the situation in the Netherlands. In this light, a fully probabilistic characterisation would be incomplete and could only be approximated.

A worst-case approach is especially valid when the loads and the response are far from each other. Comparing damage thresholds found in literature with preliminary geomechanical models of the ground surface response under deep subsidence, revealed large margins even for light damage related to the serviceability state of buildings. A fully probabilistic approach, would thus correspond to an unnecessarily large effort to verify these margins. Worst-case analyses are here for an efficient tool. Therefore, modelling checks were conducted to establish the actual margins for specific situations of vulnerable Dutch buildings. The models for these checks were fabricated using vulnerable, conservative, but realistic features of buildings and soil-foundation interactions. This appendix details the choices made regarding the Dutch building stock and their expected behaviour. In this context, a qualitative description of the likelihood of each scenario and its qualitative probability of damage is given in this appendix; this comprises the bulk of the study following the worst-case methodology employed in this report. In subsequent appendix J, a probabilistic approximation is further explored and compared to the outcome of the worst-case scenarios.

G.2 Method

G.2.1. Summary of Dutch buildings

The models employed in this study have been formulated with knowledge of vulnerable Dutch buildings. Several sources were consulted when envisioning these buildings and much is based on in-house expertise [1,2,3]. Three main sources must be highlighted: First, a case-based study [4] and additional case-based reports [5] constitute a healthy pool of exhaustive documents on actual masonry houses and the sort of damage that they display. In particular, Van Staalduinen et.al [4] looked at the context of houses and examined multiple potential causes for damage. Second, the exposure database elaborated by Arup [6], as part of the hazard and risk analyses (HRA), categorises buildings into seismic-oriented typologies and sub-typologies; the material type and structural system of walls and floors is well documented. Third, the BAG and expanded 3D-BAG database [7] contains extensive geometry information about Dutch buildings and some information about usage and year of construction. Figure G.1 details the year of construction within the 20th century for existing buildings in the Netherlands. It can be observed that there is a clear distinction between buildings before and after the second world war. The 3D-bag database also contains geometry information which can be used to obtain statistics about the size and geometry of walls. Figure G.2 presents such an example.

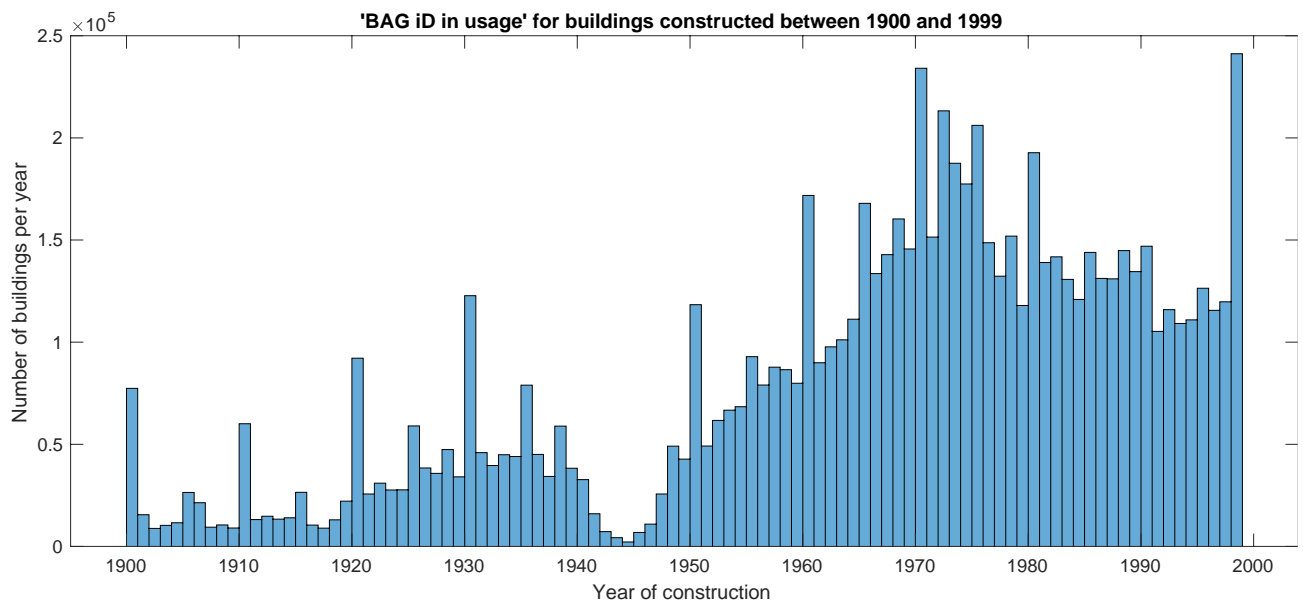


Figure G.1. Histogram of the year of construction for buildings in the Netherlands available in the BAG 3D database.

The analysis into the shape of masonry walls in houses revealed that about 70% of walls are rectangles with an upper flat edge, while the remaining correspond to gable walls of various shapes. This is reasonable since many houses with gable roofs also have at least two rectangular side walls or, even if the roof is sloped, it can be built atop rectangular walls. Furthermore, a recent study into the effect of soil-induced curvature because of local soil effects [8], revealed that longer façades, with a length greater than the height of the wall, are more vulnerable than slender walls in the context of soil deformations. Indeed, also in literature about horizontal soil strains, longer walls are found to be more vulnerable since a constant strain results in a larger displacement for a larger length. In contrast, slender walls are more vulnerable against seismic loads.

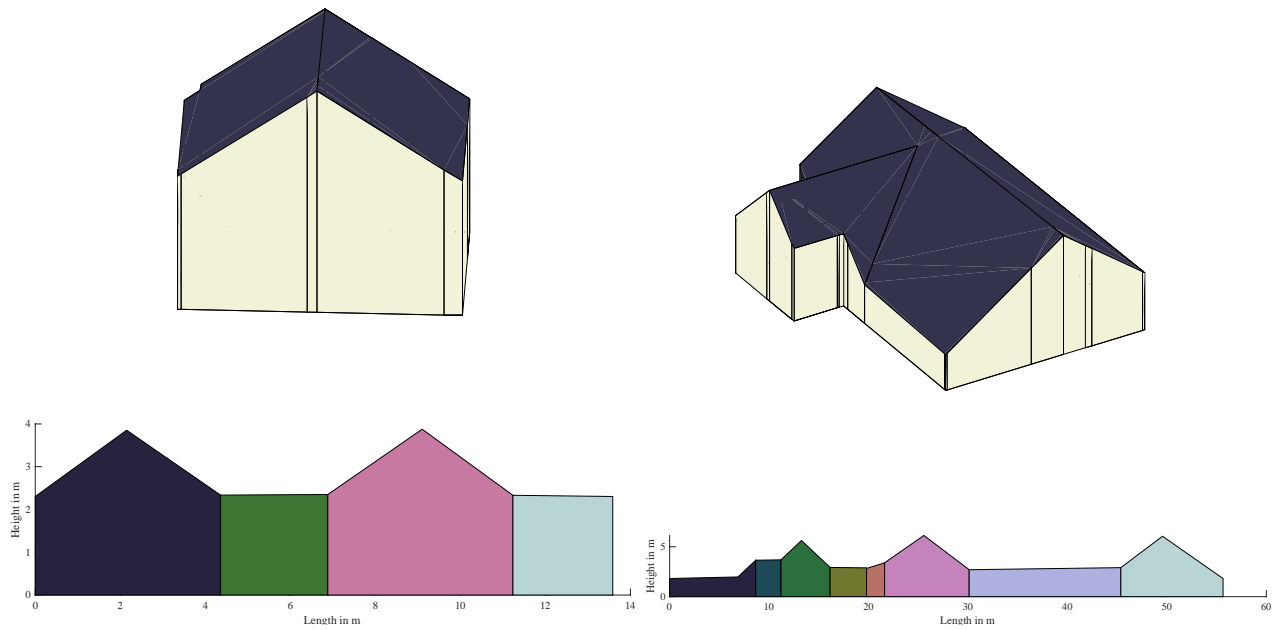


Figure G.2. Two examples of the unfolded geometry of two buildings showing the individual walls' length and height for the outer walls.

Consequently, for the modelling checks we have selected three façade geometries (Chapter 3), see two examples in Figure G.3, with vulnerable features such as:

- Many windows that make the façade more flexible and thus more likely to follow the soil deformations and become damaged. Also, windows create spots for concentration of stresses which further fosters crack formation and damage.
- A length/over ratio larger than 1, and even much larger, since longer façades are more vulnerable to soil deformations.
- Flat upper edges since the majority of walls are rectangular and this also contributes to a higher length/height ratio.

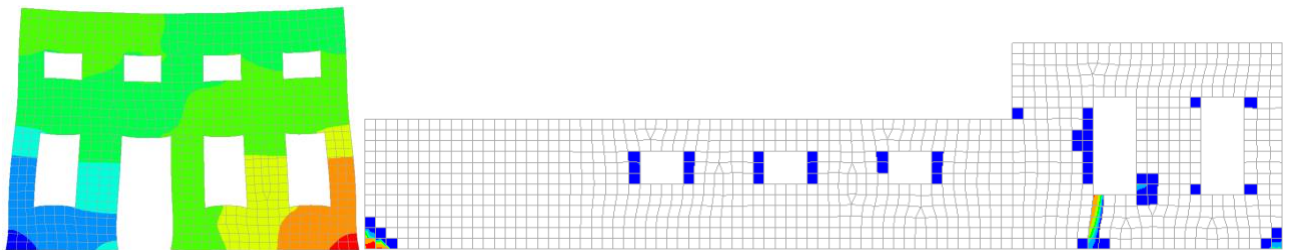


Figure G.3. Two examples of façades from this study. Left, a short façade showing exaggerated displacements; right, a long façade displaying the locations of cracks.



Figure G.4. Monumental farmhouse from 1873. Typical example of a vulnerable masonry structure [9].

G.2.2. Scenarios

Several scenarios have been analysed pertaining to the permutation of certain features or properties of the building, its context, the soil, or the hazard. These are hereafter denoted as scenario features and are detailed next:

1. Foundation

First in determining whether buildings become damaged is their foundation. An infinitely stiff and strong foundation will prevent any soil deformations from being transferred to the superstructure. Of course, such a foundation system doesn't exist but in comparison to the soil and to the building, reinforced concrete strip or beam foundations can be both very stiff and very strong. Most buildings after 1975 have such foundations. It is the older buildings, with unreinforced foundations, and especially with masonry foundations, that are most susceptible to soil deformations. These pre-1945 masonry foundations are essentially wall enlargements, usually constructed with stronger bricks and thicker mortar and becoming wider at the base. For the models, a simplified wall enlargement, rectangular in shape and with the same (weaker masonry) as the rest of the structure becomes the base case for all the scenarios with vulnerable buildings.

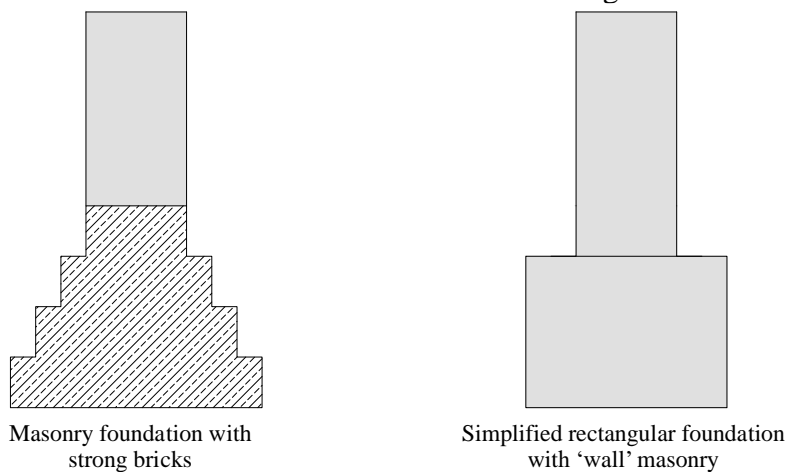


Figure G.5. Illustration of simplified foundation. Dimensions are only schematic.

2. Masonry material

The material of the building is paramount when determining the building strength and especially, its damage at light or serviceability states corresponding to narrow cracks in the order of 0.1 to 5 mm in width. In Dutch houses, several materials are employed but unreinforced masonry is most popular and the most vulnerable. Within masonry buildings however, different types of masonry can be recognised, some more vulnerable than others. Older structures sport fired-clay brick masonry with lime-based mortar while more recent buildings employed calcium-silicate brick masonry with cement-based mortars.

The NPR 9998, the Dutch guideline for design and analysis of buildings, proposes mean material values for the analysis of existing structures. These values originate from various sources: (1) the committee of TGB Steen, partially responsible for maintaining construction standards in the Netherlands; (2) CUR reports, especially on the effects of tunnelling during the construction of the North-South metro line in Amsterdam; and (3), an extensive characterisation campaign of existing Dutch masonry conducted at the TU Delft in the period 2014-2020. It follows that clay-brick masonry from before 1945 is slightly more flexible than masonry post 1945, but is much weaker. In general, stiffer structures will develop higher stresses under imposed deformations; if they are also weaker, they will become damaged earlier. For the worst-case analyses, we conceived masonry with identical stiffness as the pre-1945 masonry proposed by the NPR but reduced its strength even further, by 30%. Weaker structures are also expected to be more flexible, so this combination represents a conservative situation.

It must also be said that more flexible structures will also allow a larger deformation since the soil-structure relationship plays a role. However, for some scenarios, we assumed a 100% transfer of the soil deformations, so it is the stiffer structures that become most vulnerable; see next subsection.

A final point about the masonry typology is that of the situation at the wall corners. In most older buildings, walls are fully interlocked at the corners, with courses of bricks laid on both the analysed walls and its transversal walls. In the models, we have assumed transversal walls of one brick length at both of the walls' edges. This leads to a more accurate behaviour when replicating damage patterns of existing structures without including too much additional strength since the wall edges are only one brick in thickness. Newer buildings, with calcium-silicate elements for instance, show continuous joints without interlocking, sewed together with wall ties. In many cases, outer veneers also present dilation joints. In appendix I, the influence of these transversal walls is briefly explored.

3. Transfer of soil deformations

Deep subsidence causes horizontal deformations which originate hundreds of meters under the ground surface. Contrary to the vertical deformations due to deep subsidence, these horizontal deformations do exist but cannot be adequately measured at the surface. Yet, the soil near the surface is comparatively soft and flexible so it follows the deformations from the layers underneath. In the example presented in Figure G.5, two extremes are presented: on the left, one where the building or façade is infinitely stiff, and on the centre, one where the building is as flexible as the soil. Assuming that the soil and the building are fully coupled, the stiff façade restrains the upper edge of the top flexible layer from following the horizontal deformation that comes from the stiffer lower soil layers. The scenario in the centre would also correspond to the situation where no building is present. The right illustration depicts the situation when the soil and building are decoupled (due top slip). An analysis from literature reveals that when a building is present, the horizontal strain that is transferred to the building is about 30% (see later appendix H) of that which is computed at the surface for the case where no building is present. However, if the building is stiff and the top soil layer is flexible, this transfer will decrease. In the Netherlands, masonry buildings are relatively stiff and soils are relatively soft. When, in addition to a horizontal strain, a curvature or bending deformation of the soil is applied, determining the transfer of soil deformations becomes more complex. We assume a 50% transfer on the conservative side and have also explored the extremely conservative case of 100%

transfer. Nonetheless, soil-structure interaction for soil-induced deformations requires significant further study.

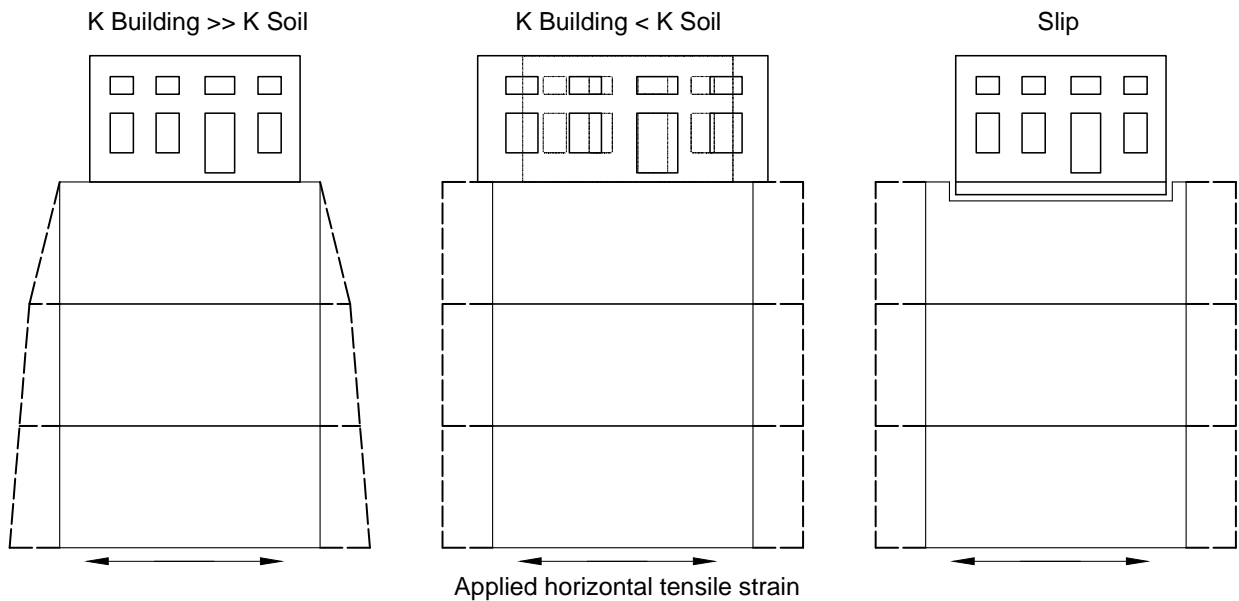


Figure G.5. Example of soil-structure interaction for a uniform horizontal strain maximum at the base of the stack. Left, flexible upper soil layer and stiff façade; centre, façade as flexible as the soil layers; and right, slip or sliding between the soil and the building. K refers to “stiffness”.

It must also be emphasized that the focus of this study is solely on the direct effects of deep subsidence. This large-scale effect considers mostly horizontal strains that are associated with very small curvatures due to the fact that the deformations occur over large areas. Other actions, such as tunnelling, or local soil drivers, like swelling of expansive clays, are perhaps better characterised by larger curvatures and negligible horizontal strains. These are not investigated herein except as potential causes for pre-existing damage (see point 6).

4. Location

Depending on the location of the building, it will be subjected to a different combination of soil deformations. Far from the area subjected to deep subsidence, soil deformations due to direct deep subsidence will be zero, while at the centre, one can expect the highest horizontal strain and curvature deformations. The area at the centre is much smaller than the perimeters; thus, fewer buildings are subjected to the highest soil demands computed. In a probabilistic study, one may determine the chance of any one building being subjected to the highest deformations considering the fact that few buildings will be in that zone. For the worst-case scenarios, we have looked at the values in the worst locations. Figure G.6. illustrates these combinations.

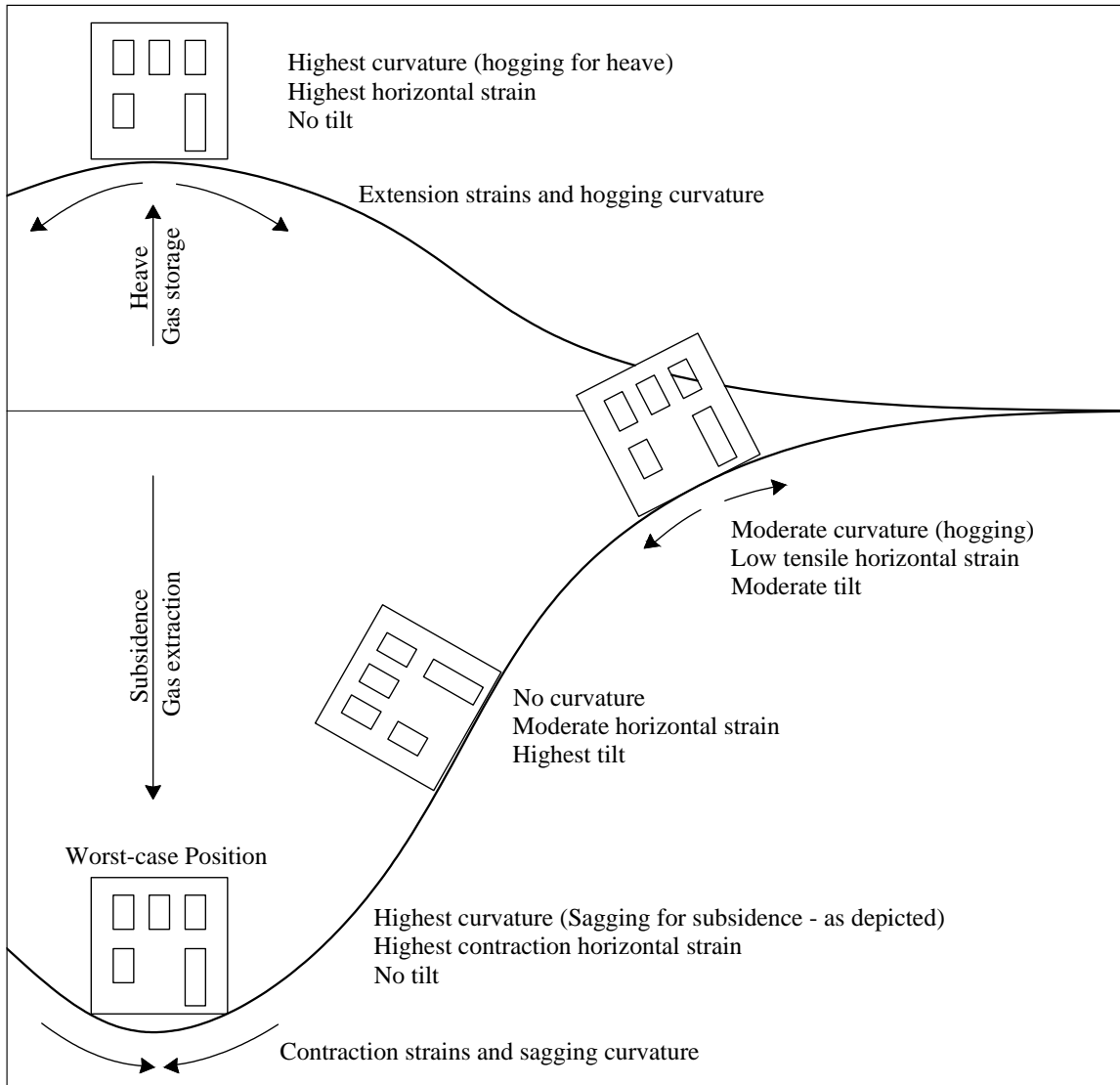


Figure G.6. Relationship between building location and strains.

5. Damage criterion

Visible damage in masonry buildings starts when cracks reach a width of about 0.1 mm. Narrower cracks on an (unfinished) masonry wall are just not visible to the naked eye. These cracks, however, have no influence on the safety of the structure nor its durability or performance. Many damage scales consider light damage to comprise cracks of 0.5 mm or wider, some begin even at a crack width of 1 mm, since repair of narrower cracks is straightforward or unwarranted in many cases. We have looked at two thresholds: one observing cracks of 1-2 mm in width, corresponding to the upper threshold of light damage, and another with a very strict criterion of 0.1 mm in width, linked to the incipient visible damage. The latter, strict scenario is used to evaluate damage in the models of the worst cases.

6. Additional Effects

There are some effects which could worsen the situation of particular buildings making them more vulnerable to deep-subsidence-induced damage. We have identified and explored two such effects, namely: existing damage and cyclic settlement movements.

Existing damage, consisting of fine, visible cracks, caused by thermal-hygral movements, settlements due to local phenomena, or traffic vibrations, will make the buildings more flexible. The increased flexibility also means that a higher percentage of the soil strains will be transferred to the structure. Moreover, existing cracks present a location where new strains can be concentrated, further aggravating the cracks in both width and length. Existing, yet invisible cracks, require smaller displacements before they can become noticeable thus increasing the apparent vulnerability of the masonry. Furthermore, already-visible cracks may noticeably widen. We have explored the effect of pre-existing damage regarding the apparent initiation and propagation of light damage; see Appendix F.

In the area of Norg, the gas field is also used as storage, with gas being pumped in during the summer and extracted in the winter. This leads to seasonal movements of the ground surface, or in other words, to cyclic subsidence-induced strains. Cyclic effects can be detrimental to materials leading to degradation and aggravation of existing cracks; over time leading to an accumulation of damage. In our analyses of worst cases, we have looked at the effect of cyclic movements on undamaged and pre-damaged masonry. For more details about cyclic effects, see Appendix C.

G.2.3 Strains and curvatures due to deep subsidence

First, a brief description about the strains and curvatures determined by the geomechanical model evaluated by TNO must be worded [10]. The model has been used to determine soil deformation values due to deep subsidence based on the gas pressures in the Norg and Groningen reservoirs. Here, for the worst year of 1995, the model computes a horizontal strain of $29 \mu\text{m/m}$, and for the regular years, the horizontal strain is $22 \mu\text{m/m}$ and is associated with a curvature in terms on angular distortion of $1.8 \cdot 10^{-8} \text{ rad/m}$. These are horizontal strains for subsidence cases which are linked with compressive strains, less damaging to buildings than tensile strains that would appear at the perimeters of the region or in the cause of heave caused by gas injection and storage. In this case, values reach $4.2 \mu\text{m/m}$ in tension and $2 \cdot 10^{-9} \text{ rad/m}$ as associated curvature. However, tensile strains also appear at the perimeter of the subsidence trough and reach higher values of up to $10 \mu\text{m/m}$; see Tables 4 and 5 in [10].

For the case of the Groningen field, recent reservoir pressure distributions, combined with a layered soil model, lead to the highest values [10]. More importantly, in the case of Groningen, tensile horizontal strains are estimated to be comparatively larger than in Norg and these tensile strains are typically more damaging to buildings.

In literature, the thresholds for damage are $200 \mu\text{m/m}$ and $1/2400 \text{ rad/m}$, or a combination thereof measured at the building, as presented in [11] adapted from Son and Cording [12]. This means that the soil distortions need first to be transferred to the buildings. The curvature from the deep subsidence phenomenon is very small and the horizontal strain dominates. For other types of settlement causes not contemplated in this study, like peat oxidation, horizontal strains are negligible, and curvatures dominate. In reference to the preliminary values of $11.4 \mu\text{m/m}$ and $8.6 \cdot 10^{-8} \text{ rad/m}$, modelling checks have been made (see Chapter 3). Note that the strain/curvature values for heave and subsidence differ; the values for subsidence are higher. Additional scenarios explored by TNO, where soil heterogeneity and a finer grid are modelled, result in values of 29 up to $34 \mu\text{m/m}$ of compressive horizontal strains and $10 \mu\text{m/m}$ tensile horizontal strains [10]. Buildings are most susceptible to the heave situation that causes hogging and tensile strains; see also Figure G.6.

G.3 Results

The previous section lists several categories and their context and explains the reasoning behind the choice of vulnerable situations. In this section, we attempt to associate a qualitative or descriptive probability to these vulnerable situations. We also detail the combination or accumulation of worst-case choices and their compound probability. Finally, we estimate the qualitative probability of failure for each of these worst cases based on the relationship between their critical thresholds and the actual values of soil strain and curvature induced by direct deep subsidence from the Norg and Groningen gas fields (see section G.2.2).

Table G.1 summarises various features or effects explored within the main report and its multiple appendixes. Their effect (or sensitivity) compared to the main case (see chapter 3) is expressed as a percentage. For example, a thinner foundation will reduce the threshold, or allowable horizontal strain at which damage appears, by up to 4% while a reinforced foundation will increase this critical value by up to 25%. It must be emphasised that many effects listed in table G.1 are considered with the direct transfer of horizontal strains. The stiffer masonry is seen to be more vulnerable, but if soil-structure interaction is considered, the stiffer material would reduce the transferred strains and thus be less vulnerable. Similarly, the reinforced foundations show a (relatively) small beneficial effect, yet the effect could be much larger if the soil demands are not enforced directly; appendix H explores these effects.

Table G.1. Approximate influence rates for various effects investigated.
 Negative values indicate beneficial effects.

Feature	Influence	Comment
Thinner foundation	1 to 4%	Not influential
Stiff masonry	30 to 40%	Strength not changed
Weak masonry	15 to 33%	Stiffness not changed
No transversal walls	-4 to 45%	Can be important
Existing damage	up to 50%	Depends on initial damage
Cyclic effects	≈ 20%	If strain values are close to critical, otherwise no effect
Reinforced foundation	-12 to -25%	With imposed 100% transfer
Common Location (not trough maxima)	- 50 to -100%	Applied strains are reduced
Strain transfer 50%	-80 to -110%	Applied strains are reduced
End of light damage	- 25 to -70%	Cracks of approx. 2 mm width
Slip interface	0 to -800 %	Between foundation and soil

A combination of models explored throughout the report and the effect of the features listed in Table G.1, and previously discussed in section G.2.1, are used to envision six scenarios, A to F. In Table G.2 next, these scenarios are listed in order of importance: for a worst-case approach, the common situations, A and B, are not so relevant as investigating the potential for damage of the vulnerable situations. Consequently, the first scenario considered is C, selected as the basic case in this study and treated in the main text (see Chapter 3). To remain on the very conservative side, the soil deformations are directly and fully (100%) applied at the base of a model with old masonry properties and damage is assessed with a strict criterion that qualifies damage already at narrow cracks of 0.1 mm in width. Next, scenario D, observes a similar case but better represents how soil deformations are transferred to the buildings. Then, scenario E includes additional effects such as existing pre-damage and damage accumulation due to cyclic effects. Other scenarios are listed on the bottom rows and complete Table G.3, where results are gathered.

Table G.2. Summary of the scenarios contemplated in Table G.3 by order of importance, where the scenarios most deserving of being studied are listed first.

Scenario	Name	Treated	Description	Building description
C	Main worst case investigated	Chapter 3	A vulnerable masonry façade subjected to 100% of the maximum deformation.	Masonry buildings with old masonry foundations, located on the worst location and examined with the strictest damage criterion.
D	Realistic transfer of deformation	Appendix B, Appendix H, Chapter 3.3	As C, but only 30% of the maximum deformation is applied.	
E	Worst case	Appendix D (material) Appendix F (pre-damage) Appendix C (cyclic effects)	As C, but with 50% of the maximum deformation and including the combined detrimental effect of weaker material, existing damage, and cyclic effects.	Buildings similar to C but with more sensitive masonry and existing cracks that can be aggravated.
A	Majority of masonry buildings	Appendix E (foundation) Reference 11	A more common situation with a good foundation, standard material, subjected to average soil deformations, and a less strict damage criterion.	This corresponds to the majority of masonry buildings, like row houses, building throughout the affected region.
B	Modern masonry buildings	Appendix E (foundation) Reference 11 Appendix I	A more modern and also common situation with explicitly reinforced foundations and no transversal walls.	Corresponds to newer masonry buildings that have better foundations but without wall interlocking at the corners (masonry elements) and can be more sensitive to displaying fine cracks.
F	Theoretical worst cases	Scenario E + Appendix I	A combination of all the effects observed to reduce the critical threshold that causes damage in buildings.	This scenario is not based on an idealised building.

On the first column of Table G.3, for scenario A, we define a common situation with a building on a strip foundation, with standard vulnerable masonry properties for existing masonry, using a direct 30% transfer of the soil strains, and consider the upper threshold of light damage, most applicable for the unfinished fired-clay brick masonry. These fired-clay masonry buildings have usually good connections with transversal walls. For these common buildings, we neglect the influence of visible existing damage and the cyclic effects present at the centre of the Norg area. The models compute a high critical value for triggering damage. Since most buildings are located on areas with moderate curvatures and horizontal strains, we estimate that the probability of incurring into damage is almost zero for these buildings, common among the building stock. Similarly, scenario B looks at the other pool of common buildings, those erected after 1975, with reinforced concrete foundations and, again, a standard type of masonry. These modern houses do not consider a connection with the transversal walls. A direct transfer of 30% the soil strains is again enforced, even though these strong foundations are likely to further limit this transfer. For these more modern buildings, we set a stricter criterion for damage. Still, a high critical value suggests that the probability of damage remains almost zero.

The focus of our study was placed, however, on scenarios C to E corresponding to a minority of vulnerable masonry buildings. For scenario C we considered an old masonry foundation and a 100% transfer of the soil strains and compared these at the location where they are maximum. We also enforced the strict damage criterion. As expected, the critical thresholds were reduced but still above those determined from the geomechanical model (see section G.2.2); these lower critical values could be linked to a higher probability of damage but still in the scope of unlikely. Scenario C was refined to consider a realistic transfer of the soil strains (becoming scenario D) which significantly increased the critical values and thus appears to the left of scenario C in the table which is accompanied by Figure G.7 which illustrates the descending likelihood of existing buildings within each scenario but the increasing probability of damage as the scenarios observe more vulnerable buildings.

Therefore, to complement scenario D, we envisioned scenario E, the worst realistic case, consisting of poor masonry foundations, a stiff, yet weak wall masonry, with a conservative 50% direct transfer of the soil strains also due to existing pre-damage, a strict limit for damage (aggravation) and applied

soils strains repeatedly to simulate cyclic effects. This combination of effects is likely to represent only a handful of real buildings and is still associated with a low probability of damage as the critical value is still large in comparison to the strains at the worst location. Note also that the lowest critical strains are in tension, while the largest strains in the field are in compression.

Lastly, appendix I, has investigated features that are used to envision scenario F where all the worst and most strict features are marked. The most influential feature is that of a stiffer masonry, where the Young’s moduli are doubled but the masonry tensile strength is kept at the value proposed by the NPR. From [2], the variability in masonry properties can be estimated. Assuming a normal distribution for the moduli of elasticity, a doubling of the mean stiffness would correspond to the upper 1%. In reality, the stiffer masonry is also linked to stronger bonds. This means that the likelihood of masonry buildings with these properties is already less than 1%; including additional vulnerable features, especially if more than one feature is included, will drastically reduce the chance that such a building actually exists. Regardless, the thought experiment of scenario F consists of adding up all detrimental effects as per table G.1; this results in a factor of 5 (against the base model of scenario C) which would bring the critical values very close to actual values in the field. However, as appendix I demonstrates, even if all effects are combined, they do not add up linearly, but result instead in a less detrimental combination. Table G.1 also shows how most effects which make the models more realistic such as a lower transfer of strains between soil and foundation, a less strict damage criterion, or a more common location, significantly increase the amplification factor required to cause damage. For scenario F, emphasis must also be placed in the value of strain transfer from the soil; if the unrealistic value of 100% is reduced to a very conservative estimation of 50% for these values of soil strains (see appendix H), then the critical thresholds would double to 36/16; these values should be compared to the highest tensile horizontal soil strains.

Finally, in the last row of Table G.3, a qualitative estimation is provided for the probability of damage based on the likelihood of a scenario and the probability of damage for buildings within the category. For example, while buildings A and B are common, they are not vulnerable to the deformations caused by the direct effects of deep subsidence, and so the final probability to observe damage is very small. Conversely, while buildings within scenario E are more likely to become damaged, few buildings will actually correspond to this category and then again, the probability to observe damage is very small. The probability of damage for the buildings of scenario E is further explored in Appendix J.

It must also be noted that the probability of the potential scenarios of subsidence or heave, presented in Table G.0, has not been accounted for. This is not discussed in this appendix; see [10].

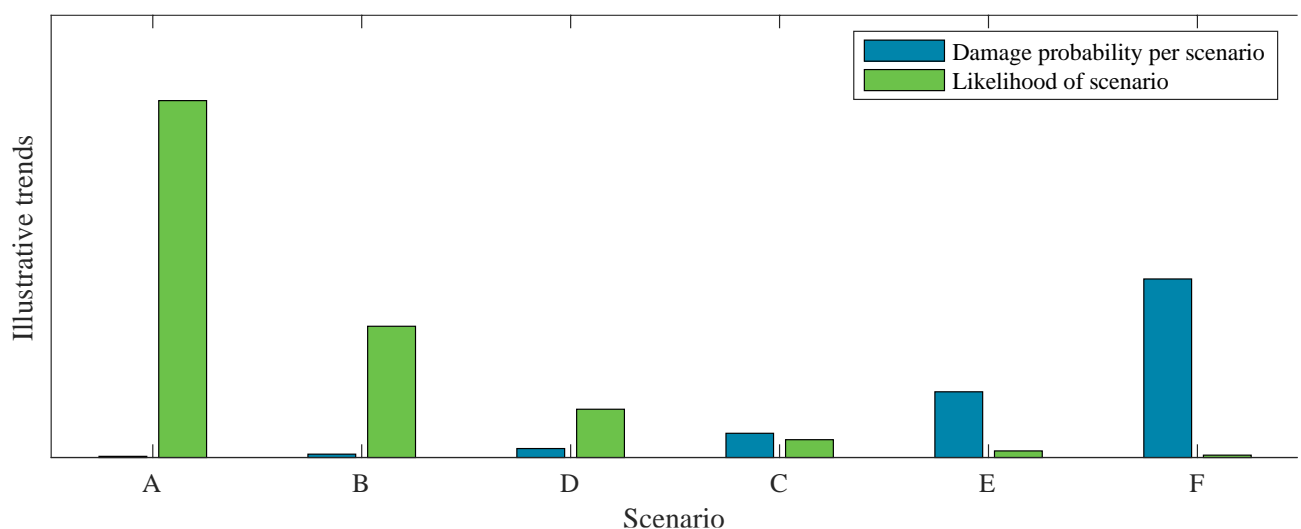


Figure G.7. Illustration of scenarios and a qualitative indication of their conditional probability detailed in Table G.3.

Table G.3. Qualitative probability of damage and by order of scenario likelihood.
 Note: *cw* refers to approximate crack width in millimetres.

Combinations Values of: Strain Curvature in 10 ⁻⁶ m/m 10 ⁻⁸ rad/m		A	B	D	C	E	F	
		Most common situation	Most modern houses	Realistic transfer	Basic case studied	Worst realistic case	Theoretical worst cases	
Foundation	Masonry Foundation (wall enlargement)			x	x	x	x	x
	Concrete strip foundation	x						
	Reinforced concrete foundation		x					
	Thin Masonry Foundation						x	x
Masonry	Standard Masonry (as defined by NPR)	x	x	x	x			
	Poor Masonry (same stiffness, reduced strength)					x	x	x
	Disconnection from transversal walls		x				x	x
	Stiff Masonry (double stiffness, same strength)						x	x
Strain transfer	30% transfer (literature agreement)	x	x	x				
	50% transfer (conservative)					x	x	
	100% transfer (unrealistic)				x			x
Additional Effects	Pre-existing visible damage					x	x	x
	Cyclic Effects (only in Norg)					x	x	x
Damage Criterion	Barely visible damage <i>cw</i> =0.1 mm ($\Psi=1$)		x	x	x	x	x	x
	End of light damage <i>cw</i> ≈2 to 3 mm ($\Psi=2.5$)	x						
Location (Applied deformation)	Moderate horizontal strain and curvature (average value in affected region)	x	x					
	Maximum horizontal strain and curvature (<1% exceedance)			x	x	x	x	x
Results (Critical deformation)	Critical value for compressive horz. strain with sagging curvature	> 550 500		360 330	109 100	60 54	45 20	22 20
	Critical value for tensile horz. strain with hogging curvature	> 370 330		290 270	88 82	50 45	36 16	18 16
Assessment	Qualitative probability of damage within given scenario	Probability nearing impossibility		Very unlikely	Unlikely	Small probability	Reasonable probability	Probable
	Qualitative frequency in building stock (likelihood of scenario)	Common		Uncommon	Exceedingly uncommon	Perhaps a few buildings	Probably not a single building	Not a single building

G.4 Conclusions

The worst-case methodology doesn't allow for the computation of probabilities of damage. However, the large margin, between soil deformation values in Norg and those required to cause damage to vulnerable buildings, permits a qualitative estimation of the damage probability for the scenarios explored. Moreover, the relative frequency of the scenarios actually appearing in the field allows to appraise an overall probability of masonry buildings displaying damage due to the direct effects of deep subsidence, which manifests itself as a combination of relatively large horizontal strains and very small curvatures at the ground surface. Other (indirect) effects have not been studied.

- The common scenario for buildings with NPR-9998-standard masonry founded on concrete foundations (scenarios A and B, Table G.3) reveals large margins, or a factor of more than 50, between soil deformations required to cause visible cracks and actual deformations appearing in the majority of the Norg or Groningen regions; this would correspond to an exceedingly small probability.
- Less common is the situation of pre-1945 buildings founded on unreinforced masonry foundations (scenario D); the weaker foundation has a large effect on the transfer of the soil deformations leading to a factor in the order of 20 over the maximum strains at the worst locations in Norg.
- If the buildings present existing damage in a way that makes the walls much more flexible and thus soil deformations are (conservatively assumed to be) fully transferred to the building (scenario C), which corresponds to an even less common situation, margins fall down to 8 to 10 times; damage is still unlikely.
- Finally, the cyclic effect of gas storage and extraction in Norg can lead to repeated cycles which degrade and accumulate damage in masonry buildings. Compounding all these effects together to create a scenario that is extremely unlikely (scenario E), a margin between soil deformations required to cause visible damage (cracks of 0.1 mm width) and those maximum due to deep subsidence still remains in the region of Norg and most of the region of Groningen. Only at the locations of highest horizontal strains in Groningen (northeast of Bedum and east of Warffum, see [10]), is the expected soil strain up to 20% larger than the horizontal strain required to lead to visible damage in the buildings of scenario E. This should be viewed in the context of this unlikely scenario explored with the worst-case methodology.

In sum, the modelling checks show that the overall probability of observing damage due to the direct effects of deep subsidence in the regions of Groningen and Norg is extremely small. Nonetheless, a true quantification of the probability of damage is not possible with the worst-cases methodology and is unfeasible with the knowledge directly available. Yet, the worst-cases approach is sufficient to verify that damage due to deep subsidence is unlikely since improbable scenarios remain undamaged when subjected to the highest soil strains estimated for most of the region.

G.5 References

1. Esposito, R., Terwel, K., Ravenshorst, G., Schipper, R., Messali, F., & Rots, J. (2017). Cyclic pushover test on an unreinforced masonry structure resembling a typical Dutch terraced house. In Proceedings of the 16th World Conference on Earthquake Engineering 2017: Santiago, Chile (pp. 1-12)
2. Jafari, S., & Esposito, R. (2017). Material tests for the characterisation of replicated solid clay brick masonry. Delft University of Technology.
3. Mirra, M., Ravenshorst, G., & van de Kuilen, J. W. (2020). Experimental and analytical evaluation of the in-plane behaviour of as-built and strengthened traditional wooden floors. *Engineering Structures*, 211, [110432]. <https://doi.org/10.1016/j.engstruct.2020.110432>
4. van Staaldouin, P. C., Rots, J. G., & Terwel, K. C. (2019). Onderzoek naar de oorzaken van bouwkundige schade in Groningen: Methodologie en case studies ter duiding van de oorzaken. Revised version 2019. Delft University of Technology.
5. A. Prospero, P.A. Korswagen, M. Korff, R. Schipper, J.G. Rots (2023). Empirical vulnerability and fragility curves for masonry buildings subjected to settlements. *Journal of Building Engineering* (UNDER REVIEW)
6. ARUP (2018). Exposure Database EDB V5 Structural Systems - Groningen Building Taxonomy analysis.
7. BAG (Basisregistratie Adressen en Gebouwen), Buildings and addresses database and derived 3D-BAG
www.3dbag.nl
8. P.A. Korswagen, M. Longo, J.G. Rots, A. Prospero (2022). Supporting analyses to determine probability of damage and fragility curves due to indirect subsidence effects. Delft University of Technology. Final Version 2, October 3, 2022.
9. Monumental Farmhouse, National Monument ID: 523688. Retrieved January 2023.
<https://rijksmonumenten.nl/monument/523688/boerderij-met-aangrenzende-bijschuren/breedenbroek/>
10. Maarten Pluymaekers (2023). Memo: Additional analysis subsidence evaluation Norg. TNO AGE 23-10.024
11. C.P.W. Geurts, M.P.D. Pluymaekers, J.G. Rots (2021). Advies IMG: Schade aan gebouwen door diepe bodemdaling en -stijging. TNO Report R10325B, Delft 2021.
12. Son, M. & Cording, E., 2005. Estimation of Building Damage due to Excavation- Induced Ground Movements. *Journal of Geotech. and Geoenv. Engineering*.

Appendix J: Convolution for the Probability of Building Damage due to Horizontal Soil Strains for Buildings of Scenario E

J.1. Introduction

In appendix G, a qualitative description of the probability of damage for the various building types and scenarios is explored. For one building type, considered the most vulnerable yet realistic building type, this description is further explored and quantified. Buildings with unreinforced masonry foundations, with old masonry, and possibly subjected to cyclic effects, corresponding to scenario E as per appendix G, are herein analysed. The probability of the appearance of visible damage ($\Psi=1$) is quantified by considering the probabilistic distribution for the horizontal soil strains over the Groningen and Norg subsidence fields [2] and the probabilistic distribution for the building allowable horizontal foundation strain summarised in Table G.3, “Results” row. The later distribution is elaborated in section J.2. Note: the allowable (A) horizontal strain (ϵ_H) applied (A) underneath the building foundations is hereon denoted as ϵ_{AHA} .

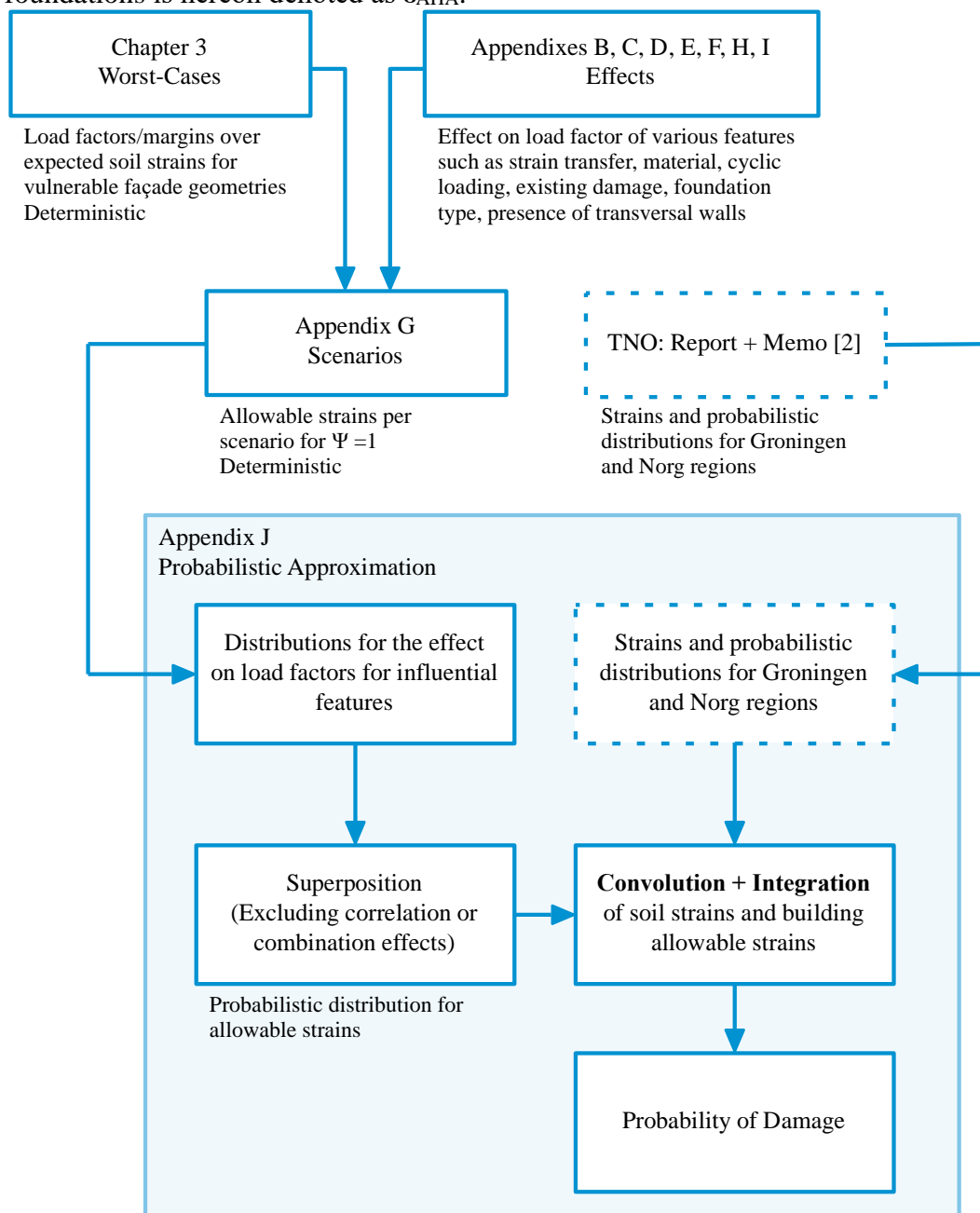


Figure J.0. Flowchart and overview of Appendix J and its input.

J.2. Distributions for Building Vulnerability

For the vulnerable buildings of scenario E, maximum allowable horizontal strains acting underneath the foundation, ϵ_{AHA} , have been determined in this report and are summarised in Table G.3. For tensile strains associated with a hogging subsidence shape, these buildings will display visible damage starting at a horizontal strain of $50\mu\text{m/m}$; while for compressive strains, linked to a sagging shape, the threshold is slightly higher at $60\mu\text{m/m}$. See also Figure G.6 which illustrates the relationship between the strains and the curvature of the soil. The subsidence deformation is characterized by a compressive strain and a relatively small concave curvature, while heave is associated with tensile strains and a small convex curvature. At the perimeter of the subsidence trough or at the heave crest, these effects are reversed.

The values stated above have been set conservatively with the method of worst-case-scenarios and one can expect that even within this building typology, many buildings will be able to safely withstand higher horizontal strains, while some may lie underneath the set allowable values.

To determine the distribution of this safety margin, various parameters are deconstructed and examined, and standard distributions are assigned. Then, the superposition (by product) of the various distributions is used to formulate the distribution of the established allowable horizontal strain, ϵ_{AHA} . The assigned distributions are determined based on material data, model assumptions and expert judgement when applicable; in all cases, these are formulated on the conservative side.

J.2.1. Material Strength

For buildings of scenario E, an old masonry material has been considered. Additionally, the strength has been reduced by 30% to consider a poor, old masonry property. This reduction corresponds to one standard deviation observed from laboratory tests on samples of existing masonry and was selected precisely to account for a more vulnerable masonry. This means that the masonry is more likely to be stronger. In appendix D, the influence of the material strength was investigated; this is also summarised in Table G.2. For weak, old masonry, the maximum allowable strain could be affected by up to 33% in comparison to the standard value. Based on these two facts, one can assume two linked distributions: one for the material strength and one for the associated ϵ_{AHA} . This is illustrated in Figure J.1, where on the left, a normal distribution is assumed for the value of the tensile strength relative to the standard value; the models investigated had a relative strength of 0.7. This lower strength is associated with a value of 1 for the allowable horizontal strain. It follows that stronger models will lead to a higher allowable strain, with a factor higher than 1 relative to the modelled case. The resulting normal distribution is shown on the right. It also presents the probability for the allowable strain to be lower than predicted if the material strength is also weaker than assumed; in this case, the probability of a lower ϵ_{AHA} would be 17%.

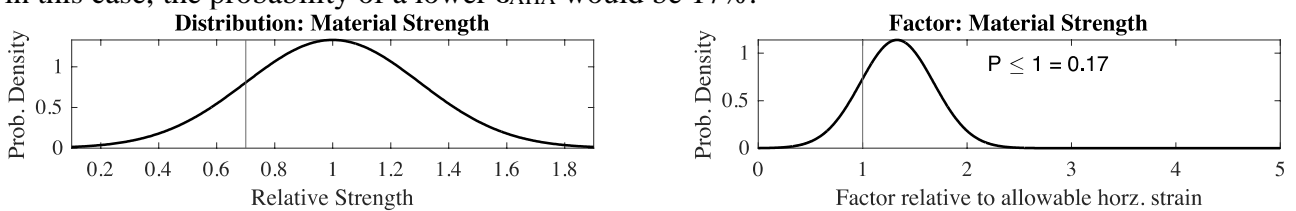


Figure J.1. Left, assumed normal distribution for the relative material strength and right, linked factor relative to the calculated allowable horizontal strain. The vulnerable situation of a weaker material was modelled, and is thus linked to a factor of 1.

J.2.2. Foundation Size

Similarly to the material strength, the influence of the foundation size was also evaluated, in this case, in appendix I. The foundation thickness has a smaller variability in the order of 10% in respect to the modelled case of 60 cm; this is determined by engineering judgement. Also, the influence of the thickness on the allowable strain is small, in the order of 5%; as per appendix I. Assuming that the modelled case corresponds to the expected value for the foundation thickness, the foundations can be both thinner or thicker and the corresponding factor slightly below or above 1; see Figure J.2.

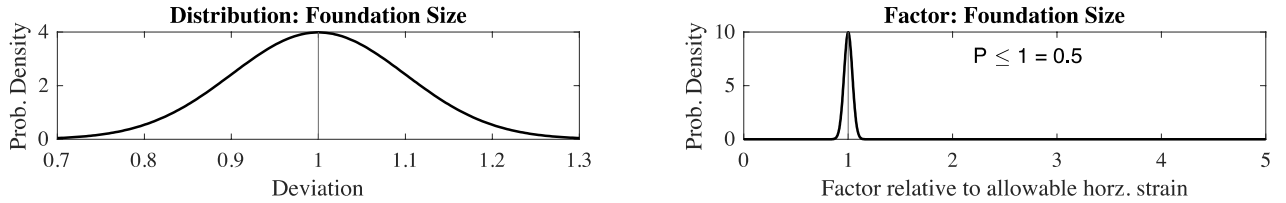


Figure J.2. Distribution of the foundation size relative to the modelled case and its associated influence on the allowable horizontal strain.

J.2.3. Geometry

Three façade geometries have been investigated. The geometries were selected so that they represent vulnerable masonry buildings, sporting long façades with several openings. To select the allowable horizontal strain, the minimum value to generate damage in any of the three geometries was used. Distinct façades responded differently to the two settlement shapes studied; for a hogging shape, façade A was the most vulnerable, while for sagging, façade B led to the lowest allowable strain. This approach is consistent with the worst-case methodology but is too conservative for a probabilistic representation of the influence of the façade geometry, where two of the three façades would allow a higher ϵ_{AHA} before exhibiting damage.

Since a full characterisation of the possible geometries is not feasible within this study, it has been assumed that the three façades are sufficiently representative of the variability in the response of the buildings. Therefore, the mean value and standard deviation of the allowable strain for the three façades is used to formulate a normal distribution for the response in hogging and sagging, respectively. Consequently, the relationship between the lowest value selected for the allowable strain and the mean is used to link the distribution of the allowable strain where the geometries' minimum is associated with a factor of 1. This is illustrated in Figure J.3, where for Sagging, for which the spread in the allowable strain was larger, the probability of the relative allowable strain being lower than 1 is only about 5%. This is expected since two of the three façades could endure a much larger horizontal strain before reaching $\Psi = 1$.

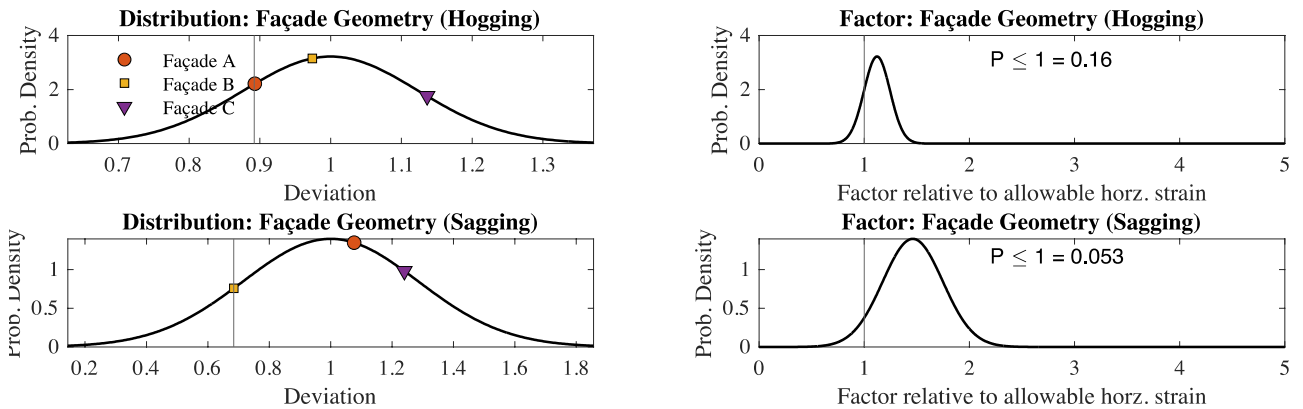


Figure J.3. Spread in the allowable strain due to geometry variations and its influence on the set threshold for both hogging and sagging independently. For hogging, façade A was more sensitive, relatively close to the mean; while for sagging, façade B was more vulnerable and comparatively much lower than the mean.

J.2.4. Pre-damage

The initial condition of the masonry façade or the amount of pre-damage before the application of the subsidence load also plays a role in the allowable strain to reach a value of $\Psi = 1$ or an equivalent increase in Ψ in respect to the initial Ψ_0 . It is not possible to characterise the degree of pre-damage on buildings without extensive research into the state of the building stock and several causes of existing damage. Instead, in the models investigated herein, discrete values of pre-damage were assumed, which could decrease the allowable horizontal strain by up to 50%; see Table G.1.

The value of allowable strain of 50 and 60 $\mu\text{m/m}$ for hogging and sagging, respectively, includes this 50% increase, consistent with the worst-case approach. However, most buildings are likely to display a smaller influence of pre-damage, and thus a higher ϵ_{AHA} ; in fact, virgin, uncracked masonry would thus tolerate up to 1.5x the set allowable strain before reaching a value of $\Psi = 1$.

If a distribution must be assigned to the spread in the effect of pre-damage, the rate of 50% is assumed to correspond to one standard deviation above the mean, which is assigned to half that value (the mean is thus assumed to be 25%); see Figure J.4 left. The effect rate cannot be lower than 0% which translates to a truncated factor at 1.5. On the other hand, the pre-damage effect could be higher, though this is less likely, which corresponds to a factor below 1 associated with a probability of 19%.

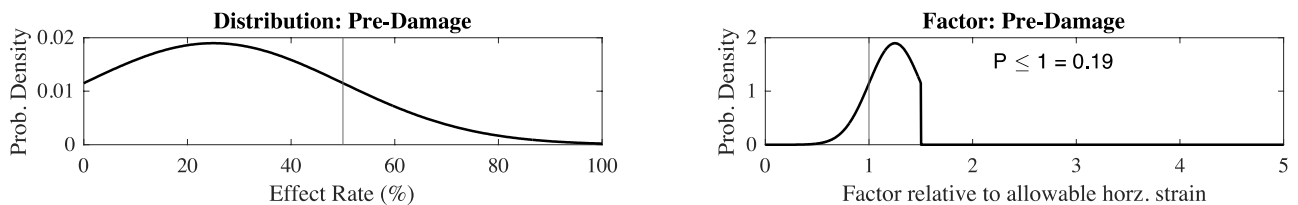


Figure J.4. Distribution for the effect rate of pre-damage.

J.2.5. Cyclic Effects

Similarly, the reported allowable soil horizontal strain includes the conservative reduction due to cyclic effects. These were observed to account for an up to 25% decrease in the allowable strain. With the same strategy as J.2.4, the rate of 25% is assumed as one standard deviation above a mean of 12.5%. Most buildings, outside of Norg, will not be subjected to cyclic effects, in this case the allowable strain could be increased by no more than 1.25.

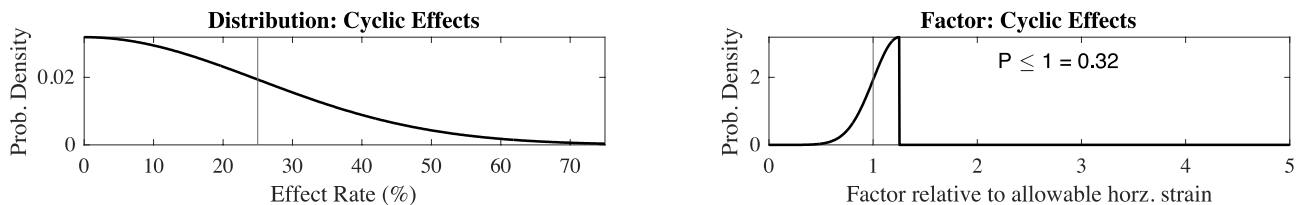


Figure J.5. Effect of cyclic effects on the allowable strain.

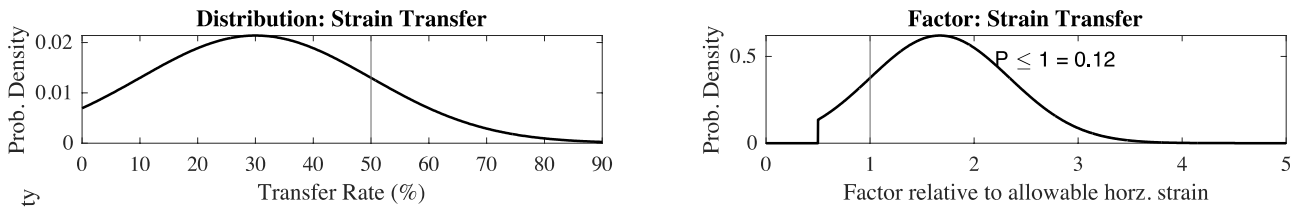
J.2.6. Strain Transfer

Only a small portion of the soil horizontal strain is transferred to the foundation of the building. This depends on many factors such as the type of soil underneath the building, the type of foundation, and the stiffness and state of the masonry; see also Appendix H. In literature, the agreed upon rule of thumb is that 30% of the greenfield strains are transferred to the foundations of masonry buildings.

To elaborate a distribution of strain transfer, a normal shape is assumed with a mean set at this value of 30%. In this work, a transfer of 50% has been set as the conservative assumption; hence, this value is placed at one standard deviation above the mean. This results in the distribution illustrated in Figure J.6 left. The transfer can fluctuate between 0 and 100%.

The threshold for the allowable horizontal strain includes a transfer of 50%. For a transfer of 100%, the allowable strain would have to be halved. This is represented in the truncated distribution on the

right of Figure J.6. Here, the probability of the transfer rate being greater than 50%, and so that the allowable strain is lower than 50 or 60 $\mu\text{m}/\text{m}$, is computed at 12%.



J.6. Effect of the strain transfer.

J.2.7. Results: Superposition for a Distribution of Allowable Strain

The six distributions shown in sections J.2.1-6 can be superimposed to determine the probabilistic distribution of the allowable building strain, ϵ_{AHA} , if no correlations or combination effects are assumed. The superposition is done by multiplying the cumulative distributions with each other.

This is done independently for the hogging and sagging cases associated with tensile and compressive horizontal strains, respectively. The result is illustrated in Figure J.7. Here it can be observed that the thresholds set for ϵ_{AHA} are indeed conservative and correspond to a low probability of exceedance. For a probability of exceedance of 10%, the thresholds can be increased to about 65 $\mu\text{m}/\text{m}$ and 85 $\mu\text{m}/\text{m}$, respectively. For the field strains summarised in [2], in particular, for the case of tensile strains in Groningen of 51 $\mu\text{m}/\text{m}$ closest to the set allowable thresholds, the expected probability of damage is below 1 in 10'000. However, the distribution associated with the field strains should also be considered; this is treated in the following section.

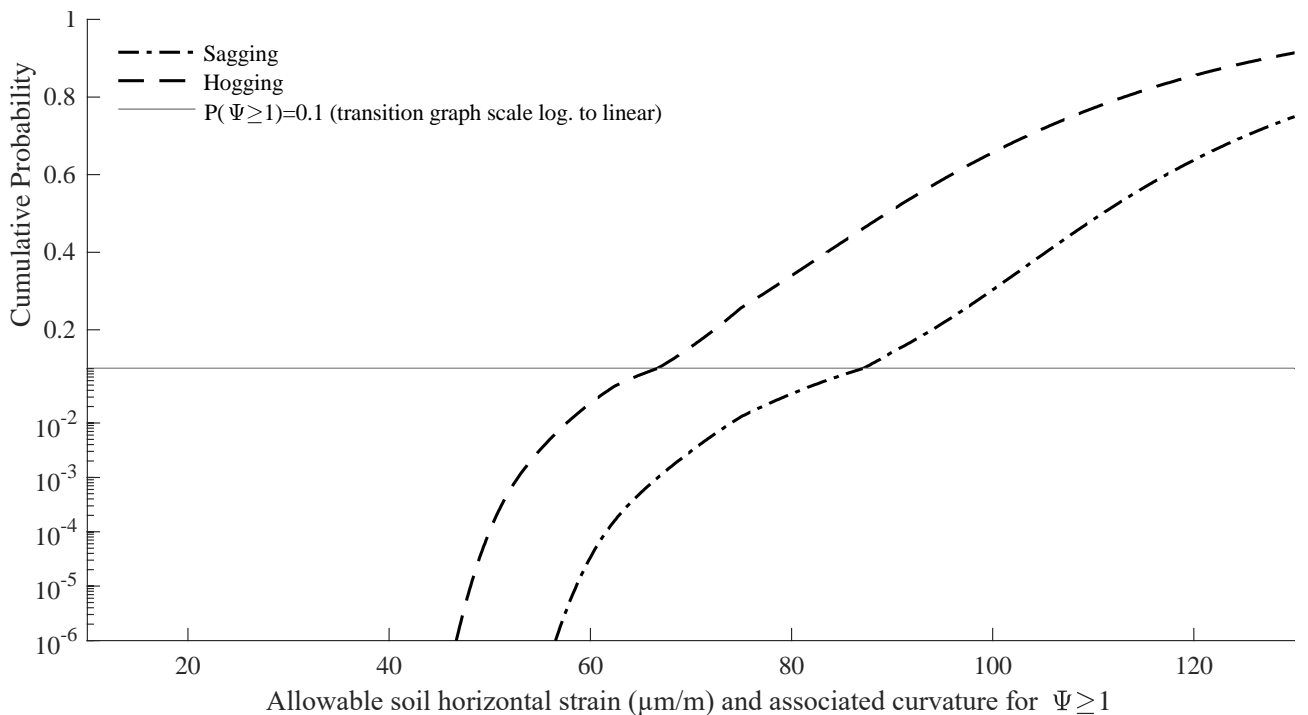


Figure J.7. Distribution for the building allowable horizontal strain, ϵ_{AHA} , against the cumulative probability of damage. This graph is also known as a fragility or vulnerability curve.

J.3 Convolution of Field Strains and Building Vulnerability

To determine the probability of damage, the building fragility, characterised by the distribution of the allowable soil horizontal strain acting underneath their foundation, should be convoluted and integrated with the distribution of expected horizontal soil strains due to deep subsidence at a given location. Distributions for these field strains are not elaborated herein but are discussed by [2]; in the following subsection, an overview of the field strains is presented.

J.3.1. Overview of Horizontal Field Strains

Three regions have been analysed with a geomechanical model to assign a probabilistic distribution to the acting greenfield strains [2]: Groningen northwest, Groningen southeast, and Norg (situation of 1995); see later Figure J.18.

The results are illustrated in the following maps (Figures J.8 – J.10) where the expected values (mean) and standard deviations are summarised. Moreover, Table J.1 identifies the six largest strains in both tension and compression for the three regions and computes the value with a 1% probability of exceedance. The largest value, relative to the corresponding building allowable strain, which is 50 $\mu\text{m}/\text{m}$ in tension, is 60.3 $\mu\text{m}/\text{m}$.

Table J.1. Summary of maximum horizontal strains in tension and compression for the three regions and the 99% confidence value assuming a normal distribution.

Region	Maximum Horizontal Strain ($\mu\text{m}/\text{m}$)			
	Tension		Compression	
	Mean	1% exc.	Mean	1% exc.
Groningen NW	51.0	60.3	57.6	68.1
Groningen SE	19.0	22.1	16.8	19.6
Norg 1995	9.8	12.3	28.2	35.6

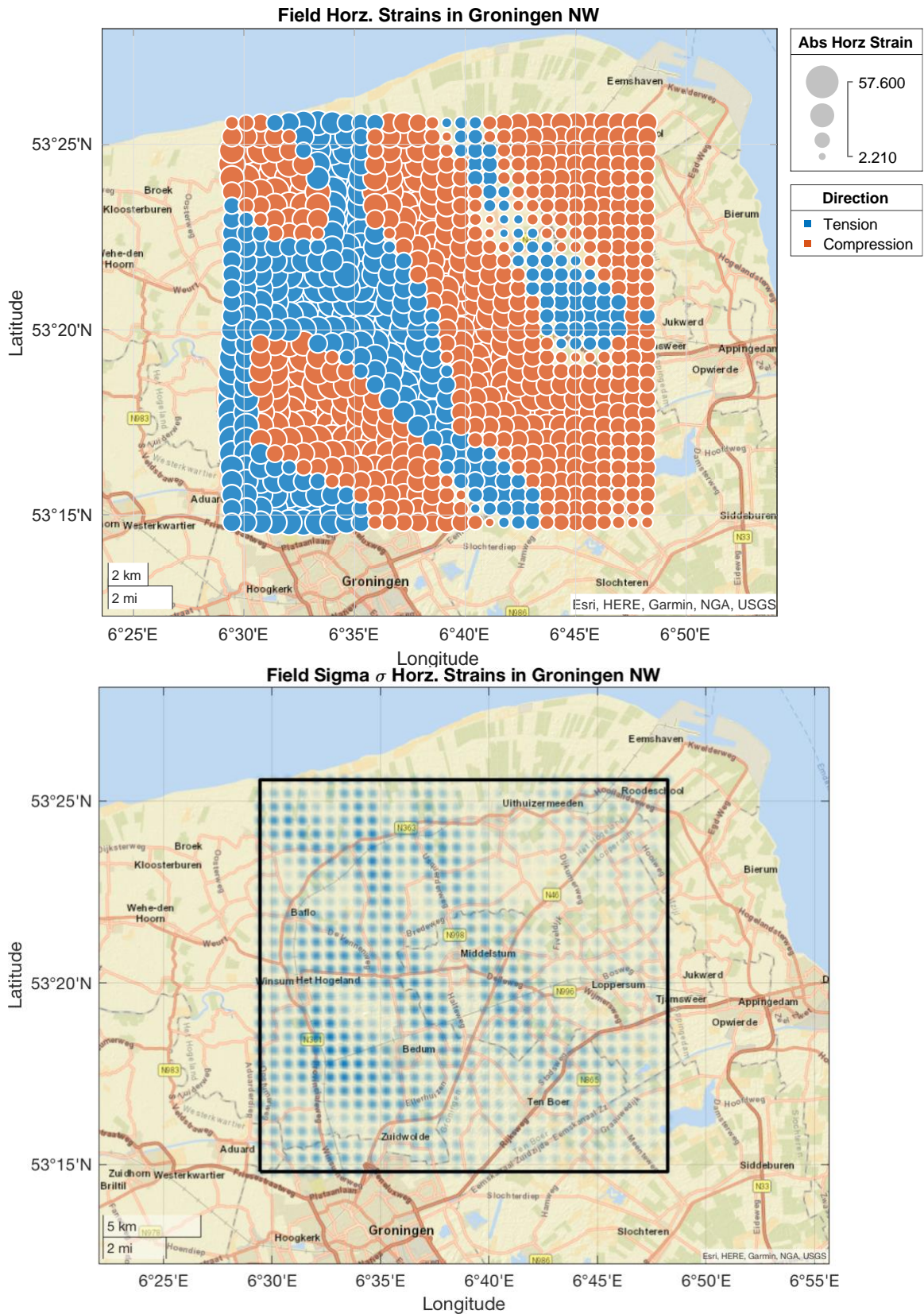


Figure J.8. Top, Mean horizontal strains in Groningen NW; bottom, standard deviation within the grid showing darker areas associated with larger uncertainty.

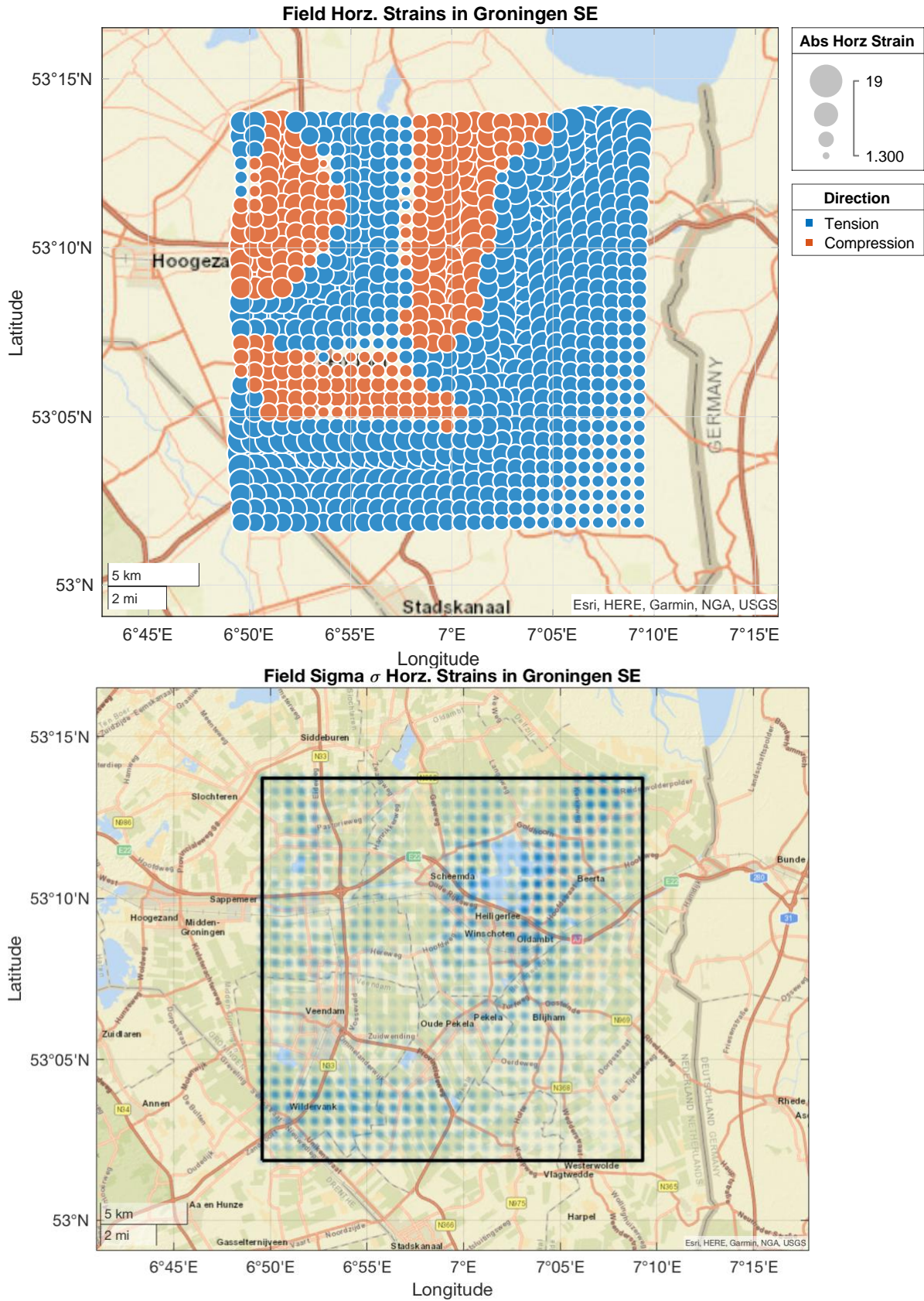


Figure J.9. Top, Mean horizontal strains in Groningen SE; bottom, standard deviation within the grid showing darker areas associated with larger uncertainty.

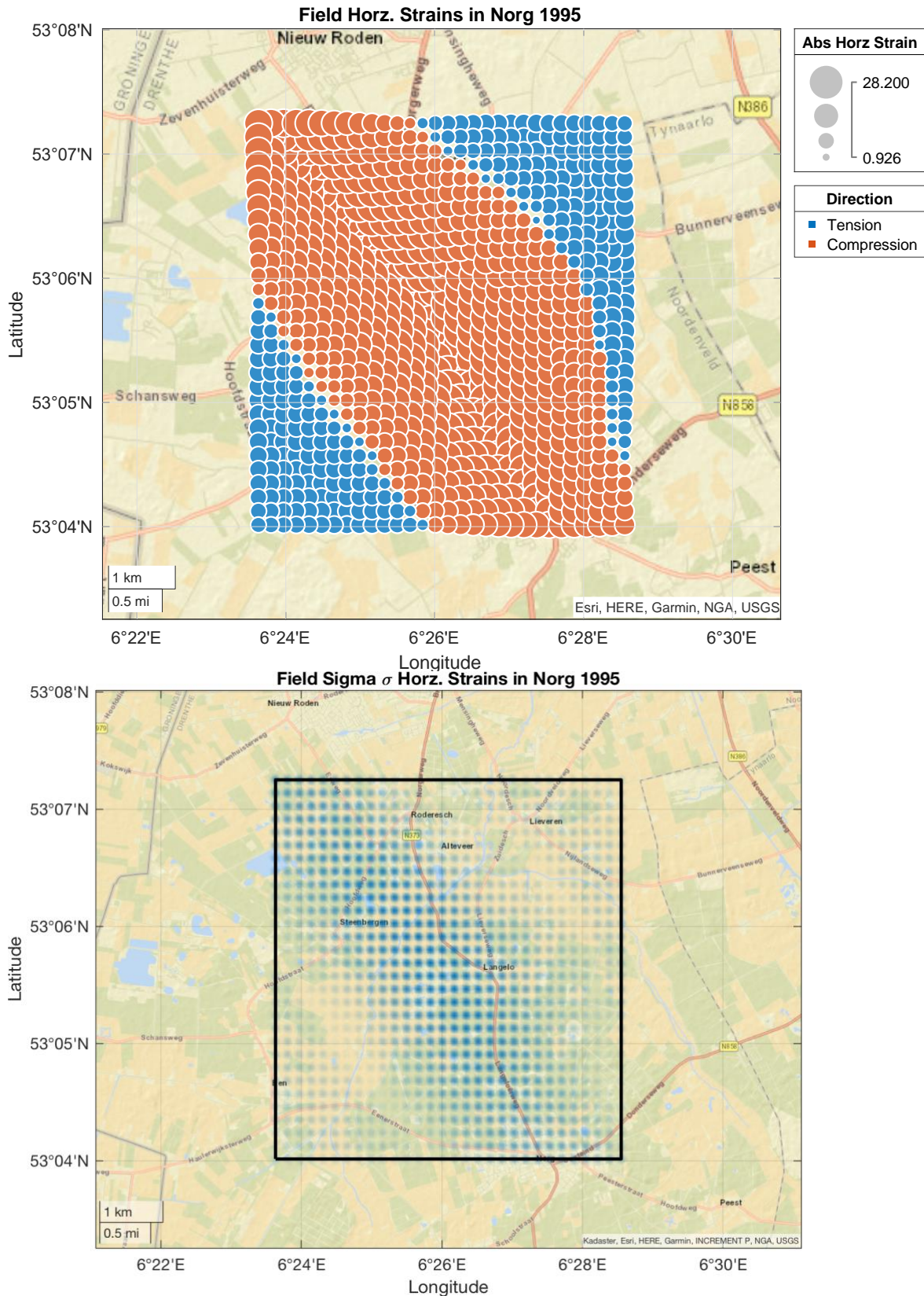


Figure J.10. Top, Mean horizontal strains in Norg (1995); bottom, standard deviation within the grid showing darker areas associated with larger uncertainty.

J.3.2. Convolution with Building Fragility

For every grid point, for which the field strains distribution is known, the probability can be convoluted and integrated with the corresponding building fragility depending on the tensile or compressive response. An example for the location with the highest probability in Groningen NW is presented in Figure J.11; the area under the intersection of both curves corresponds to the probability of damage, in this case, of roughly 0.2%. The field strains are modelled using both a normal distribution, as proposed by [2], and a lognormal distribution, which is typically more conservative due to its longer tail at the upper end. This is specially influential for very low probabilities when the mean field strains are very low.

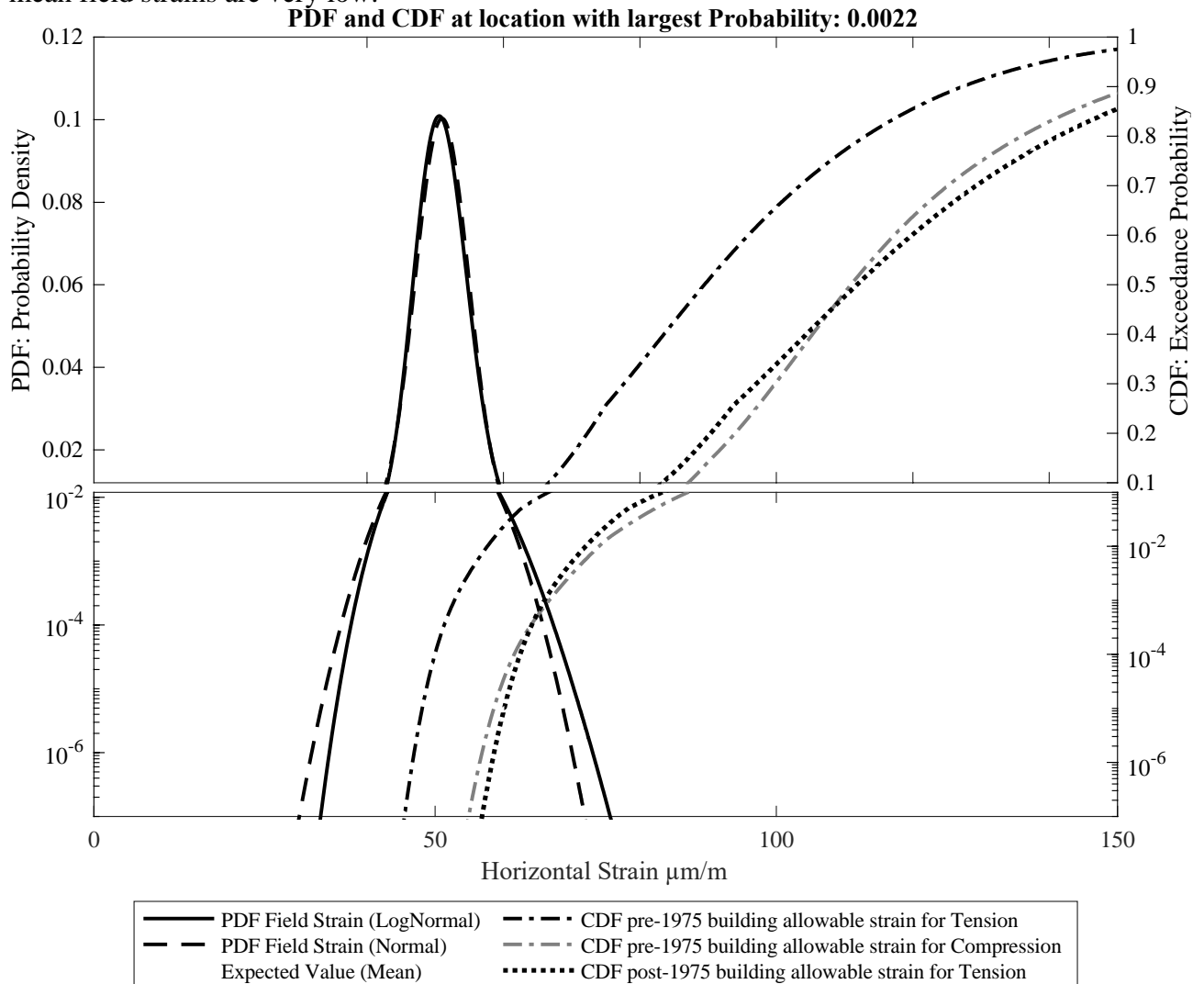


Figure J.11. Convolution field strains and building fragility from the Probability Density Function of field strains for Groningen NW and the Cumulative Density Function for the buildings of scenario E corresponding to buildings typically built before 1975. For this case, the integration between field strains and building fragility results in a probability of damage of 0.22%

The integrated convolution can be verified with a MonteCarlo simulation where unique points are sampled from the two distributions (soil strain and building fragility) and failure occurs when the field strain is larger than the allowable building strain. The number of failures divided by the total number of samples gives an indication of the probability of damage. A comparison with the analytical calculation is conducted in Figure J.12 for Groningen NW. For very small probabilities, the accuracy of the MonteCarlo simulation is affected; however, the interest lies in the larger values of probability. A summary of the results for the three regions is provided in Table J.2. The cases of Groningen SE and Norg 1995 are associated with negligible probabilities and it can be directly concluded that the

probability of damage is essentially zero in these regions. Therefore, Figure J.13 presents only the case of Groningen NW, where based on the results at every grid point, a contour can be drawn at the probability threshold encircling areas where the given probability of damage is exceeded. Only in two areas, jointly about 3.7 km², are probabilities above 1 in 10'000 expected. These locations, just outside the built environment, correspond to areas where relatively high, tensile horizontal soil strains are expected; buildings with unreinforced foundations are most vulnerable to these tensile strains associated with a hogging curvature. Newer buildings, comprising all buildings constructed after 1975 and many already after 1945, have reinforced concrete foundations; these reinforced foundations are insensitive to horizontal strains and are robust against soil curvatures. In Table G.3, buildings from scenarios A or B, with reinforced foundations, display an allowable horizontal strain more than 4 times that of the sensitive buildings of E. Hence, for these newer buildings, the computed probability of damage is essentially zero, also in the Groningen NW region. Only for the buildings of scenario E are probabilities in the order of 0.01% to 0.1% expected as shown in Figure J.13.

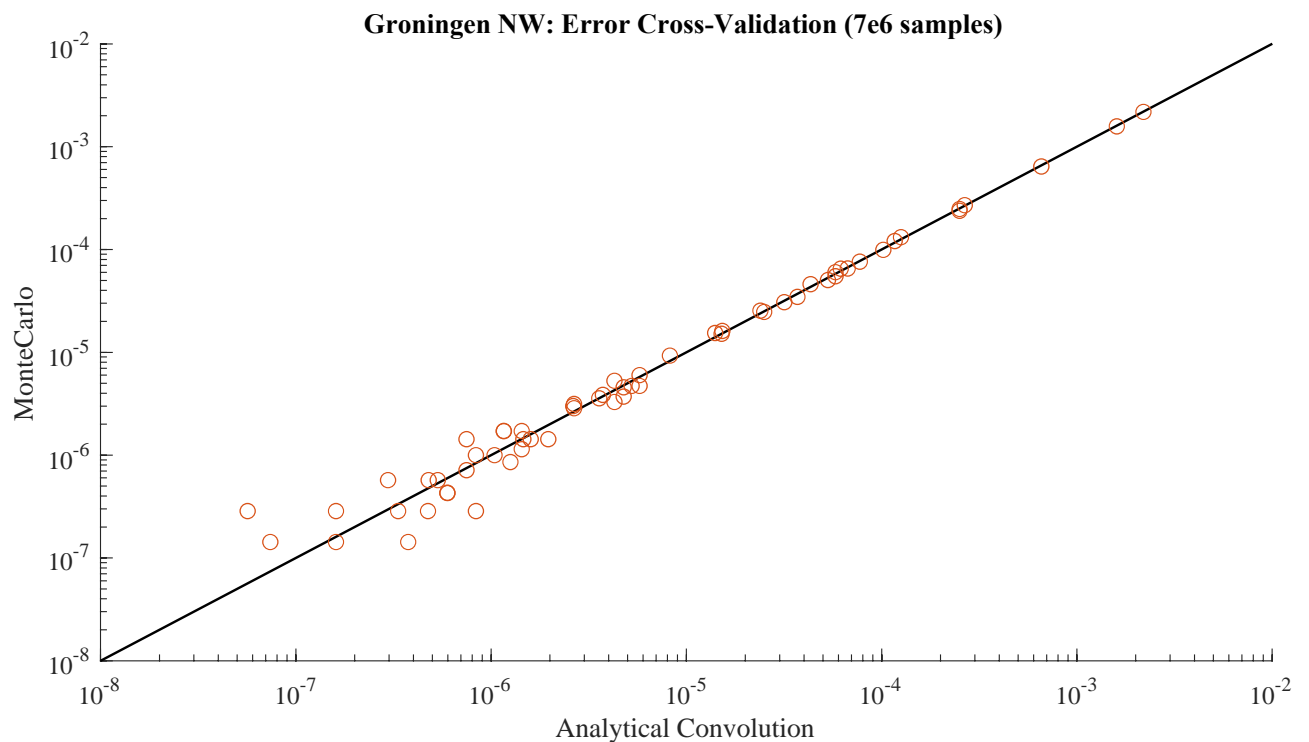


Figure J.12. Error between the analytical convolution solution and the Monte Carlo simulation.

Table J.2. Summary of results showing the maximum probability computed in every region. For very low probabilities, the number of samples of the MonteCarlo simulation is insufficient.

Calculation	Distribution	Groningen NW	Norg 1995	Groningen SE
Analytical Numerical	Normal	2.0E-03	1.5E-22	2.8E-51
	LogNormal	2.23E-03	1.4E-16	3.5E-42
Montecarlo	Normal	2.0E-03	0	0
	LogNormal	2.19E-03	0	0

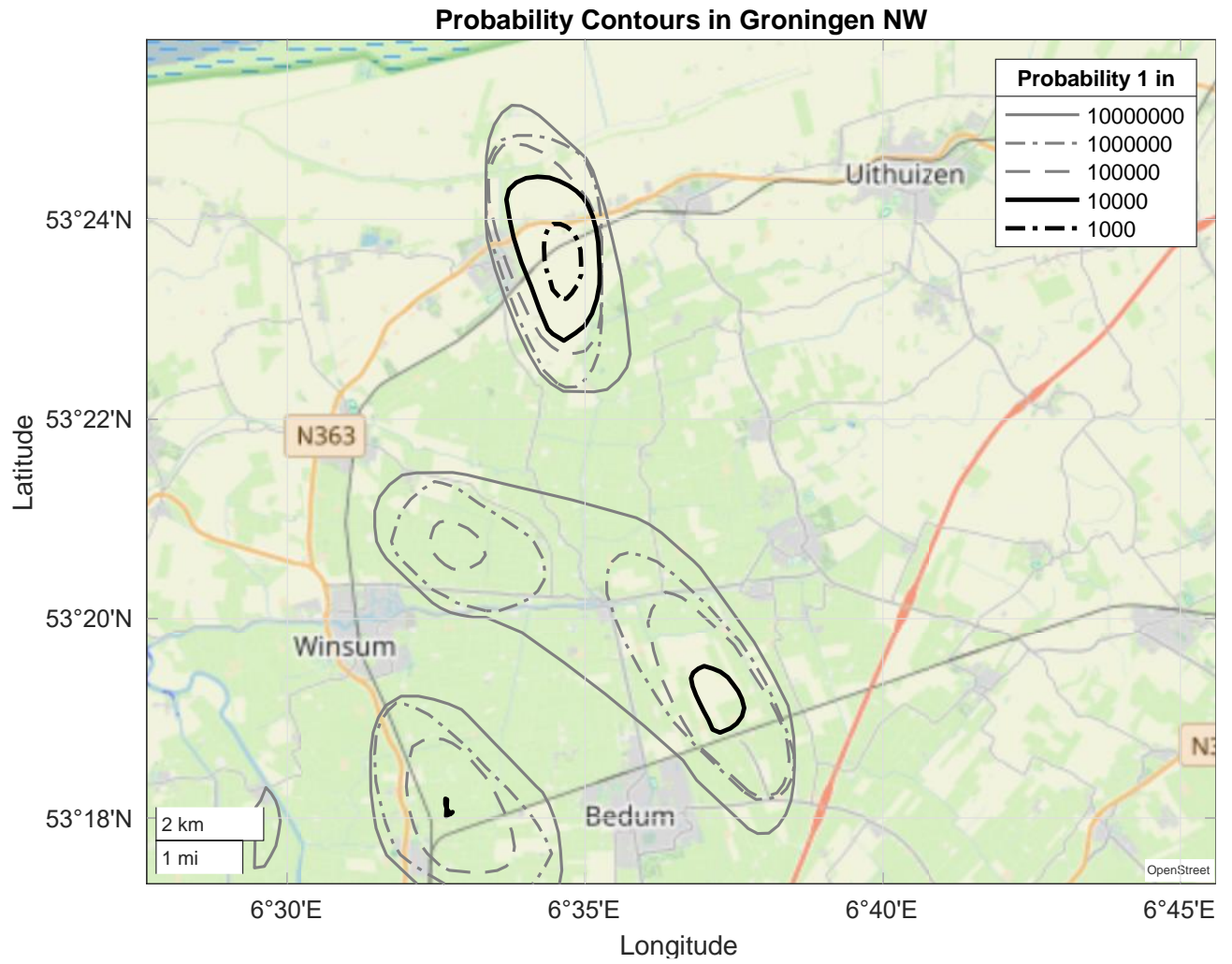


Figure J.13. Probability contours in the NW of Groningen for light damage ($\Psi=1$) of buildings with unreinforced masonry structures.

J.3.3. Intersection with BAG building database

The BAG national database registers properties about existing buildings. This database has been extended in height with aerial measurements to obtain a 3D-BAG database [3dbag.nl]; see Section G.2.1. The location, age, and footprint of 3D-BAG objects can be used to estimate the number of buildings potentially affected within the regions exceeding a probability of 1 in 10'000. Figure J.14 shows the location of about 35 thousand BAG objects or buildings within the Groningen NW grid defined by [2]. Buildings are concentrated in towns and along roads. Older buildings, like farmhouses and barns can be seen in the more rural sections.

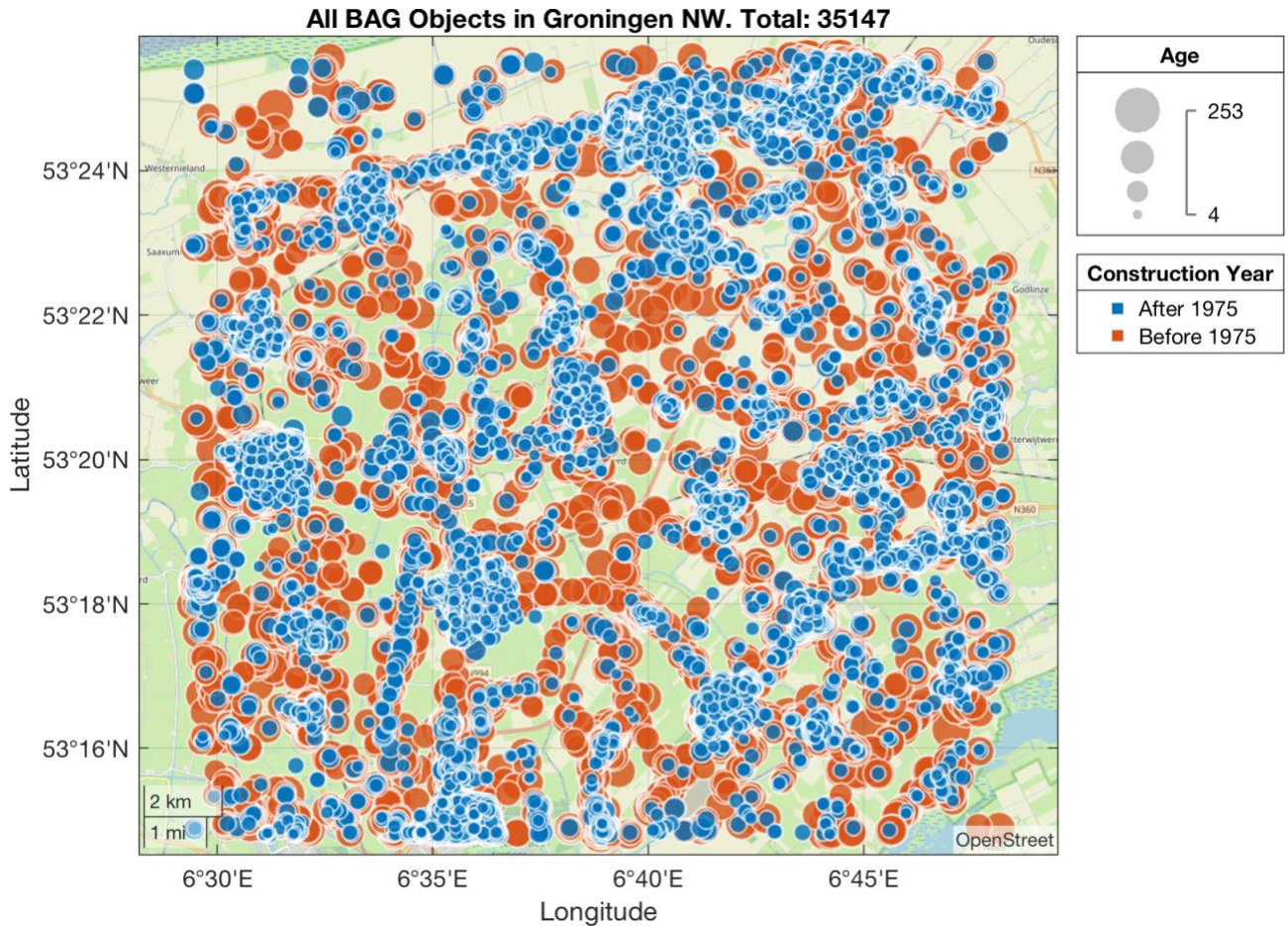


Figure J.14. All BAG objects within the Groningen NW grid.

For each of these objects, the probability of damage can be computed based on their location and fragility type. For all buildings erected before 1975, the fragility of scenario E with unreinforced masonry foundations is assigned. This is a conservative assumption since many buildings already after 1945 were constructed with improved foundations, either (reinforced) concrete or on piles. The fragility of buildings for after 1975 has not been determined; however, as a simplification, the fragility of E can be employed after increasing its mean by a corresponding factor. To remain on the conservative side, a factor of only 1.25 is employed. The buildings in scenarios A or B see allowable strains a factor of 8 higher than scenario E. Thus, the chosen factor of 1.25 is not the represent scenarios A or B specifically but any other vulnerable buildings outside typology E. This does not correspond to a defined buildings typology but instead to the group of buildings that do not have unreinforced foundations.

For BAG objects from before 1975, the contours from Figure J.13 lead to a few buildings, east of Warffum where the probability of $\Psi \geq 1$ is larger than 10^{-4} . These can be observed in the north of Figure J.15. For contrast and completeness, much smaller probabilities, down to 10^{-7} , are also

Finally, Figure J.16 presents an exceedance count associated with the probability of visible damage. Here the number of buildings decreases rapidly as the threshold probability increases. The graph summarises the last column of Table J.13 and adds a few relevant curves for comparison. First is the curve for the building typology E*; the construction of the distribution for the allowable horizontal strain is identical to that of section J.2 with the exception that the transfer of horizontal strain is reduced by changing the mean of 30% to 20%. This is the most influential component of the distribution and leads to a lower number of buildings exceeding the probability of 1 in 10⁴000; the 33% reduction in transferred strain, results in a 40% reduction in the number of expected buildings. Next, E⁺ considers the case of no cyclic effects, thus the factor on the allowable strain increases. This leads to a reduction in the expected number of buildings.

Furthermore, the curve for the more robust buildings, assigned to buildings after 1975, also appears in the left corner of the plot. This means that the number of these buildings and their probability of damage is extremely small. Lastly, the plot shows the case of the vulnerable buildings, of scenario E, convoluted with a distribution of the soil strains where the standard deviation has been increased by 50%. This is a large increase and shows how the number of buildings would increase if the uncertainty of the geomechanical calculations was larger. The sensitivity of this parameter is large, the 50% increase leads to a 10 fold increase in the number of buildings for which the probability of damage is larger than 10⁻⁴, from 20 to 200. This leads to the following two conclusions: First, that additional investigation into the geomechanical modelling of the soil, and monitoring of horizontal strains in the field, will likely lead to reduced uncertainty and thus lower probability of damage. Second, that it can be stated with confidence, that the number of buildings potentially affected by deep subsidence is limited.

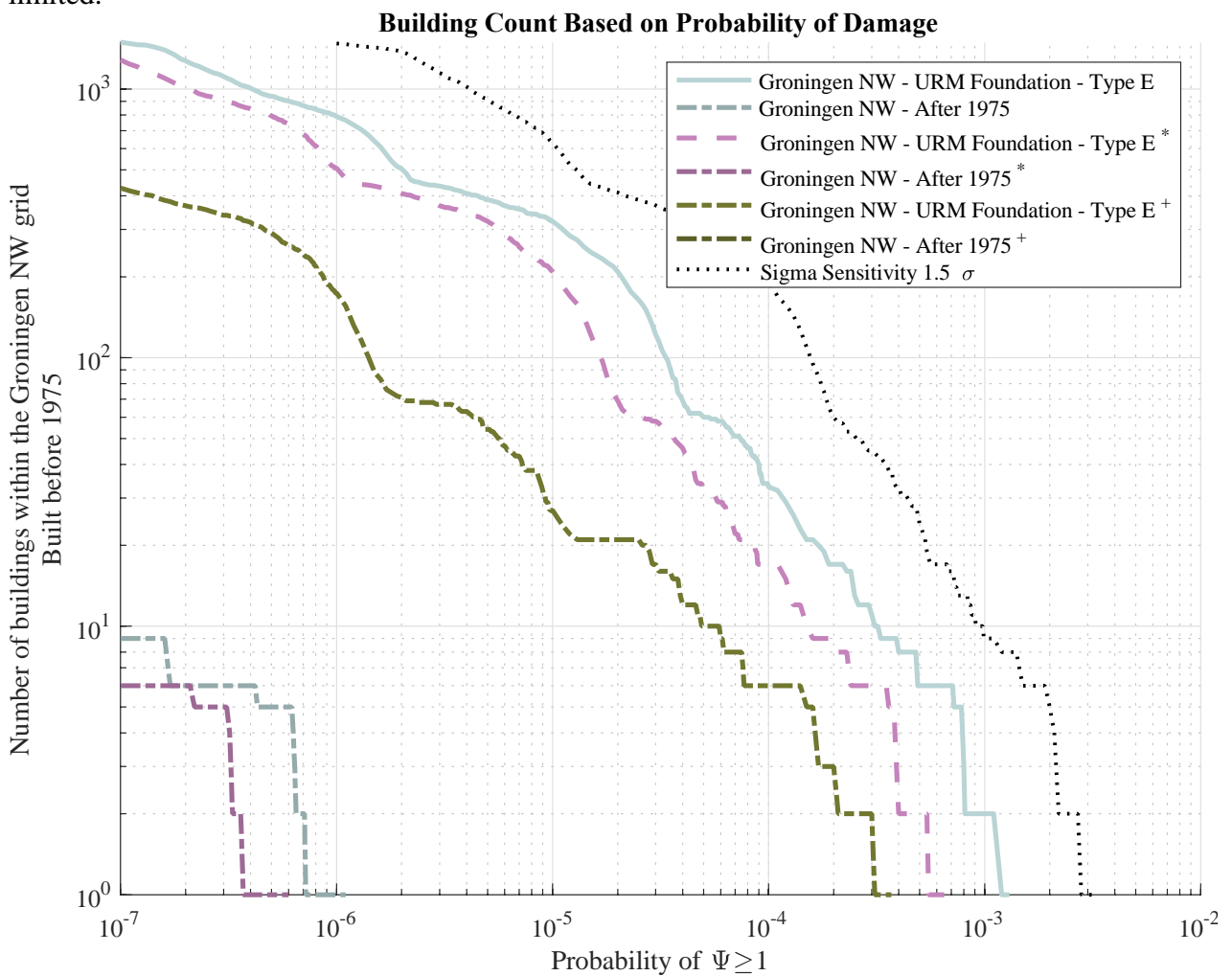


Figure J.16. Exceedance count of the number of BAG objects associated with a probability of visible damage.

J.4 Discussion

Based on the worst-case FEM models conducted in the report and its appendixes, the effect of several features, such as façade geometry or material strength, has been evaluated. The effect of each feature on the allowable horizontal building strain underneath the foundation (ϵ_{AHA}) is quantified from these models. Then, a distribution is assigned to each feature explored and linked to the expected distribution of the allowable strain. The superposition of these distributions results in a distribution of the probability of damage for increasing ϵ_{AHA} , or fragility.

To quantify the probability of damage, several assumptions and simplifications have been made, erring on the conservative side by, for instance, considering the average of the vulnerable geometries as the representative mean when many, presumably more resilient, geometries have not been explored. A complete list is not presented here, but a few of the assumptions are discussed.

First, only the effects of deep subsidence have been investigated. In reality, it is likely that several processes act simultaneously on the buildings or that indirect effects, such as the relative lowering of the water table, affect the buildings. These have not been studied; however, the aggravation of damage is considered, and an increase in Ψ of 1 ($\Delta\Psi=1$), corresponding to fully attributable damage is observed. In Appendix F, pre-damage that aggravates the effects of subsequent horizontal strains is included in the models and the horizontal strain needed to produce a $\Delta\Psi$ of 1 is calculated. Specific types of pre-damage associated with multiple causes or scenarios should be studied more in-depth.

Secondly, the probabilistic approach employed in this appendix is an approximation. It is based on a few samples at the lower tail of the fragility instead of a larger number of samples throughout the entire response. Moreover, the effect of each feature is analysed separately, and every combination is explored as independent effects. In a fully probabilistic sampling, some combinations will be more frequent than others and correlations will be present; neither have been quantified herein. For example, that the masonry is both weak (unfavourable) but stiff (unfavourable) is incredibly unlikely as weak masonry is typically correlated to lower stiffness. Furthermore, normal distributions have been implemented also based on a limited number of samples, extrapolating from experiments at the material scale, or with engineering judgment. A significantly larger number of samples would have to be considered to accurately depict the distributions assigned to each of the features. The distributions may stretch into values so improbable that they are not associated to any real case. The worst-cases approach looked at realistic cases around the lower boundaries. The distribution confirms that the values from Appendix G are associated with very low probabilities; this makes them conservative and verifies them as worst-cases.

Thirdly, the probability of damage has been determined on a per-wall or façade basis. Buildings have usually several façades (and structural inner walls) and are thus more likely to have at least one damaged wall. However, maximum soil strains are also oriented in one direction and the probability of the in-plane direction of the walls matching the maximum direction of the field strains is small. The principal axes of the strains are not aligned with the building axes. Hence, the façades are more likely to experience a reduced component of the soil strains. Consequently, in line with the philosophy employed in seismic analysis, where buildings and earthquakes vibrations are also unlikely to be aligned yet the maximum component is applied to each of the building main axes, one façade per building is linked to the principal component of the soil strain and is used as representative of the probability of damage.

Finally, scenario E and its derivatives E^* and E^+ , include many detrimental effects such as pre-damage and sensitive material properties. Figure J.16 shows that removing these factors, for example cyclic effects, can lead to a significant reduction in the number of buildings above a certain threshold probability. Other effects that have not been considered, like the combination with seasonal temperature changes or local settlement loads can be implicitly included in the effects of pre-damage or cyclic loading. Hence, the number of buildings depicted by scenario E, represent an upper threshold of the direct effects of deep subsidence.

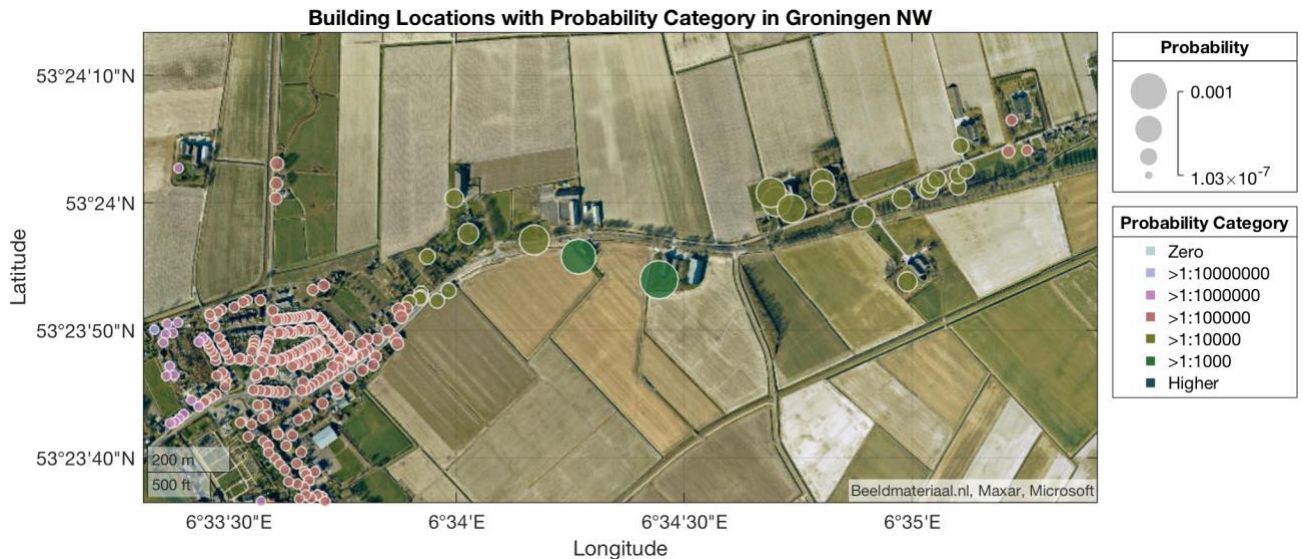


Figure J.17. Satellite view of the area with the highest probabilities, east of Warrfum. Only BAG objects from before 1975 and probabilities above 10^{-7} are shown.

Moreover, a strict criterion for damage has been implemented, namely $\Psi=1$. This corresponds to just-visible cracks of 0.1mm. This is the absolute lower threshold for damage. The probability of larger cracks is thus significantly lower. For $\Psi=2$, cracks of 1 mm in width, the probability could reduce by one order of magnitude.

To complete the picture of the probability of damage, it is also relevant to look at the buildings to which it applies. Using information from the Dutch building cadastre, buildings in the region, and buildings exceeding a probability of damage of 1 in 10'000, have been counted. The cadastre however, lists real estate objects and not individual structures. One building may be subdivided into several properties or one property may gather a few structural objects. Nonetheless, for older buildings, this discrepancy is limited. For the 30 buildings exceeding the threshold probability, the structures have been verified via satellite imagery; see Figure J.17.

A stronger building typology has also been explored. This typology doesn't correspond to any building type of Table G.3 but represents instead a typology where the mean ϵ_{AHA} is at least 25% higher than the typology E of vulnerable buildings on masonry foundations. This comprises all other building typologies expected in the region. Therefore, while no quantification can be made for other typologies in terms of probability, it is possible to conclude that their probability of damage is below the values obtained. This is sufficient to conclude that any typologies other than E are far below the threshold of probability of 1:10'000.

J.5 Conclusions

This appendix endeavoured in a quantification of the probability of damage for the vulnerable typology of old masonry buildings with unreinforced masonry strip foundations. For these buildings, the probability of visible cracks, at least 0.1 mm in width, was computed based on the horizontal strains in the soil in three regions: Groningen North West, Groningen South East, and Norg. The latter two regions fall partly outside the area where seismic damage is expected; see Figure J.18. For these regions it is thus doubly important to determine whether deep subsidence could have led to visible damage.

To determine the probability of damage, the effect of building features on the allowable, applied horizontal soil strain was decomposed and probabilistic distributions were formulated. The resulting superposition of these distributions led to the fragility of this building typology in response to the applied horizontal strain underneath the foundation. This fragility curve was then convoluted with the

distribution of horizontal strain due to deep subsidence computed throughout the region [3] and, after integration, the probability of damage was determined.

For the regions of Groningen SE and Norg (situation of 1995), the computed probability is much smaller than 1 in 10'000, concluding that deep subsidence does not lead to damage to any type of buildings. In Groningen NW, small areas have been determined where the probability of damage is between 1:10'000 and 1:800. Within this area, about 30 buildings from before 1975 are located; a portion of these buildings presumably possesses unreinforced foundations and are thus subjected to this probability. These regions are summarised in Figure J.18.

Stronger buildings, with reinforced foundations, exhibit probabilities of damage much smaller than 1:100'000 and are thus not expected to be directly affected by deep subsidence. This applies to all of the three regions mentioned.

While the probabilistic approach employed herein is simplified; it can be confidently employed to verify that horizontal strains and their associated curvatures, as a result of deep subsidence in the north of the Netherlands, are not linked to visible building damage outside of the areas already associated with seismically-induced building damage.

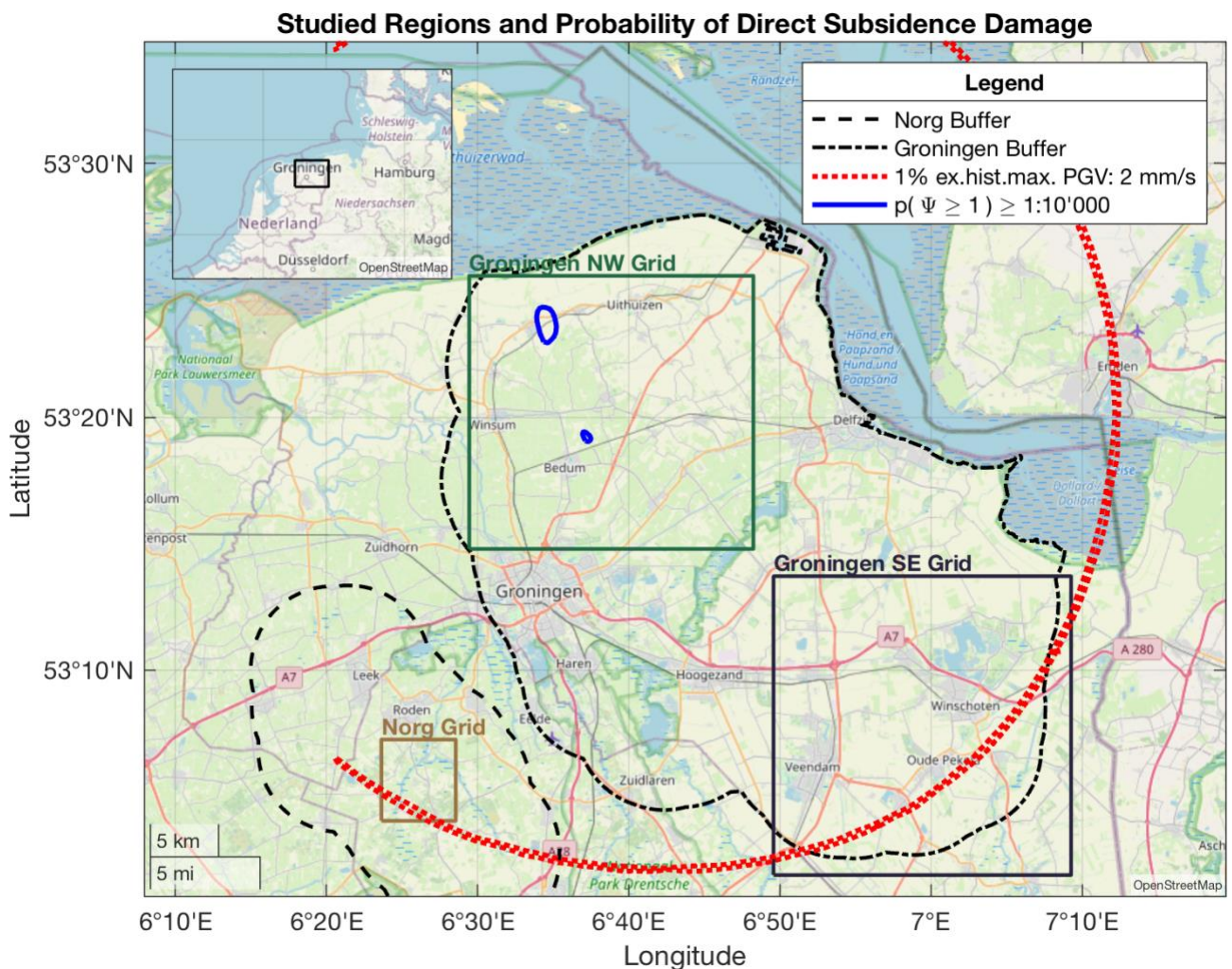


Figure J.18. Map of the Northeast of the Netherlands with the three regions studied, the 6 kilometre buffer zones of the Groningen and Norg fields, and the contour line of the 2 mm/s PGV value associated with the 1% probability of exceedance from the historical maximum. Additionally, two small regions determined in this appendix where the probability of damage due to direct effects of deep subsidence is larger than 1 in 10'000 for buildings with unreinforced masonry foundations. See also Figure J.13.

J.6 References

1. BAG (Basisregistratie Adressen en Gebouwen), Buildings and addresses database and derived 3D-BAG
www.3dbag.nl
2. Maarten Pluymaekers (2023). Memo: Additional analysis subsidence evaluation Norg. TNO AGE 23-10.024. August 2023.
3. C.P.W. Geurts, M.P.D. Pluymaekers, J.G. Rots (2021). Advies IMG: Schade aan gebouwen door diepe bodemdaling en -stijging. TNO Report R10325B, Delft 2021.

Table A - InSAR observations

Part	Page	Comment (adapted)	Reply	Action
1C	9.2	Fig 5 not identical, large curvature gradients	Figure 5 illustrates the effects of removing satellite 1 because it has partial cover. Without the additional data, the surface is expected to show higher extremes.	No actions taken.
	9.3	Comparison against GPS validates local smoothing but not spatial smoothing	This is correct; additional GPS stations would have to be compared to evaluate the goodness of the spatial smoothing employed. Also, note that the GPS comparison was done within a radius of 50m while the surface smoothing runs on a grid of 275m which will lead to damped extremes more compatible with effects from deep subsidence.	
	9.4	curvature and strain limited to section cuts, selection of geoscientific cuts could be assessed	This is a good suggestion. Plotting the derived curvature and strains would help identify areas where the effects are most pronounced. However, note that the geomechanical model has selected the section cuts with the highest values output from the model, so shifting the section cuts wouldn't lead to higher values but would help identify imperfections in the model or effects that have not been considered. Also, the derived strain/curvature are based on a simplistic Euler-Bernoulli model which would have to be adapted to 3D.	
	8.5	Uncertainty and variance in time series, confidence intervals missing	We agree that an uncertainty study was not conducted for the InSAR data. There are multiple reasons for this. Foremost, conducting a thorough uncertainty study for this type of data was unfeasible within the timeframe. Secondly, the deviations seen in the point-wise measurements are not only measuring noise; they correspond to overlapped effects such as local soil changes, temperature variations of the measured surfaces, etc. For an uncertainty study to be successful, these effects need to be quantified first. Consider the following example: measurements of mean daily temperature. The daily variations are not uncertainty, only the precision of the instruments and the number of measurement instances would be used to establish a confidence interval of the daily mean. The smoothing of the data in InSAR has been performed to look at the data that corresponds to the time scale of deep soil effects. However, unlike the example of mean temperature, determining what variations correspond to measurement imprecisions and which to local effects (throughout the day), requires a much more involved investigation, coupling perhaps the gradients from reservoir pressures to establish a relevant time scale.	
	12.1	Concerning the InSAR data analysis, given the professional level of expertise/quality employed in the data processing, there is credibility to Claim 3 – that the InSAR observations corroborate the modelling result – albeit this credibility is undermined by the absence of uncertainty quantification.		
	12.1	For the most part, it is the reviewer's opinion that while the InSAR data can reasonably be taken as support for the SADM mainly toward validating overall vertical deformation magnitudes, uncertainty may be considerably greater concerning the by-product calculations of curvature and horizontal strain – used to inform the damage indicator calculations.		
	12.1	the absence of reliable confidence intervals in the presence of data noise (see discussion above) makes the InSAR curvature and horizontal strain results difficult to evaluate – so whether those values are indeed small in a statistically-significant manner is simply unknown and not supported by the data and analysis presented.		
12.2	Likewise, it is likely that the time constraints of the projects did not lend themselves to more thorough analysis on uncertainty and model parameter sensitivity (in the case of modelling) – this is explicitly raised by the authors of 1C.			
		In sum, the uncertainty of InSAR and its processing into time-space surfaces would need to be quantified in order to increase the confidence into the results herewith obtained. Currently, efforts are being invested by other research groups into the field of processing of the raw radar data to directly obtain horizontal displacements due to the incidence angles from the various satellites. We expect that once this data is available, a richer monitoring will be obtained from InSAR.		

Table B - Computational Modelling Checks

Part	Page	Comment (adapted)	Reply	Action
1D	10.1	Masonry material model not discussed. although masonry buildings of Groningen have been widely studied numerically and experimentally, beyond refs [14,15] reported in the paper (e.g., Sarhosis et al. 2019; Blanco et al., 2018; Kallioras et al. 2018; Graziotti et al., 2016; Bal et al., 2021; Graziotti et al. 2019, etc).	The Engineering Masonry Model (EMM) for Diana has been widely employed and validated. Most references cited by the reviewer for masonry properties concern the ULS of buildings (for seismic actions) and not the SLS, some are only for calcium-silicate which are built on reinforced concrete foundations and are not vulnerable. We are familiar with many of these publications since some are own collaborations. It should be Zapico-Blanco. We can provide more detail about the material parameters.	Added discussion of existing material characterisation and properties into new Appendix G.
	10.1	the chosen masonry is relatively flexible	We have used a standard value of 5 GPa for the Young's modulus in the vertical direction. This is also the value suggested by the NPR, the dutch practical guideline, to assess existing buildings. Regardless of the stiffness of the building, its capacity to follow ground deformations without damage comes from its tensile strength. We have used a low value of 0.15 MPa and also explored the more vulnerable case of 0.10 MPa. We can explore stiffer masonry.	See appendix I with a quantification of the effect of stiffer masonry.
	10.1	foundations are stiff, should be wall enlargements	The foundations we modelled are wall enlargements; see Figure 72-0. Typically, masonry foundations have stiffer/stronger bricks but we assumed the same as the rest of the wall (conservative).	Appendix I also looks at slightly thinner foundations.
	10.1	the parametric analysis goes towards even more rigid or sliding foundations	Yes, this reinforces the fact that the situations we observed looked really at the worst case scenarios. We assumed 100% transfer when in reality the transfer is much less; we looked at poor foundations, when most buildings have better, more rigid and stronger foundations. We can discuss transfer rates.	We added appendix H that investigates transfer rates in literature and via models.
	10.1	Also, the use of calculated deformations at greenfield without façade is claimed to be worst case but is not necessarily so. The buildings can induce settlements due, for example, to their different weight distributions, soils with aquifer, soil profiles with non-homogenous layers.	The settlements at the local case are not the direct effect of deep subsidence and so were outside the scope of our study.	-
	10.1	Finally, the walls orthogonal to the facades are taken as constraint, which could have a beneficial effect, while it seems to be ignored that if these walls suffer settlements these may affect the studied facades with further damages out-of-plane in addition those in-plane discussed in the documents.	The transversal walls considered are one brick long and help provide stability to the models; they are not constraints but could be seen as reinforcement. For these type of settlements, no horizontal cracks appear at the wall edges (see Figures). Removing these one-brick long transversal walls would perhaps lead to a worse situation, but is not realistic as all walls for these types of buildings have transversal walls. Other studies show that these walls should actually be longer, so our implementation with one brick is conservative. We will compare the case without transversal walls. Out-of-plane damage has not been observed in damage claims and is presumed to be negligible for these small deformations. Indeed, as the reviewers point out, as lower stiffness leads to less damage, so are out-of-plane effects, for which walls are much more flexible, unlikely to lead to any damage due to the small deformations from deep subsidence.	Appendix I now looks at the effect of removing transversal walls.
	10.2	the use of a non-linear numerical geotechnical model, which could lead to concentration of deformation and therefore larger differential settlements, possibly detrimental for the buildings	We used a linear geotechnical model because the deformations caused by deep subsidence are so small, a non-linear model would not lead to any different results. However, it is true that horizontal heterogeneity of the soil would lead to an uneven distribution of the horizontal strains. We can explore this further.	-
	10.2	the choice of the masonry model, the foundation type, and the constraint of the orthogonal walls, could have been better justified as they do not seem to represent the worst-case conditions.	A summary table with the qualitative probabilities of each model choice would indeed have led to a clearer picture of why these are worst-case scenarios. We can elaborate a better comparison.	Appendix G focuses on providing this table.
	10.3	It appears the deep soil model is validated using 1B.	The deep soil model was used to extract a relationship between the curvature, tilt, vertical displacements and horizontal strains. These were scaled up to the worst values obtained from the geomechanical model. There was no true cross-validation.	-
	10.3	Validation with respect to comparable real structural cases would have been preferred.	There are no buildings instrumented to measure ground-based strains and deformations. Thus, no validation against structural cases can be executed. Such a study would take years of measurements to perform and would likely yield no conclusive results as the deformations from deep subsidence are too small and would be drowned by many other sources of ground-induced strains. We can include references to case-based studies.	Appendix H contains a brief literature study.
	10.4	It is claimed that different sources contribute to the settlements, however only one seems to be considered. It is not clear how it is excluded that the interaction between different sources does not determine a pejorative case.	The study had to answer the question of whether deep subsidence could lead to damage; hence, only that source was considered. However, a combination was also explored. We modelled situations where buildings had existing damage caused by other actions (or sources). Then, this initial situation was subjected to the deformations induced by deep subsidence.	In Appendixes G and J, the pejorative effect of existing damage (presumably due to the other causes mentioned) has been clearly included.
	10.4	it is not clear why the vertical strains are not relevant as well (if not the most relevant). This issue is even most relevant if the foundations decouple horizontal displacement how it is discussed at some point in the document. Emphasis seems to be given to horizontal deformations, while those vertical can cause significant damage, although apparently considered as secondary in the study.	There are no vertical strains at the ground surface. Are shear strains meant? These are considered via the curvature. The curvature is what causes damage (see literature study 1A, accepted by the reviewers). Vertical strains close to the buildings would be caused by compaction, swelling of the soil and these have no direct relationship with deep subsidence. We looked at the horizontal strains mostly, because the curvatures caused by deep subsidence are even smaller. The curvatures alone would need to be several orders of magnitude higher to cause damage (as per our study) and even larger to result in light damage according to literature (1A). This is why we took the conservative approach of combining them with the horizontal strains and enforcing the strains fully and directly (there is no decoupling).	-
	10.4	Soils-structure interaction is missing, although the vertical loads can induce differential settlements that would add-up to the effects of mining activities.	Autogenous settlements are not the cause of deep subsidence but of loads on the buildings as the reviewer points out. We included a soil-structure interface in appendix B. The interface implemented had vertical and horizontal stiffness to allow the soil to deform as the load distribution in the building changed due to the effect of deep subsidence (second order effect). This didn't lead to more damage; instead, with coupled soil-structure interaction, the soil cushions the applied soil deformation and the building deforms less. This is also why our approach of directly applying 100% of the soil deformation in the main model is conservative/worst-case.	-
	10.5	It is not clear whether further settlements are expected after the dismissal of the field; if so, it is not clear how future evolution of settlements in Groningen area is accounted for.	This is a good point but should be addressed by the values obtained from the geomechanical models.	Additional calculations consider increased values of soil strains.

Part	Page	Comment (adapted)	Reply	Action
	10.5	In one year, the settlements go from minimum to maximum cyclically due to mining activities, so there is also an effect of cumulative damage and cyclical action, which is not clearly taken into consideration. Cumulative effects were not fully accounted for. Only cyclic effect is mentioned in Appendix C, but the masonry hysteretic model used is unclear, as well as that of interfaces with soil. Moreover, the effect of ten cycles seems almost null, which let the reviewer think that cyclic modelling may be not adequate (this may be a limitation of DIANA or the reduced number of cycles).	We looked at the cyclic situation; see Section C.3. This effect does lead to an increase in damage visible in our DIANA models. We applied 10 cycles. For one façade the effect was negligible, but the others showed damage over the cycles. So, accumulation of damage is considered. We investigated this looking at the margin between the strain/curvatures needed to cause damage and the actual strain/curvatures arising from deep subsidence. The EMM has hysteresis and is a key part of our study.	In appendix G/J cyclic effects contribute to a 25% reduction of the allowable horizontal strain.
	10.6	It appears that the studied settlements are much lower than those that would cause visible damage, given that the study of the effects of settlements is very sensitive to the properties of the masonry, internal constraints between the walls, design and configuration of the foundations.	Correct. We looked at the effect of the actual values and the critical threshold that would cause damage.	This is further explored in appendixes G and J.
	11.1	It is not clear whether the settlements detected in situ were used, or if the model has only been calibrated on horizontal strains neglecting the vertical ones.	There are no measurements of settlements detected in situ from deep subsidence. Any measurement performed will be the sum of many effects, most not attributable to deep subsidence. So, our building models use the combination of horizontal strains and soil curvatures (what the reviewer refers to as vertical strains, we suspect) that the geomechanical model indicates are the product of deep subsidence. No contribution of deep subsidence is neglected.	-
	11.1	Therefore, the questions of IMG were answered, but the assumptions made are often on the side of reducing vulnerability and the parametric analysis are not necessarily on the safe side...	The reviewers have not indicated why they think our choices reduce vulnerability. On the contrary, all the choices were made with the purpose of increasing the potential for damage and thus verifying that the deformations caused by deep subsidence are far from the critical values that would cause damage on buildings.	The choices and their effects have been made clearer in Appendix G.
	11.1	... while a wider variability should be explored, and as close as possible to in-situ reality.	We argue that our worst-case scenarios are actually far from the typical building in the sense that they are more vulnerable. However, how far and what is the distribution of vulnerability is not explored. Indeed, a thorough quantification of the probability of damage due to deep subsidence was outside the scope of our study and would greatly benefit the understanding of vulnerability.	An approximation of the probability of damage is now provided in Appendix J.
	11.3	Stresses and damages in the foundations are never shown, is there any damage inferred from the FEM analysis?	Yes, sometimes cracks also continue into the foundations (which are masonry and non-linear). Stresses are shown in the foundations, for example Figure 73.	We have also added a figure with clear cracks in the foundation in new Appendix I.
	11.3	It is claimed: "Note that no damage is found for any of the cases; the stresses remain in all cases, below the assumed masonry tensile strength". Then, should a linear analysis lead to the same results? If yes, why all the hypotheses on the nonlinear modelling?	For the actual strain/curvatures caused by deep subsidence, our models show linear buildings. However, we looked at the magnification factor of these loads required to display visible damage. Then, the models need to be non-linear.	-
	11.3	Figures 20-22 show tensile stress reducing with respect to the principal stresses, which seems impossible in principle. Same for figures 27-29. Perhaps these are different loading steps. This should be clarified.	In building modelling the convention is to have tension in the positive direction. The figures show horizontal, vertical, and principal stress respectively. The principal stress is larger in both cases (figure 22 and 27).	-
	11.3	Could there be any interaction with earthquake vulnerability after damages due to settlement?	This was not part of the question from IMG. In any case, the models predict no settlement damage from deep subsidence so there is also no interaction with earthquakes. In other situations, where existing settlement damage (from other causes) is present, earthquake vibrations will undoubtedly have an effect. Yet, vibrations in the area investigated by this study are below the threshold of "presumptive evidence". This combination is more likely in regions close to the epicentres of the earthquakes, where damage from the mining activities (be it from vibrations or subsidence) is not disputed.	-
	12.4	Lastly, concerning Claim 5, the study presented in 1D contains a large number of variations including complex modelling but fail to represent the worst-case conditions or at least fail to sufficiently justify the assumptions made. This is mostly with regards to the stiff foundations used and relatively rigid masonry.	We believe that the worst-case situations are covered. More detrimental situations would be unrealistic and still likely to be above existing strain/curvatures thresholds. Additional justifications are possible and would help paint a better picture of why these are indeed worst-case scenarios. A full probabilistic characterisation is also possible and will help provide probabilities of damage.	We have combined all detrimental effects into a realistic scenario E treated in Appendix G and explored probabilistically in Appendix J.
	16.3	Furthermore, the review concluded that the masonry modelling and foundation modelling do not guarantee the worst case conditions or at least have not been sufficiently justified. Therefore damages can be more severe than reported. This is mainly due to:	We can consider a few even-more-vulnerable scenarios as per the suggestions of the reviewers.	
	16.3	Façade is modelled as relatively flexible giving relative low vulnerability to differential settlements.	We used the stiffness of the NPR and, while poor masonry should be more flexible, we kept the same high stiffness and only reduced the strength. We can explore stiffer masonry.	New in appendix I.
	16.3	Foundations are modeled relatively stiff resulting in relative low transmission of settlements to the facades.	We disagree. The masonry foundations are modelled as wall enlargements with the same Young's modulus as the rest of the wall when in reality bricks and mortar for foundations are stiffer. Also, remember that we have enforced 100% of soil deformations; in this case the stiffness of the foundation is irrelevant.	In appendix I, thinner foundations are explored.
	16.3	Orthogonal walls to facades are taken as constraints which can actually have a beneficial effect.	Transversal walls are not constraints in the model but beam elements. This leads to a realistic situation. See before.	In appendix I, the effect of transversal walls is quantified.

Memo

Send to Instituut Mijnbouwschade Groningen
Author Maarten Pluymaekers
Subject Additional analysis subsidence evaluation Norg
 and Groningen

www.tno.nl
maarten.pluymaekers@tno.nl
+31646327072

Date
10 August 2023
Our reference
AGE 23-10.024

1. Introduction

Commissioned by the Ministry of Economic Affairs and Climate (EZK), Movares (2022) conducted a review of the TNO report "Effecten diepe bodemdaling en -stijging rondom de gasopslag Norg en het Groningenveld" (TNO, 2021a). The *Instituut Mijnbouwschade Groningen* (IMG) has asked TNO, as a result of this external review, to conduct additional work to give substance to the observations and comments formulated.

To follow-up on the reviewers comments and suggestions additional work is performed to further quantify the uncertainty of the used model parameters, perform a sensitivity analysis and evaluate the model results on a 2D grid for both Norg and Groningen.

2. Subsidence modelling UGS Norg

2.1. Evaluation of results on 2D grid

The initial analysis was performed on six transects over the Norg field. To give a more extensive view of the spatial development of the subsidence and derived indicators, the initial subsidence model is evaluated on a 2D grid. This addresses two identified issues: (1) the maximum curvature and horizontal strain may not be on the selected transects; (2) the curvature and strain results of the transects were based on maximum values in the East-West and North-South directions. This lead to inconsistencies of the results most visible on the intersections of the transects.

In this analysis the horizontal strain is defined as the maximal principal horizontal strain based on the resulting strain tensor. In a 2D evaluation (e.g. [Figure 1](#)) the direction of the maximal principal horizontal strain spatially varies. In further analysis it is assumed that a building is aligned in the most unfavourable direction, the direction of the maximum principal horizontal strain. This assumption is a (true) worst case approach, since the horizontal strain is the governing loading parameter (TNO, 2021c)

The spatial development of the horizontal strain and curvature of the 'Norg 1995' reference scenario is given in [Figure 1](#).

To test the sensitivity of grid cell size, results of 500m, 200m and 100m grid cell dimensions were compared. The spatial resolution of the initial transect results is 100m.

The results are summarized in [Figure 2](#). The initial evaluation on transects underestimates the maximum value of the horizontal strain. Using a 2D grid evaluation, the maximum horizontal strain for the 'Norg 1995' reference scenario is $1.7 \cdot 10^{-5}$ m/m. The maximum curvature is unaffected by the 2D grid evaluation. From the grid cell size sensitivity analysis it is concluded that the use of a 500m grid cell size resolution slightly underestimates the maximum values of curvature and horizontal strain. Results with 200m cell resolution are comparable with 100m resolution. To reduce calculation time, in the further sensitivity analysis a grid resolution of 200m is used.

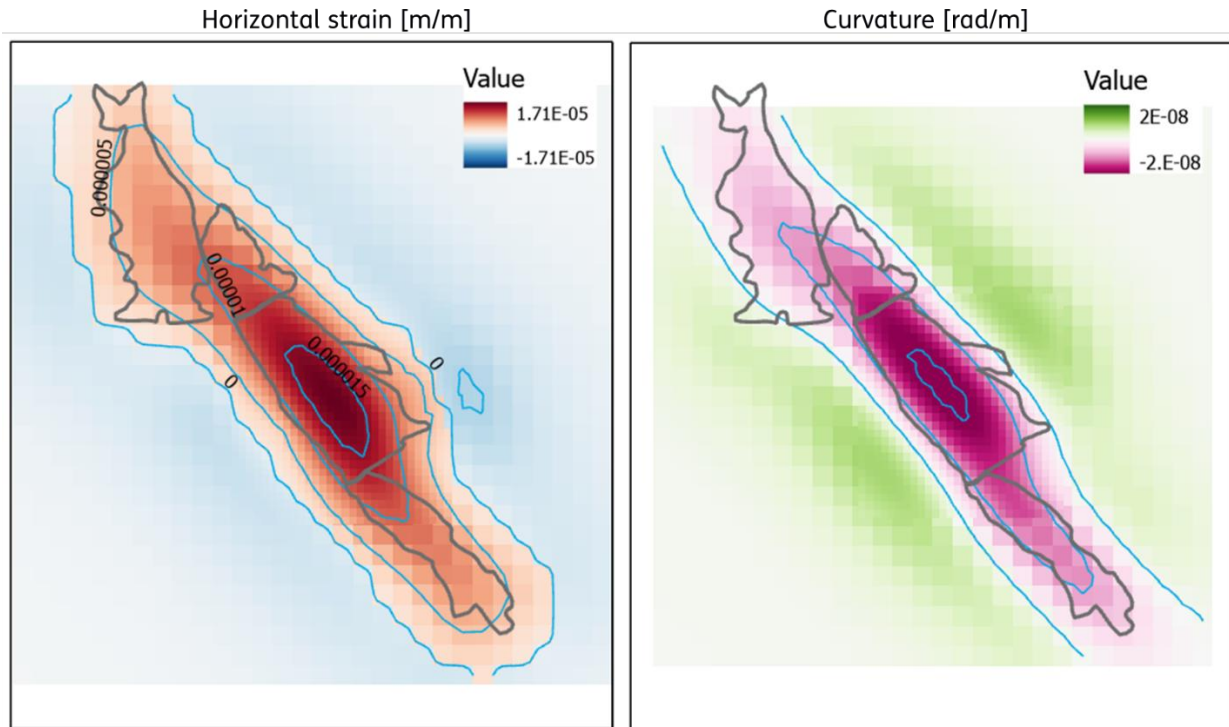


Figure 1: Reference case 'Norg 1995'. Spatial development of horizontal strain (left) and curvature (right). A grid resolution of 200m is used in the centre and 500m resolution outside that area. The outlines of the Norg field are represented in black. The horizontal strain grid is overlain by $0.5 \cdot 10^{-5}$ m/m contouring interval; the curvature grid is overlain by $1.0 \cdot 10^{-8}$ rad/m contouring interval.

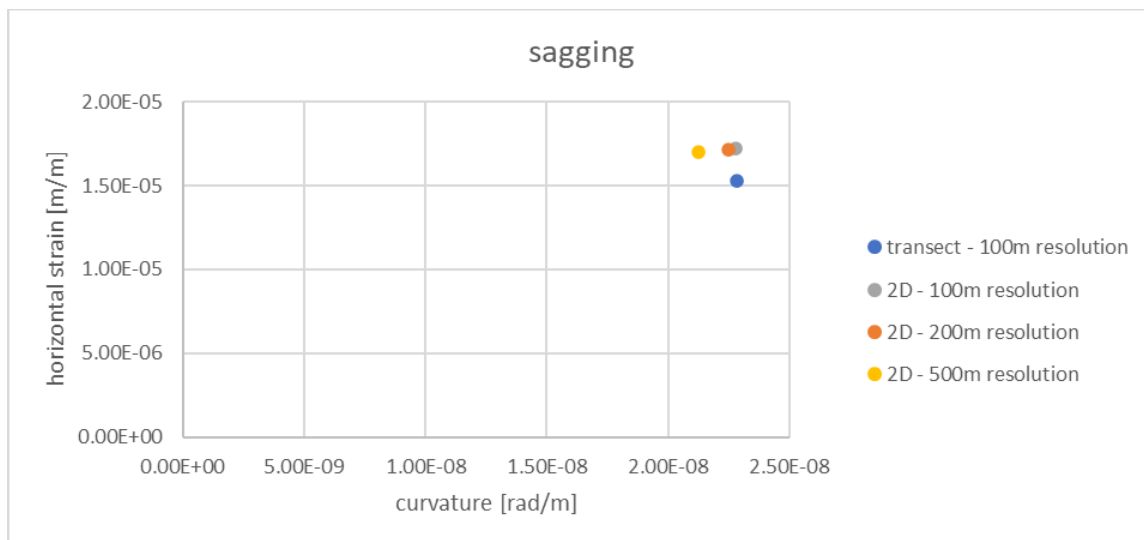


Figure 2: Reference case 'Norg 1995'. Maximum horizontal (compression) strain and curvature of the evaluated grid with different resolution (grey, orange, yellow) compared to initial evaluation on transects (blue).

2.2. Sensitivity analysis

The surface curvatures for Norg when converted at the scale of the building are far below the threshold values for expected damage (TNO, 2021b; Korswagen et al., 2021). Therefore in this sensitivity study very limited attention is given to surface curvature as a damage indicator.

Figure 3 schematically represents the SADM modelling approach, where volume loss due to compaction of a unit of reservoir rock (A) is semi-analytically transferred into an elementary subsidence bowl (B). The magnitude of compaction determines the volume of the elementary subsidence bowl. The elastic properties of the subsurface determine the shape of the elementary subsidence bowl. In the following sensitivity analysis both compaction volume (A) and elastic properties (resulting in B-B') are addressed.

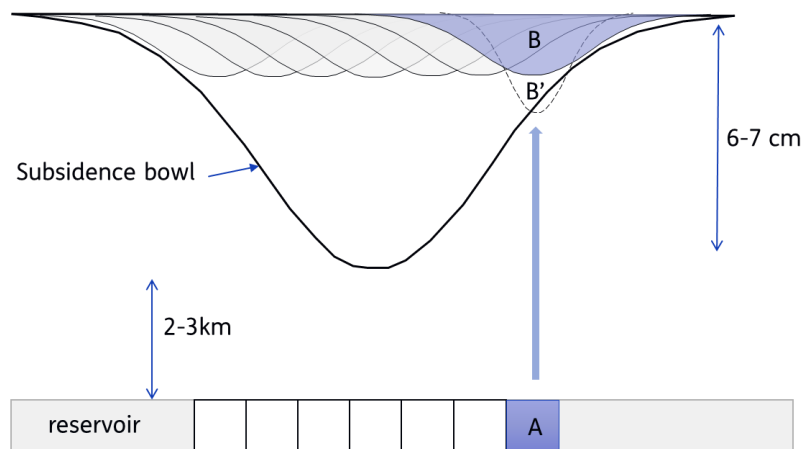


Figure 3: Schematic (2D) representation of 3D SADM modelling approach. Volume loss due to compaction of a unit of reservoir rock (A) is semi-analytical transferred into an elementary subsidence bowl (B). All elementary subsidence bowls contribute to the total subsidence bowl. Different elastic properties of reservoir and overburden rock can result in alternative shape of an elementary subsidence bowl (B').

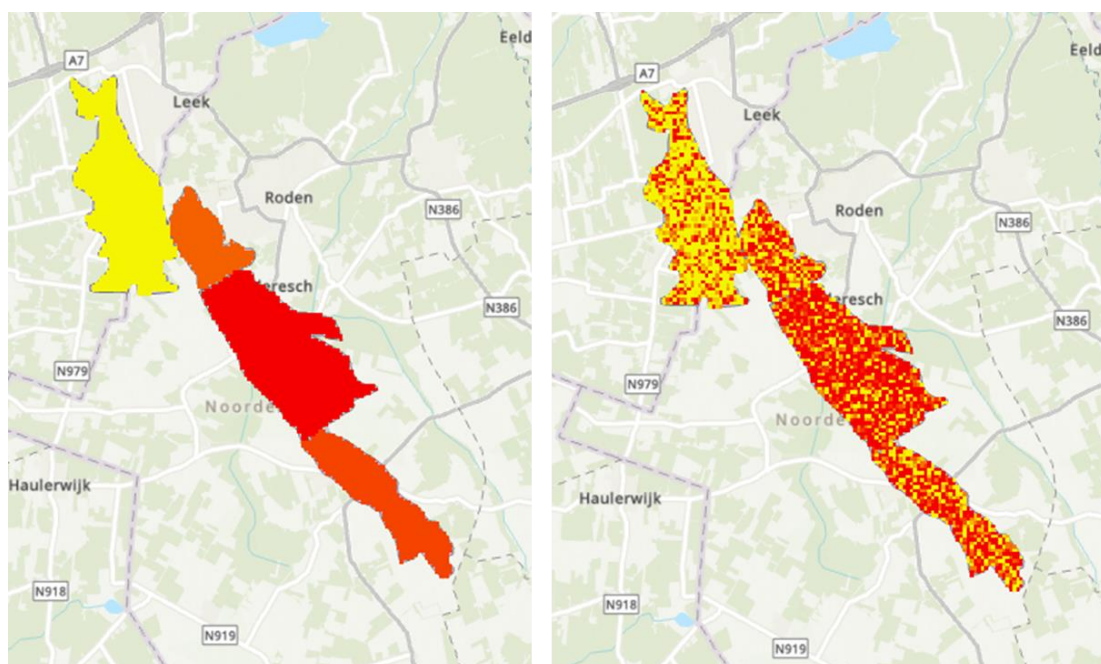
2.2.1. Reservoir heterogeneities

Heterogenous distribution of reservoir properties can effect local reservoir compaction indirectly by heterogeneous or compartmentalized reservoir depletion and directly by varying elastic and/or compacting properties of the reservoir rock. With respect to the used modelling approach, all these variables are discounted into absolute reservoir compaction (volume reduction). Several studies (Muntendam-Bos & Fokker, 2009; Fokker et al., 2012, 2016) demonstrated that inversion of subsidence observations at the surface is capable to estimate a (spatial varying) reservoir compaction field and (homogeneous) elastic properties.

To evaluate the effect of uncertainty of reservoir compaction, a single random compaction grid was constructed (**Figure 4**) based on a specified mean and standard variation assuming a normal distribution. The total compaction volume of each reservoir block is comparable to the base case regardless of the spatial variation. The spatial correlation length of compaction coefficients could not be derived from available data and therefore was assumed smaller than the grid size. This is represented in **Figure 3** as compaction volume variation per grid cell (A). The standard deviation was estimated through propagation of uncertainty of the individual variables (**Table 1**). Uncertainty estimates of pressure depletion (dP) and reservoir thickness (H) are relatively low due to availability of multiple wells and production history. Uncertainty of the compaction coefficient is estimated from core experiment data (Shell, 2008).

Table 1: Mean and standard deviation of dP (pressure depletion), H (reservoir thickness) and Cm (compaction coefficient).

variable	μ	σ
dP (Pa)	$6.6 \cdot 10^6$	$2.0 \cdot 10^5$
H (m)	184	5
Cm (Pa ⁻¹)	$4.4 \cdot 10^{-11}$	$2.0 \cdot 10^{-11}$
dP * H * Cm	0.053	0.024

**Figure 4:** Reservoir compaction based on the homogeneous 'Norg 1995' scenario (left) and reservoir compaction including normal distributed variation (right). Colours indicate the amount of reservoir compaction (yellow: low, red: high)

Using the above mentioned input data results in a maximum value of horizontal strain of $1.75 \cdot 10^{-5}$ m/m, which is slightly larger than the maximum horizontal strain for the 'Norg 1995' reference scenario: $1.7 \cdot 10^{-5}$ m/m.

2.2.2. Vertical elastic heterogeneities

In the original study homogeneous elastic properties (Young's modulus: E and Poisson's ratio: ν) of the subsurface were assumed ($E = 10$ GPa, $\nu = 0.25$). The range of representative average elastic properties for the main lithostratigraphic intervals are derived from previous studies, literature and well-log derived values (Orlic, 2016; Lele et al., 2016; Hazel, 2018; Buijze et al., 2019) and is given in [Table 2](#).

Table 2: Range of elastic properties and generalized depth intervals of the main lithostratigraphic intervals. NU: Upper North Sea Group, NL: Lower North Sea Group, CK: Chalk Group, KN-RN-RB: Rijnland – Upper & Lower Germanic Trias Group, ZE: Zechstein Group, RO: Upper Rotliegend Group.

Strat	litho	Depth (m)	E (GPa)	ν (-)
NU-1	sand	0-400	0.25 – 2.5	0.3 – 0.38
NU-2	clay	400-500	0.25 – 2.5	0.3 – 0.38
NL	clay	500-800	0.25 – 2.5	0.3 – 0.38
CK	chalk	800-1600	10 – 20	0.25 – 0.3
KN-RN-RB	sand/shale	1600-2000	15 – 20	0.25 – 0.3
ZE	halite	2000-2650	30 – 35	0.35
RO	sand	2650-2824	15 – 25	0.1 – 0.25

The impact of elastic variation in the depth domain is assessed through four different elastic scenarios. Input values are given in [Table 3](#) and visualized in [Figure 5](#), and can be described as follows:

- Scenario 1: stiff lower part of North Sea Group; low stiffness of Zechstein halite & Chalk
- Scenario 2&3: stiff lower part of North Sea Group; higher stiffness of Zechstein & Chalk
- Scenario 4: (constant) low stiffness of North Sea Group

Because of the limited number of elastic scenarios evaluated in this study the choice was made to use elastic properties outside the expected range for some intervals ([Table 2](#)) in scenario 1-3. This potentially leads to unrealistic elastic properties for some of the intervals. The aim of this approach is to explore the potentially upper and lower boundaries of the resulting horizontal strains and curvatures. Scenario 1 explores the sensitivity of the elastic properties of the thick Zechstein halite and Chalk layers. In this scenario (unrealistically) low values of Young's modulus and Poisson's ratio are chosen to evaluate the contribution to the total horizontal strain. In addition to that the lower part of the North Sea Group (NU-2 & NL) is assumed (unrealistically) stiff. In scenario 2&3 more realist elastic values for Chalk, Zechstein & Rotliegend layers are evaluated, and the lower part of the North Sea Group (NU-2 & NL) is still assumed (unrealistically) stiff. Scenario 4 is regarded the most representative for the Norg area.

Table 3: Elastic properties of the main stratigraphic intervals for scenario 1-4. NU: Upper North Sea Group, NL: Lower North Sea Group, CK: Chalk Group, KN-RN-RB: Rijnland – Upper & Lower Germanic Trias Group, ZE: Zechstein Group, RO: Upper Rotliegend Group, DC: Limburg Group. RB = Rigid Basement.

Strat	litho	E (GPa)		ν (-)		E (GPa)		ν (-)	
scenario		1		2		3		4	
NU-1	sand	0.25	0.38	0.25	0.38	0.25	0.38	1	0.38
NU-2	clay	10	0.18	10	0.18	10	0.18	2	0.35
NL	clay	15	0.23	15	0.23	15	0.23	2.5	0.3
CK	chalk	10	0.3	20	0.3	20	0.3	15	0.3
KN-RN-RB	sand/shale	20	0.3	20	0.3	20	0.3	20	0.25
ZE	halite	15	0.18	35	0.35	30	0.3	35	0.35
RO	sand	15	0.18	35	0.35	30	0.3	25	0.25
DC	sand/shale	RB	0.25	RB	0.25	RB	0.25	RB	0.25

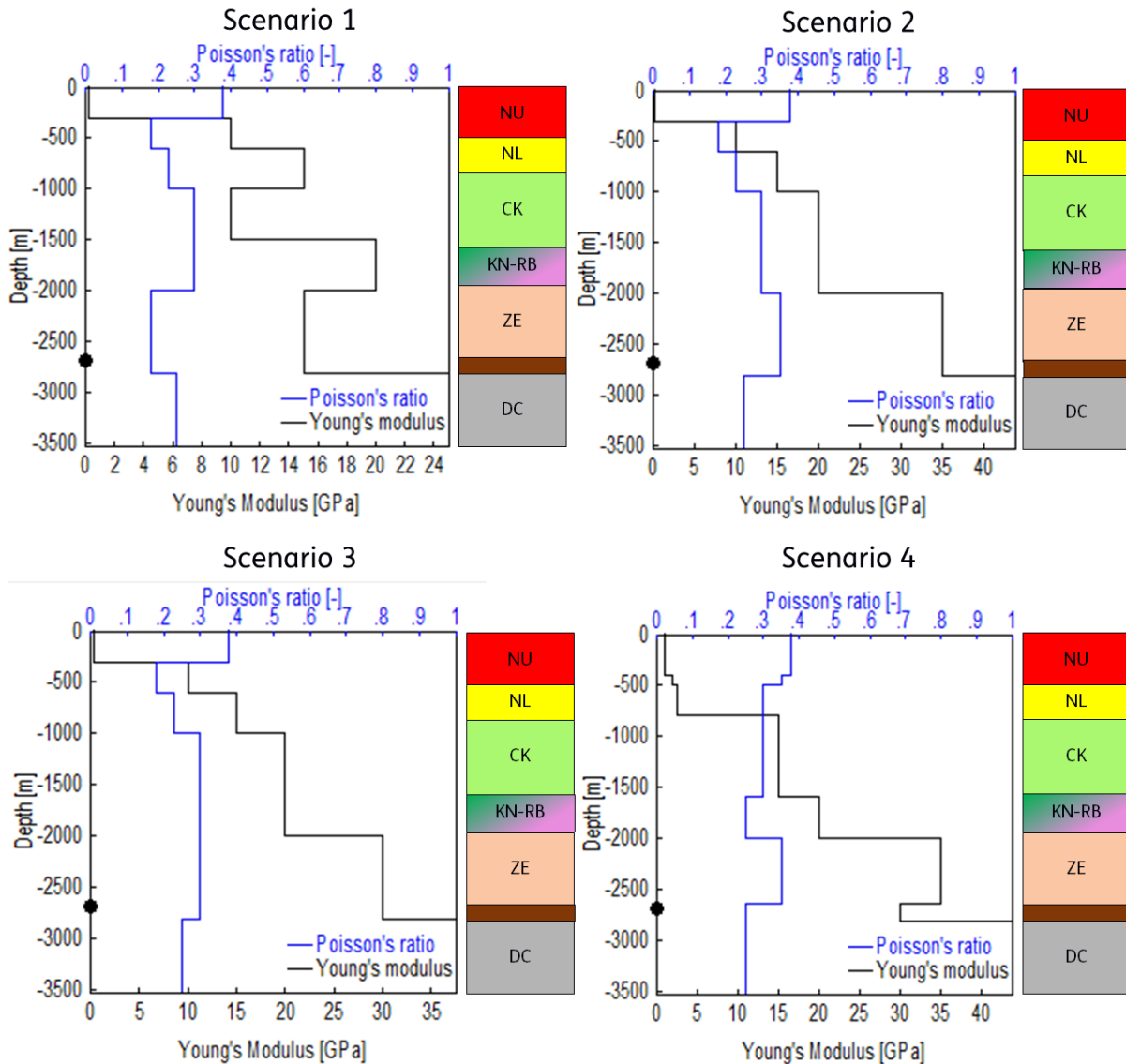


Figure 5: Generalised vertical elastic profile of scenario 1-4 of various stratigraphic units. NU: Upper North Sea Group, NL: Lower North Sea Group, CK: Chalk Group, KN-RB: Rijnland – Upper & Lower Germanic Trias Group, ZE: Zechstein Group, Brown (RO): Upper Rotliegend Group, DC: Limburg Group. The black dot shows the Norg reservoir depth.

Especially for the shallow lithostratigraphic unit (NU), a strong depth dependence of elastic rock properties is expected. The lower and upper bound of the range in Table 3 are representative for respectively the shallow and deeper part of the lithostratigraphic interval. Using a single deterministic value for this 400m lithostratigraphic interval (NU) thus likely over- or underestimates elastic properties in certain parts of the depth interval. This is further addressed in section 2.2.3.

Results of the four elastic scenarios are given in Figure 6. All four scenarios result in significantly higher values of the (maximum) horizontal strain, and ranges from $2.6 \cdot 10^{-5}$ to $3.0 \cdot 10^{-5}$ m/m. The corresponding maximum curvature shows a slight increase. Changing elastic properties results in a different shape of the subsidence bowl. The absolute depth of the deepest point of the subsidence bowls of scenario 1-4 is fairly constant. Differences in vertical deformation between the four elastic scenarios and homogeneous base case are less than 0.5 cm (regarding the deepest point).

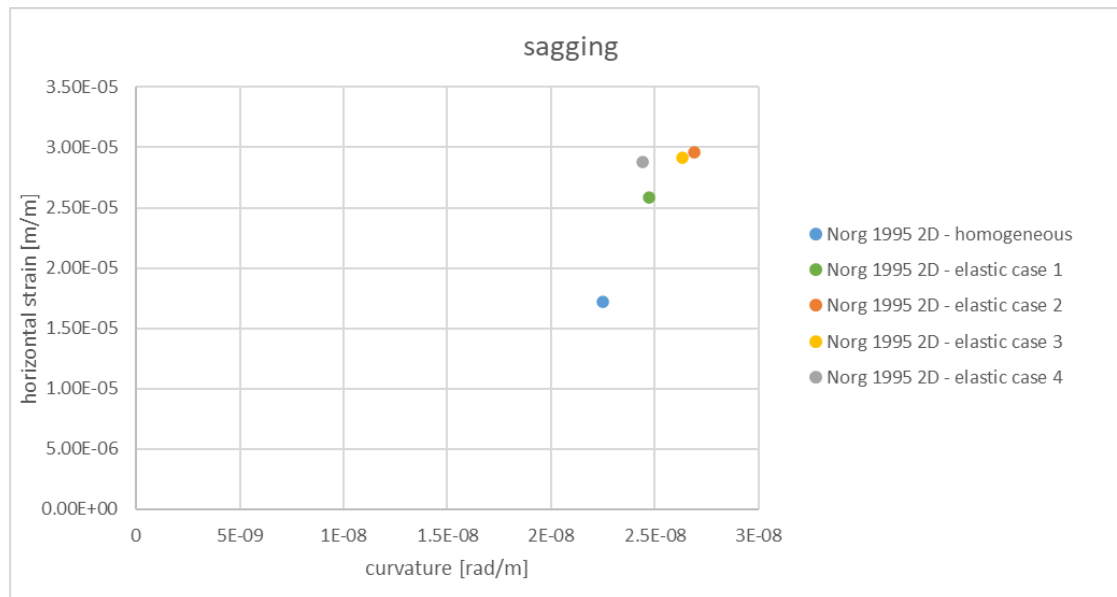


Figure 6: Reference case 'Norg 1995'. Maximum horizontal (compression) strain and curvature of the four heterogeneous scenario's (green, orange, yellow, grey) compared to the homogeneous elastic case (blue) based on 2D evaluation.

2.2.3. Near-surface elastic properties

To further explore the sensitivity of variation of elastic properties of the near-surface strata, we vary the (constant) elastic properties of the upper 400 meters (NU-1). In this analysis near-surface is defined as the upper 400m. For the scenarios 1-3 the effect of increasing the Young's modulus (E) from 0.25 to 1 GPa is assessed and additionally a decrease of the Poisson's ratio (ν) from 0.38 to 0.3. For scenario 4, Poisson's ratio of the first three layers are varied (all part of North Sea Group).

Results are shown in **Figure 7**. Per scenario the maximum horizontal strain varies 2-4% due to varying the elastic properties of the upper 400m. Increasing the Young's modulus leads to a decrease of the maximum horizontal strain and curvature. Decreasing the Poisson's ratio leads to an increase of the maximum horizontal strain and curvature. The variation of deepest point of all modelled subsidence bowls in the sensitivity analysis is less than 1 cm.

To assess the impact of averaging elastic properties of the upper 400m, two additional scenario's with a very low stiffness top layer of 15m and respectively 50m with a Young's modulus of 0.05 GPa were calculated. The properties below 400m are cf. Scenario 4. This results in a maximum horizontal strain of respectively $3.0 \cdot 10^{-5}$ and $3.1 \cdot 10^{-5}$ m/m. This effect on the maximum horizontal strain is of comparable magnitude as results from the near-surface sensitivity analysis where the elastic properties of the full 400 meter upper layer is varied. The variation of maximum horizontal strain as a result from the four different main scenarios is larger than the case where the stiffness of the very shallow top is varied.

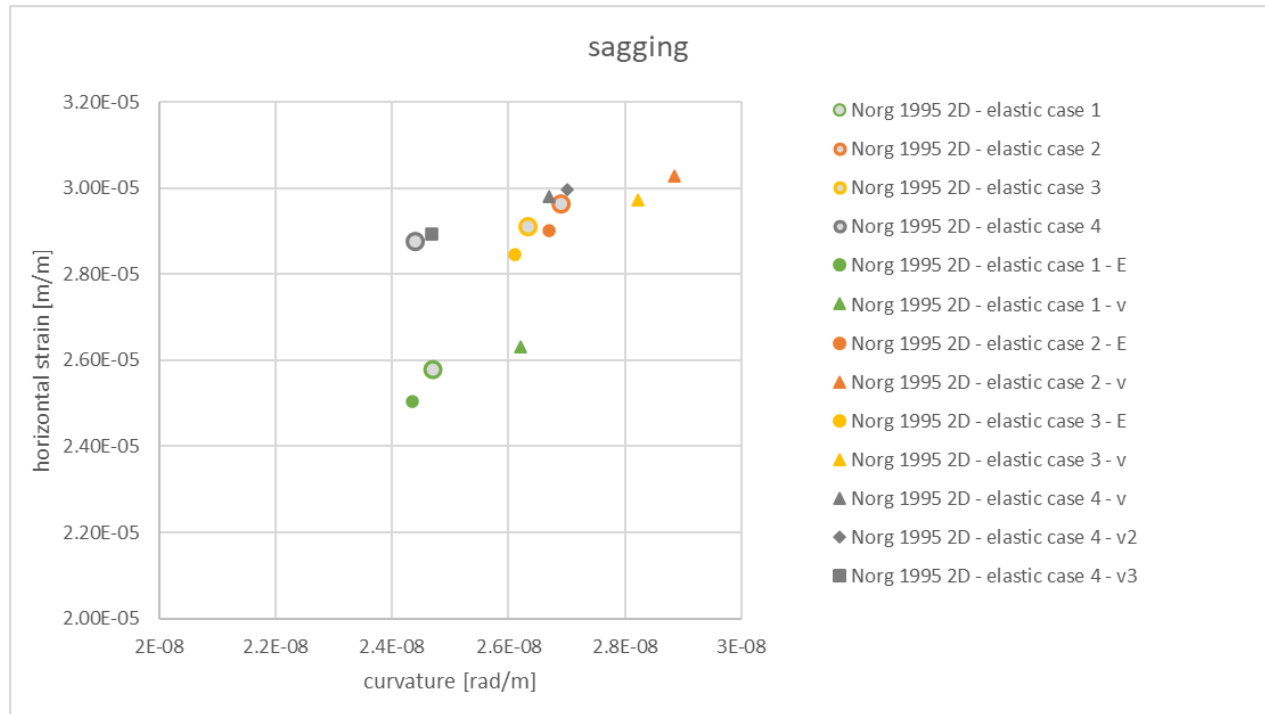


Figure 7: Reference case 'Norg 1995'. Maximum horizontal strain and curvature of the four heterogeneous scenario's (green, orange, yellow & grey circular symbols) compared elastic variations. Same colour indicate same scenario below the North Sea Group. E: 1 GPa, v: 0.3. For scenario 4 v: NU-1/NU-2/NL: 0.3/0.35/0.3, v2: NU-1/NU-2/NL: 0.3/0.3/0.3, v3: 0.38/0.3/0.3

2.3. Damage indicators Norg cases

Based on the elasticity profile Scenario 4 described in section 2.2.2 the damage indicators horizontal strain and curvature are calculated on a 2D grid for the three Norg pressure depletion cases. [Table 4](#) shows the results differentiated for the sagging and hogging results for each case.

Table 4: Maximum horizontal strain and curvature values for the Norg Scenario 4 pressure depletion cases. Compression strain is positive, tensile strain is negative.

Scenario Norg	Type	Location	Max Horizontal strain (m/m)	Max Curvature (rad/m)	
Max depletion 1995	subsidence	centre	29 10 ⁻⁶	24 10 ⁻⁹	sagging
		perimeter	-10 10 ⁻⁶	11 10 ⁻⁹	hogging
UGS full depletion	subsidence	centre	22 10 ⁻⁶	18 10 ⁻⁹	sagging
		perimeter	-8 10 ⁻⁶	8 10 ⁻⁹	hogging
UGS full injection	heave	centre	-4 10 ⁻⁶	2 10 ⁻⁹	hogging
		north & south	2 10 ⁻⁶	3 10 ⁻⁹	sagging

Note that the maximum pressure depletion of the reservoir during the gas extraction phase of the Norg field in 1995 is used as the reference scenario. For the transition from gas production to UGS, cushion gas was injected to increase the reservoir pressure. The current pressure range of the Norg gas storage facility is limited by the prevailing storage license. The minimum reservoir pressure allowed by the use of the gas storage is more than 30 bar above the 1995 level. This means that the surface deformation resulting from the current use of the gas storage is considerably less than occurred in 1995 (reduction

of approx. 25% in case of an empty gas storage and a reduction of approx. 85% in case of a full storage). The scenario "maximum gas extraction Norg 1995" is therefore the most unfavourable situation that has occurred to date with respect to the maximum deformations and the related strains and curvatures.

Figure 8 shows the spatial distribution of horizontal strain as a result of the 'Max depletion 1995' case using the Scenario 4 elasticity profile. This figure focuses on the main reservoir block where the pressure depletion is largest. Horizontal strain and curvature above the other reservoir blocks is significantly lower.

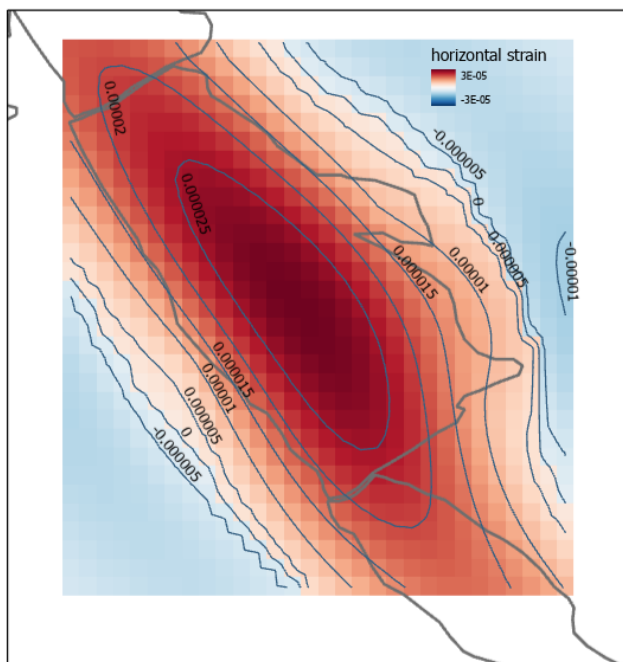


Figure 8: Horizontal strain (m/m) cf. Scenario 4 for the case maximal depletion in 1995 for the Norg main block.

2.4. Horizontal strain distribution Norg case 'Max depletion 1995'

2.4.1. Uncertainty elastic properties

Although the model results based on elastic profile Scenario 4 is regarded as the most realistic, all cases served as input for defining a probability density function of the horizontal strain. Because of the limited number of elastic scenarios evaluated in this study the choice was made to use elastic properties outside the expected range for some intervals in scenario 1-3 in order to capture the full range of the potential horizontal strain distribution. A weighting of the four cases was applied to derive the mean and standard deviation of the horizontal strain for each grid cell. Scenario 4 was weighted double because this is regarded the most realistic case where the other cases deliberately contain unrealistic elastic properties of some layers. Scenarios 2 and 3 were both weighted half, because both scenarios are from a geological perspective very similar, and therefore overrepresented in this limited set of four simulations. A single weighting is applied to scenario 1.

Figure 9 shows the resulting probability density function for the weighted scenario's, in this example for the surface location where the maximum horizontal strain is reached. The horizontal strain is assumed to be normal distributed. As a result of combining these four elastic scenario's in some areas the

horizontal strain has the probability to be positive (tensile strain) as well as negative (compressional strain) especially around the tipping point between a sagging to a hogging situation. If one prefers to evaluate the tensile and compressional strain cases separate, the use of a lognormal distribution is an obvious approach. Differences especially reflected in the shape of the tails of the distribution.

Note that the results of the near-surface variations (section 2.2.3) lie within the P95 interval of the distribution based on the weighting of the four scenario's.

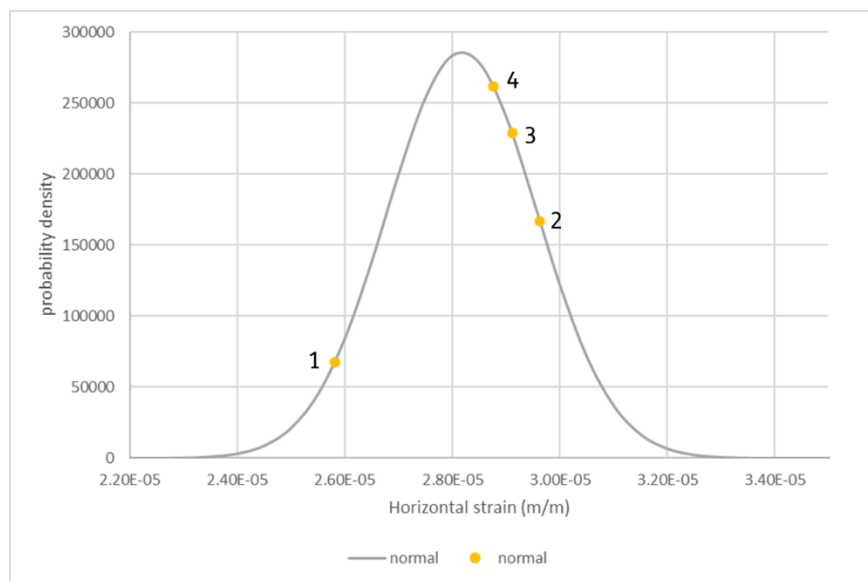


Figure 9: Probability density function of the maximum horizontal strain for the weighted Norg scenario's. Yellow markers indicate the four individually numbered cases. The grey curve represents a normal distribution with mean $2.8 \cdot 10^{-5}$ m/m and standard deviation $1.4 \cdot 10^{-6}$ m/m.

For each evaluated grid cell, the resulting probability density function of horizontal strain can be described by a mean (μ_{strain}) and standard deviation ($\sigma_{elastic}$) due to the uncertainty of elastic properties. Analysis of the results show that $\sigma_{elastic}$ is dependent on μ_{strain} , therefore the uncertainty can be expressed as a coefficient of variation where

$$\sigma_{elastic} = 0.05 * \mu_{strain}$$

This is valid for all the evaluated grid cells in the Norg modelling area.

2.4.2. Uncertainty reservoir compaction and total uncertainty

Variation in elastic subsurface properties is not the only source of uncertainty. Uncertainty due to variation of reservoir thickness, pore pressure depletion and the compaction coefficient of the reservoir rock also exist and should be taken into account. For simple (bowl shape) subsidence cases the increase/decrease of vertical surface deformation can be assumed to have linear relation with (horizontal) surface strain. For example a 10% increase of vertical surface deformation results in approximately 10% increase in horizontal surface strain. This relation allows us to estimate the horizontal strain uncertainty due to uncertainty of reservoir compaction (combining the uncertainty of reservoir thickness, pore pressure depletion and compaction coefficient)

To incorporate this source of uncertainty we introduce $\sigma_{\text{reservoir}}$, representing the horizontal strain uncertainty due to uncertainty of the various components defining reservoir compaction combined with the uncertainty introduced by model imperfections.

Modelling results of vertical deformation are constrained by surface deformation measurements. The typical uncertainty bounds (P95 or 2σ) of the measurement in the Norg area is 1 cm (NAM, 2018). The equivalent standard deviation is then approx. 0.6 cm. The deepest point in the subsidence bowl is approximately 6 cm.

The horizontal strain uncertainty ($\sigma_{\text{reservoir}}$) due to reservoir compaction and model imperfection can therefore be approximated by a coefficient of variation where

$$\sigma_{\text{reservoir}} = 0.1 * \mu_{\text{strain}}$$

The total uncertainty is the product of both components.

$$\sigma_{\text{total}} = \sqrt{\sigma_{\text{elastic}}^2 + \sigma_{\text{reservoir}}^2}$$

$$\sigma_{\text{total}} = 0.112 * \mu_{\text{strain}}$$

As noted, elastic variation leads to a different shape of the modelled subsidence bowl, that is reflected in both the horizontal surface strain and the vertical deformation. Combining the both uncertainty components is a conservative approach because the variation of vertical deformation is now captured by $\sigma_{\text{reservoir}}$ and additionally also by σ_{elastic} .

3. Subsidence modelling Groningen gas field

3.1. Evaluation of results on 2D grid

To give a more extensive view of the spatial development of the subsidence and derived damage indicators, the initial subsidence model is evaluated on a 2D grid.

An example is given in [Figure 10](#) for the ‘Groningen 2016’ scenario with homogeneous elastic properties. Using a 2D grid evaluation, the maximum horizontal strain for the ‘Groningen 2016’ scenario is $2.6 \cdot 10^{-5}$ m/m. The maximum curvature is $2 \cdot 10^{-8}$ rad/m. The maxima are located in the Bedum area. Note that absolute maximum value of the strain evaluation is dependent on the grid cell size resolution as discussed in section 2.1. A grid resolution of approx. 700m was used to keep computational times within acceptable ranges, but this comes at a cost of numerical accuracy. The absolute maximum strain value is therefore likely to be underestimated.

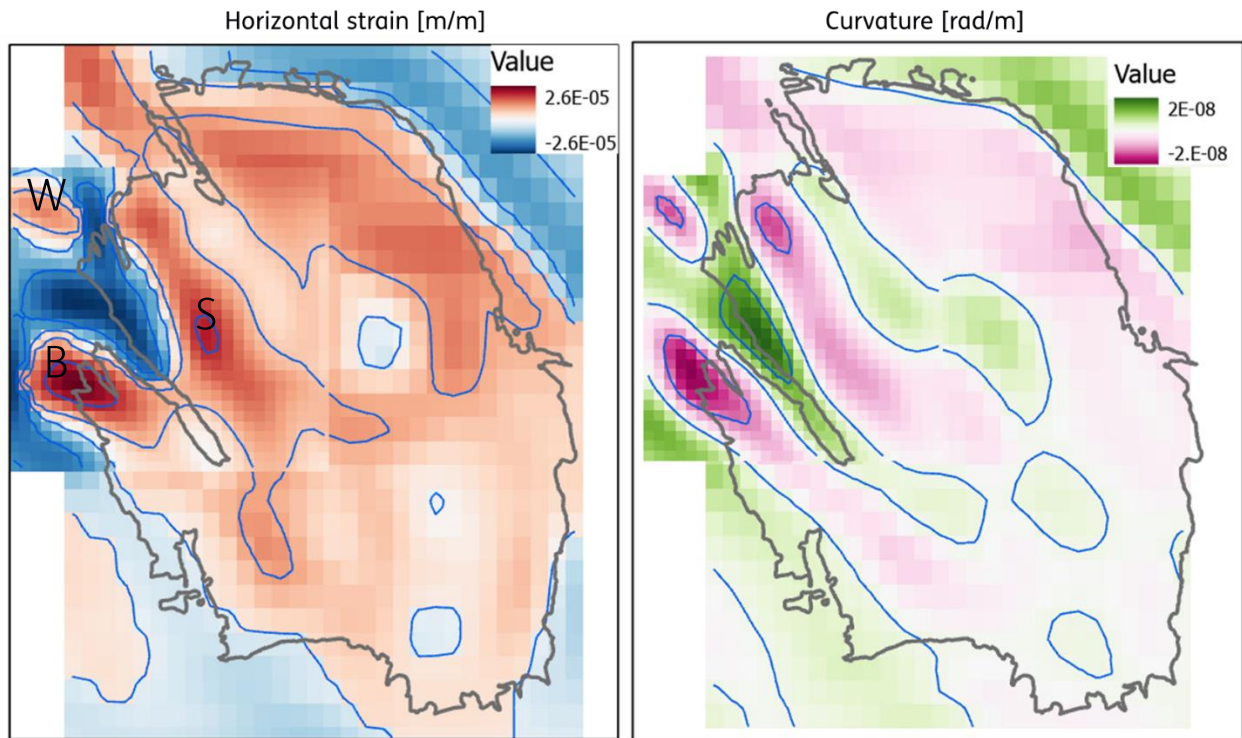


Figure 10: Homogeneous elastic case ‘Groningen 2016’. Spatial development of horizontal strain (left) and curvature (right). A grid resolution of approx. 700m is used in the north west area and approx. 1400m resolution outside that area. The outlines of the Groningen field are represented in black. The horizontal strain grid is overlain by $1.0 \cdot 10^{-5}$ contouring interval, the curvature grid is overlain by $1.0 \cdot 10^{-8}$ contouring interval. B: Bedum area, W: Warffum area, S: Stedum area.

3.2. Vertical elastic heterogeneities

Similar to the Norg analysis, a vertical heterogeneous elasticity profile was applied for the Groningen model. The elastic profile is shown in **Figure 11** (left panel) and was adopted from Fokker and Van Thienen-Visser (2016).

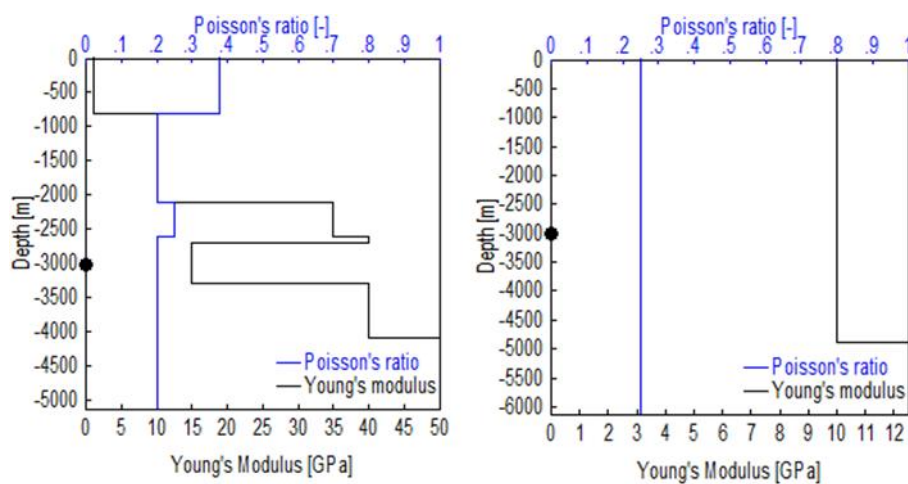


Figure 11: Vertical elastic profile (left) applied to the Groningen model after Fokker and Van Thienen-Visser (2016). For reference the homogeneous elastic profile is shown on the right.

The results are summarized in [Table 5](#). Compared to the homogeneous case (section 3.1) the maximum horizontal strain values are doubled. The spatial pattern of the resulting surface strain ([Figure 12](#)) is very similar to the homogeneous case ([Figure 10](#)). The maxima for the sagging case are likewise located around Bedum, Warffum and the Stedum areas.

The maximum horizontal strain values for the hogging situation (tensile strain) are of the same order of magnitude as the sagging situation (compression strain). This is very different from the Norg area where subsidence for the 'maximum depletion 1995' case results predominantly in a sagging situation with compressional strains.

For two areas a finer grid resolution was used to calculate the model results based on the heterogeneous vertical elastic profile. This was applied for the Groningen NW area where the highest horizontal surface strains are present, and for the Groningen SE area that covers the IMG 'effect area 2'. Horizontal strain results for the Groningen SE area is visualized in [Figure 13](#). In the IMG effect area 2, predominantly tensile horizontal strain is expected. Within that specific contour a maximum horizontal strain of ca. $-15 \cdot 10^{-6}$ m/m (tensile strain) is expected.

Table 5: Maximum horizontal strain and curvature values for the Groningen cases with vertical heterogeneous elastic properties. Compression strain is positive, tensile strain is negative.

Scenario	Type	Max Horizontal strain (m/m)	Max Curvature (rad/m)	
Groningen NW 2016	subsidence	54 10^{-6}	35 10^{-9}	sagging
		-46 10^{-6}	31 10^{-9}	hogging
Groningen NW post 2020	subsidence	58 10^{-6}	39 10^{-9}	sagging
		-51 10^{-6}	34 10^{-9}	hogging
Groningen SE post 2020	subsidence	17 10^{-6}	6 10^{-9}	sagging
		-19 10^{-6}	6 10^{-9}	hogging

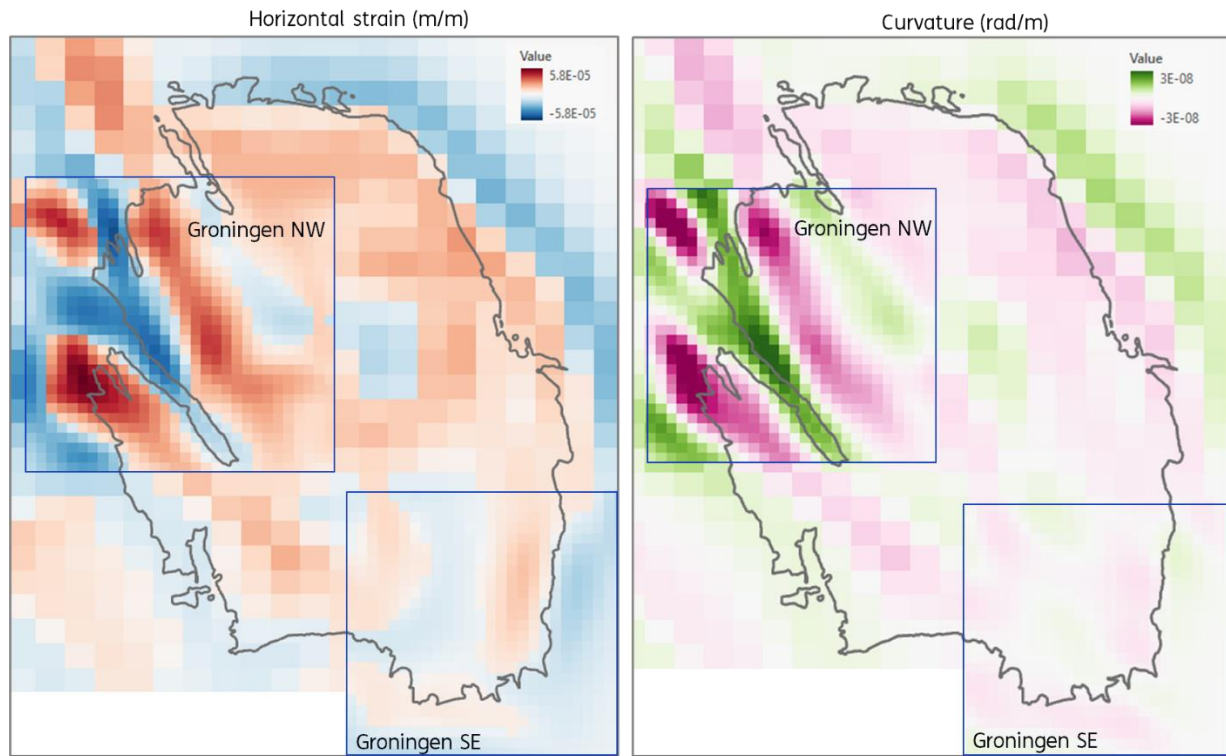


Figure 12: Case 'Groningen Post 2020' with heterogeneous vertical elastic properties. Spatial development of horizontal strain (left) and curvature (right). A grid resolution of approx. 700m is used in the north west and south east areas and approx. 1400m resolution outside that area. The outlines of the Groningen field are represented in black.

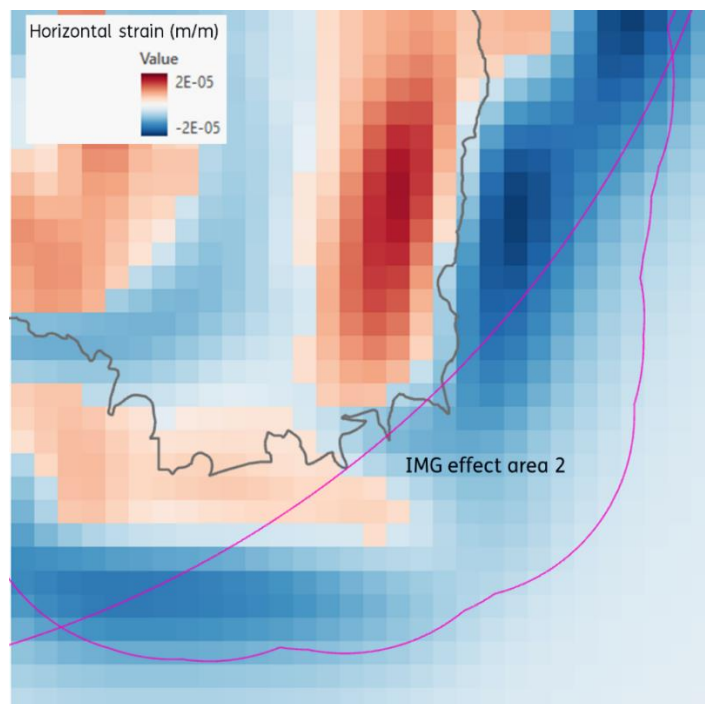


Figure 13: Case 'Groningen Post 2020' 2020' with heterogeneous vertical elastic properties. Spatial development of horizontal strain (grid resolution of approx. 700m) for the south east area, covering the IMG 'effect area 2'. The outline of the Groningen field is represented in black. The purple lines define the IMG 'effect area 2'. Note that the results are equal to Figure 12 but plotted with a different colour scale.

3.3. Horizontal strain distribution Groningen case ‘Post 2020’

For the Groningen area results are only obtained for one single realisation of a heterogeneous vertical elasticity profile. This single realisation is considered as the median value. In order to estimate the uncertainty due to elastic variations, the results from the Norg case were used as a first estimate. The uncertainty due to elastic variation ($\sigma_{elastic}$) is then likewise formulated as:

$$\sigma_{elastic} = 0.05 * \mu_{strain}$$

To determine the horizontal strain uncertainty due to uncertainty of the various components defining reservoir compaction combined with the uncertainty introduced by model imperfections ($\sigma_{reservoir}$) we distinguish between the Groningen SE and for Groningen NW area's because the magnitude of vertical deformation is different.

Modelling results of vertical deformation of the Groningen field have a typical uncertainty bounds (P95 or 2σ) of approximately 1.5 - 3 cm depending on the location (NAM, 2021).

For the Groningen SE a representative figure of the maximum uncertainty bounds (2σ) is 2 cm, resulting in a standard deviation of approx. 1.2 cm. For the Groningen NW area a representative figure is 2.5 cm, resulting in a standard deviation of approx. 1.5 cm

For the Groningen SE area an increase of 5% reservoir compaction leads to 1.2 cm additional vertical deformation at the deepest point (23 cm):

$$\sigma_{reservoir\ Groningen\ SE} = 0.05 * \mu_{strain}$$

For the Groningen NW area an increase of 6% reservoir compaction leads to 1.5 cm additional vertical deformation at the deepest point (25 cm):

$$\sigma_{reservoir\ Groningen\ NW} = 0.06 * \mu_{strain}$$

Combining the uncertainty of both components result in:

$$\sigma_{total\ Groningen\ SE} = \sqrt{\sigma_{elastic}^2 + \sigma_{reservoir\ Groningen\ SE}^2} = \sqrt{0.05^2 + 0.05^2} * \mu_{strain} = 0.071 * \mu_{strain}$$

$$\sigma_{total\ Groningen\ NW} = \sqrt{\sigma_{elastic}^2 + \sigma_{reservoir\ Groningen\ NW}^2} = \sqrt{0.05^2 + 0.06^2} * \mu_{strain} = 0.078 * \mu_{strain}$$

As noted, elastic variation leads to a different shape of the modelled subsidence bowl, that is reflected in both the horizontal surface strain and the vertical deformation. Combining the both uncertainty components is a conservative approach because the variation of vertical deformation is now captured by $\sigma_{reservoir}$ and additionally also by $\sigma_{elastic}$.

4. Conclusions

Maximum curvature and (in this case especially) horizontal strain at surface level are important intensity measures to assess possible risks of damage to buildings. This additional analysis shows a 2D evaluation of expected surface curvatures and horizontal surface strains. This was done assuming homogeneous elastic subsurface properties as well as assuming heterogeneous vertical elastic properties. Using a more realistic heterogeneous vertical elastic profile results in significant higher values of horizontal strain. Compared to using homogeneous elastic properties, the estimated values of

horizontal strain are roughly doubled in magnitude. Surface curvatures also show an increase in case of using heterogeneous vertical elastic properties.

In general the expected surface curvatures for Norg and Groningen when converted at the scale of the building are far below the threshold values for expected damage (TNO, 2021b; Korswagen et al., 2021). Therefore no further attention is given to surface curvature as a damage indicator and no probability distributions are derived for this parameter.

In addition to the new results, uncertainty of the horizontal strain was estimated, combining both the uncertainty contribution from elastic parameters and reservoir compaction. The resulting probability distribution of the horizontal strain can subsequently be used to calculate exceedance probabilities for a certain damage state (not part of this report).

4.1. Norg

Evaluation is now based on a 2D grid instead of the original transects. Taking a vertical variation in elastic properties into account for the Norg case results in a maximum horizontal strain value of $2.9 \cdot 10^{-5}$ m/m for the most realistic elasticity profile.

A weighting of the four available elasticity cases was applied to derive the mean and standard deviation of the horizontal strain for each grid cell. It turns out that the coefficient of variation due to variation in elastic subsurface properties is nearly constant over the Norg field. Additional variation of near-surface elastic properties (upper 400 meter) shows a sensitivity up to plus or minus 4% with respect to the maximum horizontal strain. These model realisations lie within the P95 interval of the distribution based on the weighting of the four scenario's. In general the impact of near-surface elastic variations is smaller than the variation as a result from the four different main scenarios.

Besides uncertainty of elastic properties, the effect of subsidence model uncertainty (vertical deformation) caused by uncertain reservoir compaction on horizontal surface strain is taken into account. These two uncertainty components are combined and resulted in a single coefficient of variation that is applicable for the all grid cell within the 2D grid.

The surface deformation resulting from the current use of the Norg gas storage is considerably less than occurred in 1995 (reduction of approx. respectively 25% and 85% in case of an empty and full gas storage). This is caused by the injection of cushion gas (resulting in increased reservoir pressure) when the gas field was converted to an UGS.

4.2. Groningen

Evaluation is now based on a 2D grid instead of the original transects. Taking a vertical variation in elastic properties into account for the Groningen case results in a maximum strain value of $5.8 \cdot 10^{-5}$ m/m for a realistic elasticity profile. The maximum horizontal strain values for the hogging cases (tensile strain) are of the same order of magnitude as the sagging cases (compression strain). This is very different from the Norg area where subsidence results predominantly in compressional strain.

For Groningen only one single elastic profile was used that is representative for the Groningen area. In order to take elastic uncertainty into account, the coefficient of variation resulting from the Norg analysis was used as an estimate for Groningen.

Similar to Norg the contribution of subsidence model uncertainty caused by reservoir compaction, and its effect on horizontal strain is estimated. This was done for the Groningen NW area where the largest horizontal strains are expected, and the Groningen SE area covering the 'IMG effect area 2'. This results for both areas in a combined coefficient of variation acknowledging both elastic uncertainty and uncertainty of reservoir compaction.

5. References

Buijze, L., van den Bogert, P. A. J., Wassing, B. B. T., & Orlic, B. (2019). Nucleation and arrest of dynamic rupture induced by reservoir depletion. *Journal of Geophysical Research: Solid Earth*, 124, 3620– 3645.

Candela T, Chitu AG, Peters E, Pluymaekers M, Hegen D, Koster K and Fokker PA (2022). Subsidence Induced by Gas Extraction: A Data Assimilation Framework to Constrain the Driving Rock Compaction Process at Depth. *Front. Earth Sci.* 10:713273.

Fokker, P.A. , K. Visser, E. Peters, G. Kunakbayeva, A.G. Muntendam-Bos, 2012, Inversion of surface subsidence data to quantify reservoir compartmentalization: A field study. *Journal of Petroleum Science and Engineering*, Volumes 96–97.

Fokker, Peter A. and Karin Van Thienen-Visser, 2016, Inversion of double-difference measurements from optical leveling for the Groningen gas field. *International Journal of Applied Earth Observation and Geoinformation* 49.

Fokker, P.A., B.B.T. Wassing, F.J. van Leijen, R.F. Hanssen, D.A. Nieuwland, 2016, Application of an ensemble smoother with multiple data assimilation to the Bergermeer gas field, using PS-InSAR. *Geomechanics for Energy and the Environment*, Volume 5.

Hazel, William, 2018, On the Impact of Reservoir Overburden Heterogeneity on Subsidence Modelling. MSc thesis TU Delft.

Lele, Hsu, Garzon, DeDontney, Searles, Gist, Sanz, Biediger and Dale, 2016, Geomechanical Modeling to Evaluate Production-Induced Seismicity at Groningen Field. SPE-183554-MS.

Movares, 2022, Peer Review: Direct and indirect cause of building damages related to deep subsidence and heave, Reference D79-CWS-HS-RAP-22007458, 2 November 2022.

Muntendam-Bos, A.G., Fokker, P.A., 2009, Unraveling reservoir compaction parameters through the inversion of surface subsidence observations. *Comput Geosci* 13, 43–55.

NAM, 2018. Aanvraag Instemming Opslagplan Ondergrondse Gasopslag Norg (actualisering september 2018).

NAM, 2021. Groningen long term subsidence forecast. Reference EP202008201822, 12 February 2021.

Orlic, Bogdan 2016, Geomechanical effects of CO₂ storage in depleted gas reservoirs in the Netherlands: Inferences from feasibility studies and comparison with aquifer storage. *Journal of Rock Mechanics and Geotechnical Engineering*, Volume 8, Issue 6.

TNO, 2021a, Effecten diepe bodemdaling en -stijging rondom de gasopslag Norg en het Groningenveld. Reference TNO2020_R12068, 24 February 2021.

TNO, 2021b, Schade aan gebouwen door diepe bodemdaling en -stijging. Reference TNO2021_R10325, 19 February 2021.

TNO, 2021c, Literature Review: Effects of subsidence on buildings. Reference TNO2020_R12073, 2 February 2021.

Shell, 2008, Cyclic Compaction Experiments on Samples from Norg-5. Reference EP 2008-5189.

Appendix A – Response to peer review

The authors thank the review panel for their constructive comments. In this appendix the main questions and concerns of the review are addressed.

On the use of SADM (semi-analytical deformation modelling)

The reviewers state that 3D numerical solvers are state-of-the-art in production geomechanical modelling and that likely SADM was chosen for simplicity and numerical convenience.

With respect to the scope and timeframe of the study we indeed opted for a SADM approach for numerical convenience.

Reviewers identify two potential issues: (a) Discrepancies caused by separate 2D transect calculations as opposed to full 3D geomechanical simulation and the ambiguity of not producing 2D-gridded maps by the SADM approach. (b) Heterogeneous compaction properties are approximated via the SADM which in turn is designed for laterally homogeneous media.

In general an analytical or semi-analytical approach for modelling subsidence due to gas extraction at a depth of multiple kilometres is widely used and scientifically well-accepted, despite the potential loss of accuracy. Besides this a full 3D geomechanical simulation may be more accurate, but one should keep in mind that results are dependent on (elastic) input parameters of which its values and the (spatial) variability is not well-constrained. In such a case a single, deterministic, 3D geomechanical analysis will be of limited added value and very likely a more extensive (e.g. probabilistic) approach is required in case of a 3D geomechanical analysis.

- (a) Although the initial plan was to evaluate subsidence and derived strain & curvature properties on 2D-gridded maps, it was computational demanding at desired grid resolution, especially for the Groningen field. In our view wisely chosen transects could provide insight in the maximum values for horizontal strain and curvature. We acknowledge that the visualisation of results on transects introduced some discrepancies that could have been avoided by using evaluation of the results on a 2D-gridded map. In the additional analysis performed for Norg and Groningen 2D-gridded results of the analysis are presented.
- (b) The SADM is indeed benchmarked with full 3D numerical solvers for homogeneous compaction properties. Several studies (Muntendam-Bos & Fokker, 2009; Fokker et al., 2012, 2016) demonstrated that inversion of subsidence observations at the surface is capable to estimate a (spatial varying) reservoir compaction field using a SADM approach. Although a heterogeneous case was not explicitly validated with a full 3D numerical model, a good match of model results with surface observations in above mentioned studies provides confidence in the SADM capabilities in case of a heterogeneous compaction field as used in the subsidence analysis for the Groningen case.

On the potential importance of near-surface properties

Reviewers pose that the absence of treatment of near-surface heterogeneity in modelling may lead to potential blind spots such as: (a) Underestimation of strain magnitudes, because the near-surface is always more compliant than the deeper overburden rocks. Given the same input stress the resulting strains may be higher. (b) Unknown scale of lateral strain variations possibly related to discontinuities in near-surface properties at building scales and unknown potentially local contributions to geographically-dependent variations on subsidence-related damage risk.

Possible near surface effects due to heterogeneous near-surface properties were disregarded in the initial analysis due to the foreseen timeframe of this project. Well-motivated statements on near surface effects would require an extensive 3D numerical (FEM) study and thorough characterisation of near-surface properties at the area of interest.

- (a) The authors acknowledge that assuming homogeneous elastic properties of the overburden rock lead to an underestimation of the horizontal strain at the surface compared to a vertical heterogeneous case, despite the fact that vertical surface deformation in both cases is comparable. In the additional analysis performed for Norg and Groningen the extent of this underestimation is assessed.
- (b) Subsidence induced by reservoir compaction and possible variations on reservoir depth level potentially lead to relatively long wavelength variation at the surface due to the smoothing effect of multiple kilometres of overlying rock. The effect of heterogenous variations in the overburden and the capability to contribute to small-wavelength fluctuation at the surface is not well-understood or quantified. To answer this question a full 3D numerical study is required. However, results of unpublished comparative TNO studies between 3D FEM analysis (Abaqus) and semi-analytical stress models (comparable with SADM) show that semi-analytical models are capable to capture the range of stress (and related strain) variations due to elastic heterogeneities. Although this is not validated for subsidence modelling, the sensitivity analysis of elastic properties as applied in this additional analysis for Norg and Groningen provides insight into the range of the possible effect of elastic heterogeneity on the subsidence evaluation.

On the absence of uncertainty quantification

Reviewers state that multiple simulations could have been performed based on a defined uncertainty range of model parameters to yield confidence intervals for resulting surface deformations. Though reviewers acknowledge that this may well have been beyond the resources/scope of the project, the absence of uncertainty analyses does lead to important considerations: Unknown range of extreme deformation values and unknown statistical significance of final results.

Applying a full probabilistic workflow could provide more insight in the bandwidth of the results, but was in view of the foreseen timeframe of the initial analysis disregarded. A probabilistic workflow is especially of added value if for the building damage modelling initially also a probabilistic approach was followed.

In the additional analysis performed for Norg and Groningen the uncertainly range of the results were estimated, and also the building damage modelling was addressed probabilistically.

References

Fokker, P.A. , K. Visser, E. Peters, G. Kunakbayeva, A.G. Muntendam-Bos, 2012, Inversion of surface subsidence data to quantify reservoir compartmentalization: A field study. Journal of Petroleum Science and Engineering, Volumes 96–97.

Fokker, P.A., B.B.T. Wassing, F.J. van Leijen, R.F. Hanssen, D.A. Nieuwland, 2016, Application of an ensemble smoother with multiple data assimilation to the Bergermeer gas field, using PS-InSAR. Geomechanics for Energy and the Environment, Volume 5.

Muntendam-Bos, A.G., Fokker, P.A., 2009, Unraveling reservoir compaction parameters through the inversion of surface subsidence observations. Comput Geosci 13, 43–55.